

STUDY AND INTEGRATION OF
PHOTOVOLTAIC SYSTEMS

A Thesis
presented to
the Faculty of Engineering
at Notre Dame University-Louaize

In Partial Fulfillment
of the Requirements for the Degree
Master of Science In Electrical and Computer Engineering

by
PETER R. SALAMEH

AUGUST 2022

© COPYRIGHT

By

Peter Salameh

2022

All Rights Reserved

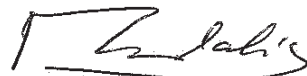
Notre Dame University - Louaize
Faculty of Engineering
Department of Electrical, Computer and Communication Engineering

We hereby approve the thesis of

Peter Salameh

Candidate for the degree of Master of Science in Electrical and Computer Engineering

Dr. Nassar Mendalek



Supervisor, Chair

Dr. Semaan Georges



Committee Member

Dr. Elias Nassar



Committee Member

Acknowledgments

This thesis is the result of being a Master's candidate in electrical and computer engineering at Notre Dame University-Louaize Lebanon.

This work would not have been possible without the vision of my master's advisor, Dr. Nassar Mendalek, who was always present to help me and guide me toward the correct path. Dr. Mendalek encouraged me to pursue my master project in this research domain and guided initially the project's work to the Modular Multilevel Converters to which this thesis is based. Dr. Mendalek was also the solver of numerous problems that I faced and he deserves all thanks and appreciation.

Moreover, I am very grateful for Dr. Semaan Georges and Dr. Elias Nassar for being part of this work's committee, Dr. Georges and Dr. Nassar supports were always available during graduate and undergraduate academic years.

Furthermore, I am very thankful to all professors of Electrical, Computer and Communications Engineering Department who allowed me getting to this academic level and knowledge from my undergraduate to the graduate studies. Thanks to every member of the faculty of engineering, Dean, Chairperson, Doctors, staff and colleagues, they all leaved a trace in my academic journey.

Finally, it is impossible for me to forget thanking my parents, family, friends and colleagues who were supporting and encouraging me in my life and through the difficulties I faced.

Table of Contents

Acknowledgments.....	iii
Table of Contents.....	iv
List of Figures.....	vii
List of Tables.....	ix
Abbreviations and Symbols.....	x
Abstract.....	xii
1. Chapter 1: Introduction.....	1
1.1 Background.....	1
1.2 Main Purpose.....	4
1.3 Outline.....	4
2. Chapter 2: Photovoltaic Power Systems.....	6
2.1 Photovoltaic Cell, Electronic Structure.....	6
2.1.1 Equivalent Circuit of a PV Cell.....	7
2.1.2 Solar Panel.....	8
2.2 Power Conditioning Units.....	10
2.3 Photovoltaic system and topologies.....	13
2.3.1 Centralized converter topology.....	13
2.3.2 Series-connected string converter topology.....	14
2.3.3 Multi-string parallel-connected topology.....	15
2.3.4 Cascaded dc-dc converters topology.....	15
2.4 Specifications and standards for grid connected PV systems.....	17
2.5 Maximum power point controller and algorithm.....	18
2.6 The power electronic interface.....	23
2.6.1 DC/DC Boost converter.....	24
2.6.2 Modular multilevel converter.....	26
2.7 The system topology.....	28
2.8 Problem Statement.....	28
3. Chapter 3: Modular Multilevel Converter.....	29
3.1 Mathematical Model of the MMC.....	30
3.2 State Space Matrix presentation.....	32
3.3 Reverse Model Predictive Control (RMPC).....	35
3.4 Grouping-Sorting Optimized Control.....	36
3.5 Simulation and Results.....	42
4. Chapter 4: Solar System Study at Notre Dame University Lebanon.....	49

4.1 System Design and Objectives	49
4.2 Methodology.....	49
4.2.1 Simulation Software: PVsyst	49
4.2.2 Site Assessment	50
4.2.3 Meteorological Data.....	53
4.3 Selection of Module and Inverter	57
4.4 Module Orientation and Inter-Row Spacing	58
4.4.1 Number of Modules to be installed.....	61
4.5 System Design	62
4.6 Shading	64
4.7 Economical Evaluation of the PV System.....	65
4.8 Results and Discussion	68
4.9 Conclusion	71
5. Chapter 5: Case Study - Grid Connected Photovoltaic Project in Lebanon	72
5.1 Overview and Location Description.....	72
5.1.1 Port of Beirut Existing Electrical Infrastructure	73
5.2 Executive Summary.....	81
5.3 Description of the Project.....	82
5.3.1 POB demand load	82
5.3.2 PV Panels location & type of installation	83
5.4 Selected Material for the Port's Project.....	90
5.4.1 PV Panels	90
5.4.2 Inverter	91
5.5 System Configuration.....	93
5.5.1 Determining number of Inverter and number of PV panels per inverter	93
Using block design and String Inverters.....	95
5.5.3 Estimated monthly PV output in KWh for 1MWp PV installation	96
5.6 PV KWh output compared to POB KWh consumption	98
5.7 Energy captured from solar carports according to orientation	99
5.8 Connecting the renewable energy to the POB grid	101
5.9 Approximate Cost Estimate and Return on Investment	101
5.10 Connecting the renewable energy to the POB Grid	103
5.10.1 Excavation and routing to main substation.....	104
5.10.2 Converting the received energy to medium voltage	105
6. Chapter 6: Conclusion.....	107

Appendices	108
Appendix A: PVsyst Report for NDU Main Campus	108
Appendix B: PV panel Jinko JKM590-610N-78HL4-BDV-F1-EN	109
References	110

List of Figures

Figure 2.1– Energy Conversion process in solar cells.....	7
Figure 2.2 – Equivalent circuit of a photovoltaic solar cell.....	7
Figure 2.3 – Series parallel connection of the centralized converter topology.....	13
Figure 2.4 – Total cross tied connection of the centralized converter topology.....	13
Figure 2.5 – Series connected string inverter topology.	14
Figure 2.6 – Multi-string parallel connected topology.	15
Figure 2.7 – Cascaded DC-DC converters topology.	16
Figure 2.8 – Power vs. Voltage and Current vs. Voltage curves.....	19
Figure 2.9 – Flow chart of P&O method	21
Figure 2.10 – Simulink Model of the MPPT controller with Perturb and Observe MATLAB script.....	22
Figure 2.11 – Equivalent circuit of Boost converter.....	24
Figure 2.12 – Equivalent circuit of Boost converter when T is on and off.....	25
Figure 2.13 – Boost Converter including the control comparator.	25
Figure 2.14 – Structure of Modular Multilevel Converter.....	26
Figure 2.15 – Multilevel converter’s sub module.....	27
Figure 2.16 – Conduction paths of sub module.	27
Figure 2.17 – Complete PV system connected to grid.....	28
Figure 3.1 – Structure of a three-phase MMC-based inverter and its SM.....	29
Figure 3.2 – Control scheme of the reverse MPC.....	35
Figure 3.3 – GSOC 1 st and 2 nd levels.....	37
Figure 3.4 – Complete model of the MMC including the RMPC	42
Figure 3.5 – Circuit of the MMC system tied to ideal grid through grid impedances, and the R-MPC control block.	43
Figure 3.6 – Illustration of the phase-a upper arm subsystem showing the twenty submodules and the block (s-function) that determines the gate signals.....	43
Figure 3.7 – Half-bridge submodule used in the MMC.....	44
Figure 3.8 – The inside of the R-MPC control block showing the subsystems to derive the RMPC control law for each arm.	44
Figure 3.9 – Implementation of the RMPC control law for the two arms of phase-a.	45
Figure 3.10 – Output-side line-to-line voltages and line currents.	47
Figure 3.11 – Arm voltages and inner currents of phase-a arms.	47
Figure 3.12 – Capacitor voltages and phase-a common-mode current <i>idiff</i>	48
Figure 4.1 – Steps taken in PVsyst design.....	49
Figure 4.2 – Satellite imagery of the location - Notre Dame University Louaize-Zouk Mosbeh Main Campus [16]	51
Figure 4.3 – Engineering Labs, Building Dimensions: 80mx19m, Perimeter: 198.5m, Rooftop Area: 1523m ² [16].....	52
Figure 4.4 – Faculty of Engineering & Faculty of Natural and Applied Sciences, Building Dimensions: 34.5mx53m, Perimeter: 175m, Rooftop Area: 1827m ² [16]... ..	52
Figure 4.5 – Computer Labs, Building Dimensions: 80mx12.3m, Perimeter: 183m, Rooftop Area: 982m ² [16].....	52

Figure 4.6 – Zone 1, Building Dimensions: 36mx18m, Perimeter: 107m, Rooftop Area: 629m ² [16].....	53
Figure 4.7 – Area 2, Building Dimensions: 33mx18m, Perimeter: 118m, Rooftop Area: 768m ² [16].....	53
Figure 4.8 – PVGIS source of data depending on the geographical site location	54
Figure 4.9 – NSRDB data available for the colored areas.....	55
Figure 4.10 –Solcast data available in the highlighted areas.....	55
Figure 4.11 – SolarAnywhere TGY data, twelve months of various years	56
Figure 4.12 – Inter-row spacing for a ground mounted PV system.....	60
Figure 4.13 – Solar Paths at Zouk Mosbeh [17].	60
Figure 4.14 – 3D distribution of PV panels on NDUs buildings roofs.....	62
Figure 4.15 – Loss diagram over the whole year [17].....	68
Figure 4.16 – Normalized productions (per installed kWp) [17].....	69
Figure 4.17 – Performance Ratio [17]	70
Figure 5.1 – POB General Layout [21].....	72
Figure 5.2 – Port of Beirut Power Plant Buildings [22]	73
Figure 5.3 –POB Power Plant’s Single Line Diagram [23].....	75
Figure 5.4 – POB Complete Single Line Diagram [24].....	80
Figure 5.5 –Example of floating PV installation (Kelseyville country, California, USA, 252 kW)	84
Figure 5.6 –Example of PV roof installation: SMLC PEPSICO Lebanon	87
Figure 5.7 –Example of Solar Carports Installation: 16.3 MW solar array on a car park in Corbas, France.....	89
Figure 5.8 – Port Parking PV layout.....	89
Figure 5.9 – Current Voltage relation of LR5-72HBD-530M at different cell temperature [26].....	90
Figure 5.10 – Current Voltage relation of LR5-72HBD-530M at different incident irradiance [26].....	91
Figure 5.11 –Power Voltage curve of LR5-72HBD-530M at different incident irradiance [26].....	91
Figure 5.12 –Circuit diagram of a Huawei SUN2000-105KTL-H1 string inverter [27]	93
Figure 5.13 –Lebanon Solar GHI Map [28].....	96
Figure 5.14 –PV installation Schematic.....	101
Figure 5.15 –Excavation and routing to Poste Principale.....	104

List of Tables

Table 1.1 - Lebanese power plant and related generation capacities [3]	3
Table 2.1 – Summary of Hill Climbing and Perturb and Observe algorithm	20
Table 3.1– System parameters adopted in the simulation.....	46
Table 4.1– Geographical location of Notre Dame University Louaize Lebanon [16].	51
Table 4.2– Identified roof areas that are useful for PV installation.....	51
Table 4.3 – Meteorological data based on the PVGIS imported from the TMY [17].	56
Table 4.4– Jinkosolar JKM-600N-78HL4-BDV specification [17]	57
Table 4.5 – Huawei SUN2000-40KTL-M3-400V inverter specification [17]	58
Table 4.6 – Supports angles and azimuth	61
Table 4.7 – Identified roof areas that are useful for PV installation.....	61
Table 4.8– Identified roof areas that are useful for PV installation.....	64
Table 4.9 – Economical Assumptions [17].....	66
Table 4.10 – Financing Evaluation [17]	67
Table 4.11 – Payback Time and NPV	68
Table 4.12 – Results Overview	69
Table 5.1 – Relation between Number of Operating Generators, STSs and Load [22]	76
.....	76
Table 5.2 – POB Monthly Load Report over one year	83
Table 5.3 – Yearly GHI chart and table [28]	96
Table 5.4 – Estimated monthly PV output in KWh for 1MWp PV installation at POB [28].....	97
Table 5.5 – PV KWh output compared to POB KWh consumption	98
Table 5.6 – South Orientation PVout calculation for 1MWp installation	99
Table 5.7 – East Orientation PV out calculation for 1MWp installation.....	100
Table 5.8 – South West Orientation PV out calculation for 1MWp installation	100
Table 5.9 – Cost Estimate of the project.....	102

Abbreviations and Symbols

Chapter 2	
Symbols	Description
I_{ph}	Current produced by the photoelectric effect.
I_D	Diode reverse saturation current.
I_{SH}	Current through shunt resistance.
I	PV cell/array current.
R_p	Shunt resistance.
R_s	Series resistance
N_p	Number of PV cells in parallel.
N_s	Number of PV cells in series.
Q	Electron charge.
k	Boltzmann's constant.
a	Ideality factor modified.
T	Cell working temperature.
V	Voltage across PV array terminal
D	Duty Cycle of the Converter
Chapter 3	
Symbols	Description
j	Represent the three phases and could then be either a, b or c
m	Represent which arm in a particular leg and could be either u (upper arm) or l (lower arm)
n	Represent the number of sub-modules and could be 1, 2, 3, ..., N
u_{jm}	Arm voltage
i_{jm}	Arm current
u_j	AC side voltage
i_{oj}	Output current
i_{cj}	Circulating current
L_{oj}	Load inductance
R_{oj}	Load resistance
U_{dc}	DC source voltage
$u_{jm,n}$	Capacitor voltage
C	Sub module capacitance
X	State Vector $[i_{oj}, i_{cj}, u_{ju}, 1, \dots, u_{ju}, N, u_{jl}, 1, \dots, u_{jl}, N]^T$
D	Perturbation Vector $[u_j, U_{dc}]^T$
gc	Group Combination
M	Number of groups in Grouping Sorting Optimized Control
X	Number of submodule in a group M in Grouping Sorting Optimized Control
G	Cost Function
λ_o	Weighing factor of the cost function g
λ_c	Weighing factor of the cost function g
λ_w	Weighing factor of the cost function g
$M_{jui/l}$	Sorting Index of the submodules
N	Number of on state submodules

N	Number of submodule per arm
L	Arm inductance
C_{sm}	Submodule Capacitance
Udc	DC bus voltage
F	Frequency
T_s	Sampling period
Chapter 4	
Symbols	Description
Vmp	Voltage maximum power
Voc	Open Circuit Voltage
d_{row}	Inter row spacing
w_m	Panel width
β_m	Tilt angle
γ_m	Azimuth angle of the module
γ_s	Azimuth angle of the sun
α	Altitude angle of the sun
Chapter 5	
Symbols	Description
B_n	Expected benefit at the end of the year n
C_n	Expected cost at the end of year n
i	Discount rate
n	Project duration in years
N	Project period
PVB	Present value benefit
PVC	Present value cost
ROI	Return on Investment

Abstract

This thesis aimed to study the structure of an on grid photovoltaic system and to get by the aspect of integration of such system to the power network. The integration method can have different topologies and is usually based on power electronic devices controlled by dedicated controllers. In order to transform the direct output signal of the PV panels to an alternative signal connected to the utility network, the Modular Multilevel Converter (MMC) was used in this study. The challenges linked to this type of converters are associated with its sub-modules balancing control, the suppression of the circulating current, the complexity of its control, and its related performance. Simulation of the converter dynamic behavior including the related control technique is done through Matlab Simulink [1]. The adopted control strategy used is based on the reverse model predictive control and was used in order to reduce the computational burden by calculating the number of inserted MMC's submodules directly, based on the reverse prediction of arm voltages. Preliminary results showed that the output of the used system presents reasonable accuracy when compared to the parameters of the tied-to electrical network. In addition a case study of a grid connected photovoltaic system is presented in this work: the site conditions, power aspects, topology, economical study are all presented for a particular application.

Chapter 1: Introduction

In this Chapter, the main purpose of this project is presented in addition to the motivations that led to its selection. Furthermore, an outline of the main chapters included in this report is given.

1.1 Background

Power generation is lately changing toward dispersed system while it had been for several decade relying on centralized large power plants. In other words, instead of fulfilling most of the power demand using a single large power plant, trends in countries are currently directed toward providing several generation units placed closer to the consumers' sides. These units could be renewable such Photovoltaic (PV), wind turbine, wave generator, fuel cell... or nonrenewable sources such fossil fuel and nuclear power plant...

PV renewable energy sources' power generation is estimated to have increased by 22% in 2019, to 720 TWh. Global grid-connected solar capacity reached 707.5 GW at the end of 2020 according to the International Renewable Energy Agency [2]. With this increase, the solar PV share in global electricity generation is now almost 3%. In 2019, PV generation overtook bioenergy and is now the third-largest renewable electricity technology after hydropower and onshore wind.

Lebanese power generation sector is currently suffering from problems and the financial deficit of Electricité Du Liban (EDL) reached 1.8 billion USD in 2018 [3]. This situation was reached due to several factors that one can highlight among them: The freezing of the

tariff at a level below the average cost of production, the operation of old low efficiencies and high operating cost plants, high rates of technical and non-technical losses and the additional load that was lately imposed by the Syrian refugees whose consumption is estimated to be around 0.5 GW. The total electric power capacity (generated and imported) that is currently available in Lebanon is around 2403MW while the peak demand reaches 3670MW in 2019 [3]. Table 1.1 lists the available power plant in Lebanon and their generation capacities.

Beside the hydro power generation, other renewable power plant such Photovoltaic are almost not relied on in Lebanese market. However the exploitation of renewable energy will give the investor or the nation the power to both ameliorate the environmental conditions, by reducing harmful emission, and to reduce the cost of production of power.

The efficiency, reliability and cost-effectiveness of the power electronics devices that are used to interface PV systems to the mains grid and other types of off-grid loads are of major concern in the process of system design. In order to improve the efficiency and convert low voltage direct current (DC) source into usable alternating current (AC) source, the power electronics converters are used to transform DC into AC.

Table 1.1 - Lebanese power plant and related generation capacities [3]

	Name of the Facility	Fuel Type	Installed Capacity (MW)	Effective Capacity 2018 (MW)
Existing EDL	Zouk 1 Thermal Power Plant	Heavy Fuel Oil	607	440
	Jieh 1 Thermal Power Plant	Heavy Fuel Oil	343	180
	Zouk 2 ICE Power Plant	Heavy Fuel Oil / Natural Gas	198	157
	Jieh 2 ICE Power Plant	Heavy Fuel Oil / Natural Gas	78	63
	Zahrani I Combined Cycle Power Plant	Diesel Oil / Natural Gas	469	420
	Deir Ammar I Combined Cycle Power Plant	Diesel Oil / Natural Gas	464	430
	Baalbeck Open Cycle Gas Turbine	Diesel Oil	64	57
	Tyr Open Cycle Gas Turbine	Diesel Oil	72	56
	Richmaya-Safa Hydro	-	13	3
	Naameh (Landfill Gas)	-	7	7
Existing Barges	Power Barge Zouk	Heavy Fuel Oil/Natural Gas	187	195
	Power Barge Jiyeh	Heavy Fuel Oil/Natural Gas	187	195
Existing Independent Power Plants	Litani Hydro	-	199	47
	Nahr Ibrahim Hydro	-	32	17
	Bared Hydro	-	17	6
	Kadisha Hydro	-	21	15
	Hrayche Thermal Power Plant	Heavy Fuel Oil	35	46
Power Wheeling	Imports from Syria	Syria	276	69

1.2 Main Purpose

Power electronic converters used to process the DC electrical energy out of the PV panels are aimed to provide stable and regulated AC power. To guarantee adequate performance of these converters, dynamic models are derived and used in the design of advanced control techniques (nonlinear control, model predictive, or others). The system dynamic and steady-state behaviors will be validated by conducting necessary simulations in MATLAB/Simulink environment. The work also included studies of a grid connected PV power plants installed on the shores of the eastern side of the Mediterranean Sea.

1.3 Outline

In chapter 2, the electronic structure and the equivalent circuit of the PV cell is provided, then the equation of the solar panel, composed of series and shunt connected PV cells, is given. In addition, PV system' topology are listed and a small briefing of the available grid tied standard are listed. Then after, the used system topology will be described, modeling the photovoltaic array and elaborating the maximum power point controller and algorithm will also be stated. And finally the power electronic interface will be described.

Chapter 3 elaborates details related to the modular multilevel converter used in the application to connect the PV panels to the power grid. In this chapter a mathematical model of the converter will be derived, in addition, the control technique used to control the behavior and output of the converter are also provided. In addition, based on the selected modular multilevel converter and control technique, simulation model of the system is implemented with Simulink and the obtained results are elaborated.

Chapter 4 consists of a solar system study done for Notre Dame University Main Campus at Zouk Mosbeh. In this chapter the simulation using real components for a PV project is done using PVsyst software. Meteorological data acquisition is explained, selection of modules and inverters and defining the ultimate installation orientation and spacing is shown. The simulation goes through the detailed information that the installer shall know to guarantee optimal installation and the highest yield. The simulation goes through shading scenarios and also allow the user to evaluate the economic aspect of the project as well.

Chapters 5 is composed of a case study related to the PV grid connected system. In this chapter the complete installation, selection, technical and economic aspects are elaborated.

Finally, Chapter 6 concludes with a summary of the main results of the project and suggestions on possible ways to supplement and enhance the work.

Chapter 2: Photovoltaic Power Systems

2.1 Photovoltaic Cell, Electronic Structure

The operation of PV solar cells are based on the formation of a pn junction. PN junctions are formed by two different types of semiconductor materials. Semiconductor materials, such as Silicon, lies in the fourth column of the Periodic table of elements. The important feature of the pn junction is that they form a strong electric field due to diffusion. This electric field pulls the electrons and holes in opposite directions.

By irradiating the pn junction with light, the semiconductor pn device can be switched on. This is the basis of solar photovoltaic cell. The incident solar radiation passes through the p type material to reach the junction. This is perceived as a flux of particles (photons) which carry the energy. Some of these photons with energy exceeding the band gap energy ($E_c - E_v$) collide with the valence electrons of the semiconductor material and thus are absorbed. This will yield a release of electrons to the conduction band and holes will be left behind in the valence band. The absorption process generates then electron-hole pairs. When the silicon cell is electrically isolated on open circuit a direct voltage will appear across the terminals. If the cell has an external electrical circuit connected to its terminal then a direct current will flow.

A pn junction photovoltaic cell performs two functions simultaneously:

- a. It harvests sunlight by converting photons to electric charges
- b. It conducts the charge carriers from where the charges can be collected as electrical current.

Figure 2.1 shows an illustration of the energy conversion process in the solar cell.

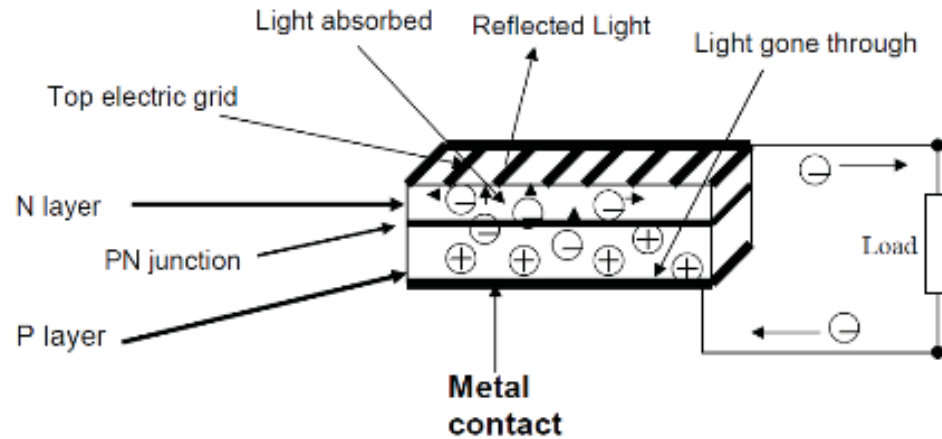


Figure 2.1– Energy Conversion process in solar cells

2.1.1 Equivalent Circuit of a PV Cell

An ideal PV cell is modelled by a current source in parallel with a diode. However no solar cell is ideal and thereby shunt and series resistances are added to the model as shown in the PV cell equivalent circuit in Figure 2.2. In this circuit R_s is the intrinsic series resistance whose value is very small. R_p is the equivalent shunt resistance which has a very high value.

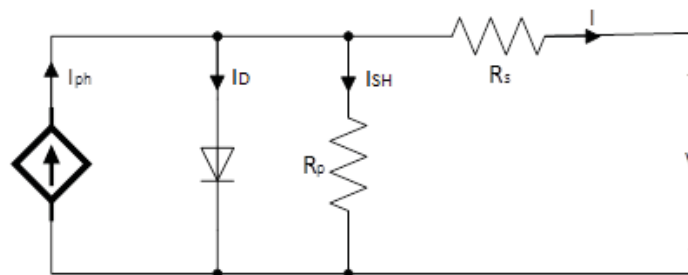


Figure 2.2 – Equivalent circuit of a photovoltaic solar cell

Applying Kirchhoff's Current Law we get Eq. 2.1:

$$I_{ph} = I_D + I_{SH} + I \quad 2.1$$

Where:

I_{ph} : Current produced by the photoelectric effect.

I_D : Diode reverse saturation current.

I_{SH} : Current through shunt resistance.

I : PV cell current.

R_p : Shunt resistance.

R_s : Series resistance

2.1.2 Solar Panel

In general a PV cell generates a voltage of 0.5V and in order to obtain the required voltage and current, PV cells are arranged in series and parallel configuration to form what is called module or arrays of PV cells [4]. For an array of PV cells the current equation Eq. 2.2 is given by:

$$I = N_p I_{ph} - N_p I_D \left[e^{\frac{(V+IR_s)q}{akTN_s}} - 1 \right] - N_p \frac{(V + IR_s)}{R_p} \quad 2.2$$

Where:

I : PV array current.

N_p : Number of cells in parallel.

N_s : Number of cells in series.

I_{ph} : Current produced by the photoelectric effect in a cell.

I_D : Reverse saturation current of the diode.

R_s : Resistance in series associated with the cell.

R_p : Resistance in parallel associated with the cell.

q: Electron charge.

k: Boltzmann's constant.

a: Ideality factor modified.

T: Cell working temperature.

V: Voltage across PV array terminal.

When choosing the solar panel to be used in a project, the most important key feature that a designer must check are:

1. Electrical Data (Standard Test Conditions (STC): Irradiance 1000W/m², Cell Temperature 25°C, Air Mass AM1.5): Maximum Power, Maximum Power Voltage, Maximum Power Current, Open Circuit Voltage, Short Circuit Current.
2. Electrical Data (Normal Operating Cell Temperature (NOCT): Irradiance at 800W/m², Ambient Temperature 20°C, Wind Speed 1m/s): Maximum Power, Maximum Power Voltage, Maximum Power Current, Open Circuit Voltage, Short Circuit Current.
3. Mechanical Data: Dimensions, Weight, IP rate, Cell orientation
4. Temperature Rating
5. Maximum Ratings: Operational Temperature, Maximum System Voltage, Max Series Fuse Rating
6. Linear Performance Warranty

In addition to the above, one can expect when checking the datasheet of a particular PV panel to find some informative curves such Current-Voltage Curve for different cell temperature, Current-Voltage Curve for different Incident Irradiance, Power-Voltage Curve...

All these characteristics in addition to the cost allow to differentiate between panels and to choose the one that fit most for a particular project.

2.2 Power Conditioning Units

By power conditioning units it is meant the devices used to control the DC power produced by the PV panels and arrays. Depending on the number of stages the PV system is divided into either single stage: where inverter is used to perform all the required control tasks; or two stages: where a converters precedes the inverters and the control tasks are divided among the two power electronic devices.

DC-DC converters are power electronic circuits that convert a dc voltage to a different dc voltage level, often providing a regulated output. There are various different kinds of converters mainly linear and switching and their operation mode depends on the duty cycle of the power switch [5]. Some of these converters and their key features are listed here below, for wider comparison refer to [6].

1. Basic Converters: Their use is limited to application when the change in the input to output voltage is very small. The generation of noise is large in these converters.
 - a. Buck Converter: the average output voltage is lower than the input. It is used in application such solar charged electric cars to charge the battery or when array voltage is higher from the battery voltage [6].
 - b. Boost Converter: the average output voltage is higher than the input. Stepping up the voltage is done without transformer.

2. Cascaded Converter: it is a combination of series and or parallel connection of Buck and Boost converters.
 - a. Buck-Boost Converter: output voltage could be either less than or higher than the input voltage.
 - b. Sepic Converter: the output voltage can be less equal or more than the input voltage. This converter has the ability to shut down immediately when the converter is switched off.
 - c. Zeta Converter: used to reduce the ripple and noise in the output current. It provides better isolation between input and output.
 - d. Cuk Converter: Switching losses for this converter are low and therefore it has a good efficiency.
3. Interleaved Converter: used for high current and power application. They reduce ripples significantly, increase the efficiency, reduce electromagnetic and improve response of the module in transient state.
 - a. Interleaved Dual Boost Converter: Ripple cancellation is done on both input and output sides. And improvement of the efficiency is done by activating a suitable number of converters that are interleaved and installed between load and source.
 - b. Interleaved Flyback Converter: The output voltage is higher in this case and due to interleaving operation the ripple in input and output are reduced.
4. Isolated converter: Used to protect the output from any disruptions on the input side. Among the commonly known isolated converter the following can be listed:
 - a. Full bridge Transformer Isolated Buck Converter

- b. Forward Converter
- c. Flyback Converter
- d. Single Ended Two Transistor Forward Converter.
- e. Phase Shift Full Bridge Converter

Inverters are circuits that convert DC to AC. They transfer power from a DC source to an AC load. In the search to improve PV system's efficiency and shrink the system total cost, transformer less PV multilevel inverters form an alternative that increases the total interest. But some topologies of this category has efficiency degradation problems and other safety issues related to the connection between grid and PV.

Traditional inverters were heavy, large, difficult to install and their efficiency was in the 85-90% range [7]. Other problems with traditional inverters were low power factor and the relatively increased harmonic content in the AC current output. Today, some inverter technologies use line frequency transformer that allows galvanic isolation between PV array and grid and thus removes the DC current injection problems. However, line frequency transformer is considered as a poor component in inverter since it leads to an increased size, weight, and price.

The use of a high frequency transformer, embedded in modern inverter, reduces the scale of the system (size and weight). And many inverters do not even include a transformer at all. Topologies with no transformer have better efficiencies and are more economic than inverters equipped with transformers. But for transformer less inverter the problem of DC current injection shall be handled separately.

2.3 Photovoltaic system and topologies

In order to choose the optimal system for future PV project, the analysis of common architectures being used for photovoltaic systems is provided here.

2.3.1 Centralized converter topology

In this topology, the PV panels are wired in a single common array (in series and or parallel) and the array is connected to a single inverter. This topology is economic due to the small number of inverters, but the partial shadowing of the one panel will affect the whole array power output. This topology has two kinds of connection:

1. Series-parallel (SP) as shown in Figure 2.3

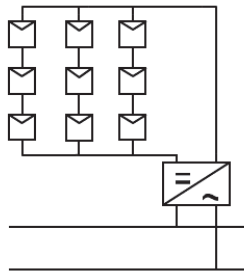


Figure 2.3 – Series parallel connection of the centralized converter topology.

2. Total cross tied connection (TCT) as shown in Figure 2.4

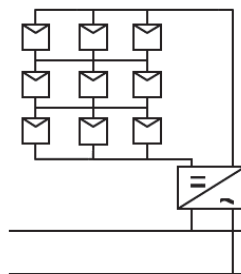


Figure 2.4 – Total cross tied connection of the centralized converter topology.

In the TCT connection, the system element mismatch problem is reduced. Each of the PV-modules gets equipped by parallel diode that allows bypassing the module if it is shadowed or even damaged.

2.3.2 Series-connected string converter topology

Here the array of the PV panels is split to the several strings in series. Losses due to electric conductors are important when the voltage is low [8]. This topology is characterized by the high voltage and low current, or in other words it allows reduction in the cost of wires, decrease in the voltage drops and thus power losses the conductors. Strings are connected one by one to inverters with MPPT and the outputs of the inverters are connected to the transmission lines. Figure 2.5 shows this topology.

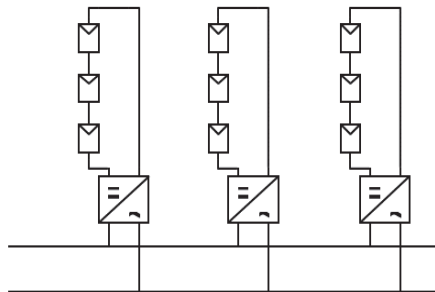


Figure 2.5 – Series connected string inverter topology.

When one or several panel is shadowed in a string, other string are not affected and irradiance level remains same for other string. Each PV modules is equipped by parallel diode to bypasses it if its output voltage is low. The topology is appropriate for installation where the irradiance is regularly altered for complete panel string, while irradiation of other panel strings is not disturbed.

2.3.3 Multi-string parallel-connected topology

This topology as shown in the Figure 2.6 is similar to the series connected string topology with the difference of having separate inverter and dc-dc converter with MPPT. Here the converters are simpler and thus are cheaper and at the time more efficient. Every string of the PV panels is connected to dc-dc converter and converters connected to common inverter that is in turn connected to the grid.

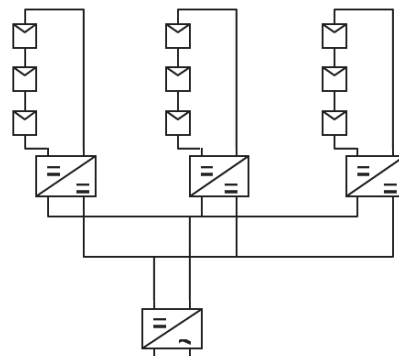


Figure 2.6 – Multi-string parallel connected topology.

The separate MPPT and inverter control reduces the cost of the PV system. The other advantage of this topology is that the inverter provides high power rate and the system efficiency is higher.

2.3.4 Cascaded dc-dc converters topology

MPPT function in this topology, as shown in Figure 2.7, is performed for each of the PV panels. Each PV module is equipped by its own converter and MPPT controller. Converters are then connected in parallel or series, however the series connection is more common. In the series connection if a panel is shadowed the converter is gaining maximum available

power, but other panels are not affected, the output current of each converter must have the same value.

This topology assures the optimal power generation process and maximal total yield if efficiency is not taken into account.

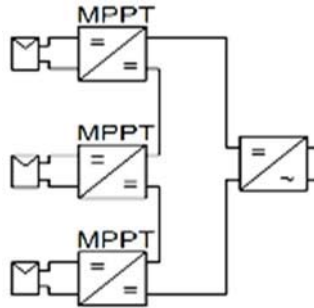


Figure 2.7 – Cascaded DC-DC converters topology.

The cascaded converter topology with central inverter provide better distribution level and performance during the partial shadowing and thus is recommended for the building integrated photovoltaic. Higher distribution level implies higher number of converters that allows better performance and increases the harvested power.

But the large number of converters decreases the overall efficiency because of the decrease of power rate of the converters (and small power rate converters are relatively less efficient than high power converter). But this topology is able to reach higher total energy than other systems when the shadowing is significant. On the other side centralized and multi string inverter topologies are common for the solar plants and roof-top systems, which are not affected by surrounding, since high efficiency can be reached at higher power rates.

To sum up, less distributed systems in case of low irradiation disturbance presents higher performance due to higher efficiency that could be achieved relatively easy. Systems that

are more distributed have better performance in cases of the frequent partial shading close to the location of the PV panel and thus can shade the panels partially.

2.4 Specifications and standards for grid connected PV systems

There are special standards and requirements related to connection of the PV to the grid. These standards aim to maintain the quality of the power produced by the photovoltaic distribution system. The grid-connected standards covered the topics about voltage, current injection, flicker, frequency, harmonics, maximum current, total harmonics distortion (THD) and power factor. Some definitions used in grid connected PV are:

1. Grounding: NEC 690 standard requires that the system and interface equipment should be grounded and monitored. It gives more safety and protection in case of ground faults inside the PV system.
2. Voltage disturbances: The utility company set the voltage of grid network. The output voltage of the PV has to be within the operating range defined by the standards. The voltage operating range is detailed in IEEE standard 929
3. DC component injection: According to IEC 61727, the DC current injected should be less than “0.5% of rated inverter output current into the utility AC interface.”
4. Total harmonic distortions: Modulation scheme of inverters should give an AC current with low level of harmonic distortion (IEEE Std. 929-2000):
 - a. Total harmonic current distortion shall be less than 5% of the fundamental frequency current at rated inverter output.
 - b. Even harmonics shall be < 25 % of the odd harmonics limits.

5. Voltage flicker: The voltage flicker should not exceed the maximum limits in IEC 61727.
6. Power factor: The IEEE standard 929 specifies that the power factor of the PV system should be > 0.85 (lagging or leading) when output is $>10\%$.
7. Frequency: According to IEEE standard 929, the PV systems should have a quasi-fixed frequency and should stay synchronized with the grid.

As for the Lebanese recommendations and guidelines for interconnection of PV plants, it should be noted that Lebanon does not have a published RE-related grid code yet. This is due to the fact that Lebanon suffers from a critical deficit between electricity generation and demand, therefore, the grid is susceptible to high deviations in voltage and frequency and regular outages due to load shedding.

In 2016 The United Nations Development Programme (UNDP) in collaboration with the Ministry of Energy and Water (MoEW), Electricity of Lebanon (EDL), the Lebanese Center for Energy Conservation (LCEC), and the “grid code” committee, published a report titled “Solar PV Grid Interconnection Code for Lebanon – Recommendations and Guidelines”. The objective of this report is to be used as guidelines in the absence of a clear Lebanese code and to be used as a draft when elaborating the Lebanese codes.

2.5 Maximum power point controller and algorithm

One of the major disadvantage of the PV cell is their low efficiencies when compared to conventional or other renewable power sources. Therefore it was important to create techniques that operate the solar system at its maximum power and under the changing

environmental conditions. Figure 2.8 shows the power and current plotted versus the voltage for a PV array

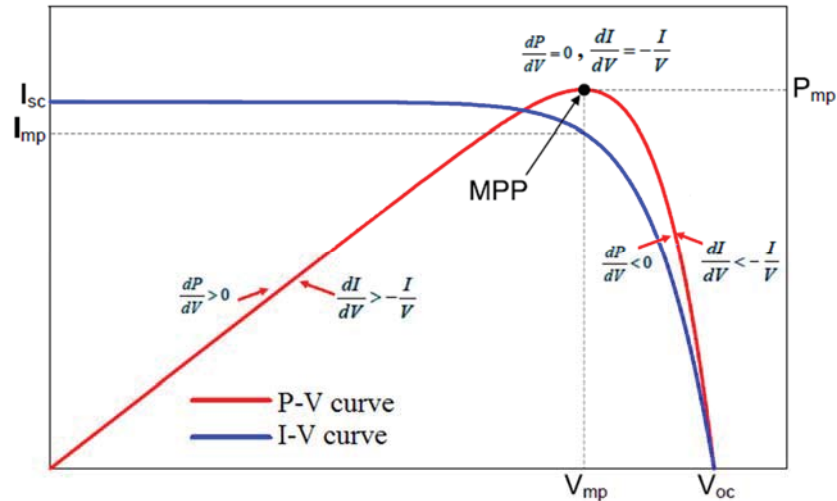


Figure 2.8 – Power vs. Voltage and Current vs. Voltage curves

The problem considered by Maximum Power Point Tracking (MPPT) techniques is to find periodically and automatically the voltage V_{mp} or current I_{mp} at which an array should operate to get the maximum power output P_{mp} under certain given temperature and irradiance. Some of the MPPT techniques are:

1. Hill Climbing/Perturb & Observe (P&O)
2. Incremental conductance
3. Fractional open circuit voltage
4. Fractional short circuit current
5. Fuzzy logic control
6. Neutral network
7. Ripple correlation control
8. Current sweep
9. DC-link capacitor droop control

10. Load Current or Load Voltage Maximization

11. dP/dV or dP/dI Feedback Control

In general each MPPT technique has different characteristics and therefore based on the applications a specific technique may be chosen. In this report the Hill Climbing/P&O will be described.

Due to its simplicity and its low computational demand Perturb and Observe technique is commonly used in the PV systems. This technique works according to the following sequence:

1. The voltage of the PV panel is perturbed by a very small amount (called ΔV) by changing the duty cycle of the DC-DC converter.
2. Based on the change in the voltage, the change in power (ΔP) is observed.
3. If there is an increase in power, the following perturbation should be kept the same to reach the MPP and if there is a decrease in power, the perturbation should be reversed. This can be seen in Figure 2.8 since incrementing the voltage increases the power when operating on the left of the MPP and decreases the power when on the right of the MPP.

A summary of this algorithm is shown in Table 2.1.

Table 2.1 – Summary of Hill Climbing and Perturb and Observe algorithm

Perturbation	Change in Power	Next Perturbation
Positive	Positive	Positive
Positive	Negative	Negative
Negative	Positive	Negative
Negative	Negative	Positive

This algorithm also works with instantaneous PV array voltage and current as long as sampling occurs once in each switching cycle. The process is repeated until reaching MPP, then the system oscillates around the MPP. Two sensors are usually required to measure the PV array voltage and current from which power is computed [9].

The flow chart of the P&O method is summarized and shown in Figure 2.9.

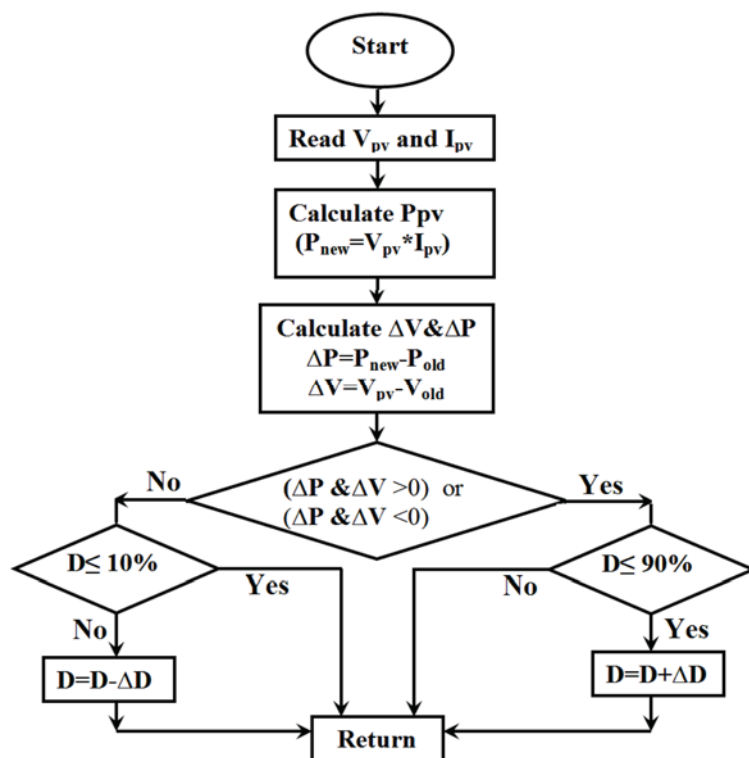


Figure 2.9 – Flow chart of P&O method

Simulink Model of the Perturb and Observe used is show in Figure 2.10:

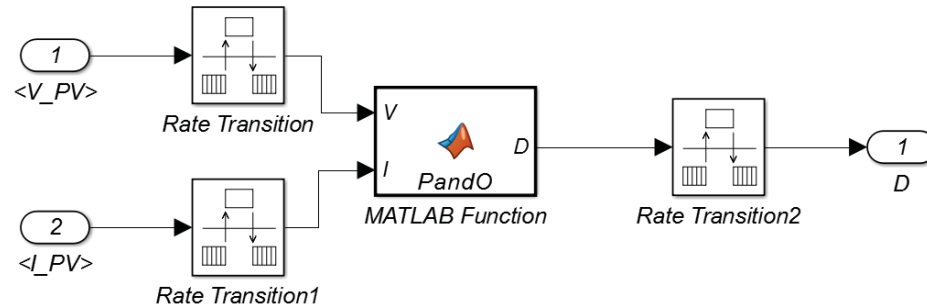


Figure 2.10 – Simulink Model of the MPPT controller with Perturb and Observe MATLAB script

Input used in this model consists in the output voltage of the PV array block (V_{PV}) and current of the PV array block (I_{PV}).

The used Matlab script related to the Perturb and Observe function in this model is as follows:

```
function D = PandO(V, I)
% MPPT controller based on the Perturb & Observe algorithm.
% Dp:
Dint = 0.6;
Dmax = 0.9;
Dmin = 0.1;
deltaD = 1/100;

persistent Vpre Ppre Dpre;

dataType = 'double';

if isempty(Dpre)
Dpre = Dint;
Vpre=0;
Ppre=0;
end

P= V*I;
dV= V - Vpre;
dP= P - Ppre;

% if dP ~= 0
if dP < 0
if dV < 0
D = Dpre - deltaD;
else
if dV > 0
D = Dpre + deltaD;
else
D=Dpre;
```

```

        end
        end
    else
        if dV < 0
            D = Dpre + deltaD;
        else
            if dV > 0
                D = Dpre - deltaD;
            else
                D=Dpre;
            end
        end
    end
end
% else D=Dpre;
% end

if D >= Dmax || D<= Dmin
    D=Dpre;
end
Dpre=D;
Vpre=V;
Ppre=P;

```

2.6 The power electronic interface

Power electronic interface refers to the power electronic devices and the related controllers that are used to enhance the output of the PV panel and tune it in order to allow a safe connection to the grid. The power electronic devices used in this grid connection PV application are composed of the boost converter, the MPPT controller, the modular multilevel converter and the related controller. The MPPT controller used in conjunction with boost converter extract the maximum power of the PV array at each instant. On the other hand, the modular multilevel converter used in this application is used as an inverter to transform the resulting DC output of the boost converter to AC three phase signal that is finally connected to the grid.

2.6.1 DC/DC Boost converter

The Boost Converter is a switching converter that operates by periodically opening and closing an electronic switch. It is called boost converter because the output voltage is higher than the input voltage. The equivalent circuit of a Boost converter is shown in Figures 2.10, 2.11 and 2.12. For steady state operation, the input and output voltages of the boost converter are related by the Eq. 2.3:

$$V_{output} = V_c = \frac{V_{in}}{1 - D} \quad 2.3$$

Where D is the duty cycle of the converter or in other words for a switching period T, the converter switch is closed for time DT and open for (1-D)T.

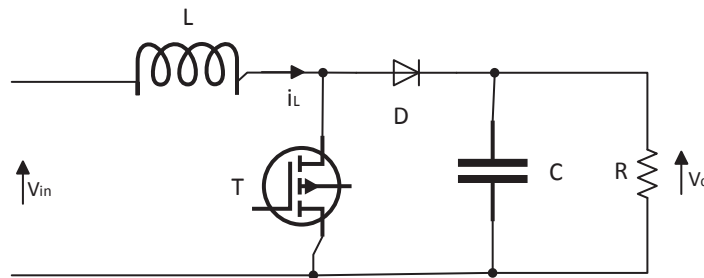


Figure 2.11 – Equivalent circuit of Boost converter.

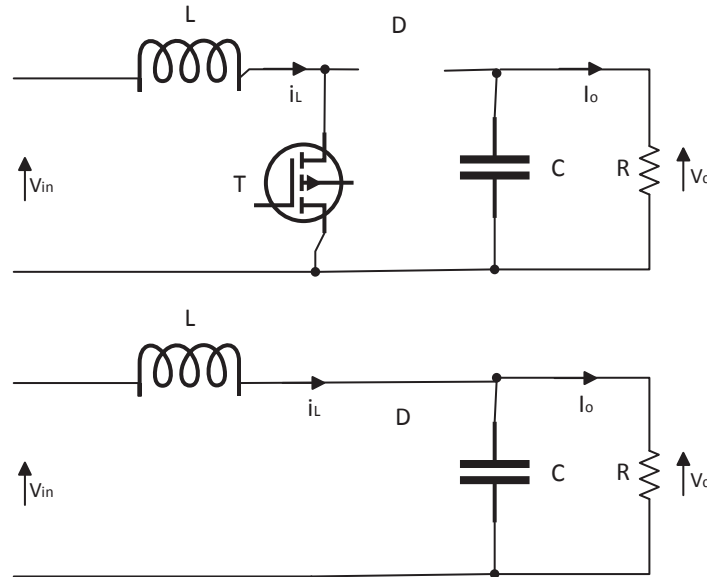


Figure 2.12 – Equivalent circuit of Boost converter when T is on and off.

The boost converter is used in this application to boost the voltage provided by the PV array described in the previous section. It is then connected to the output of the PV array.

Figure 2.13 shows the Simulink model of the used boost converter.

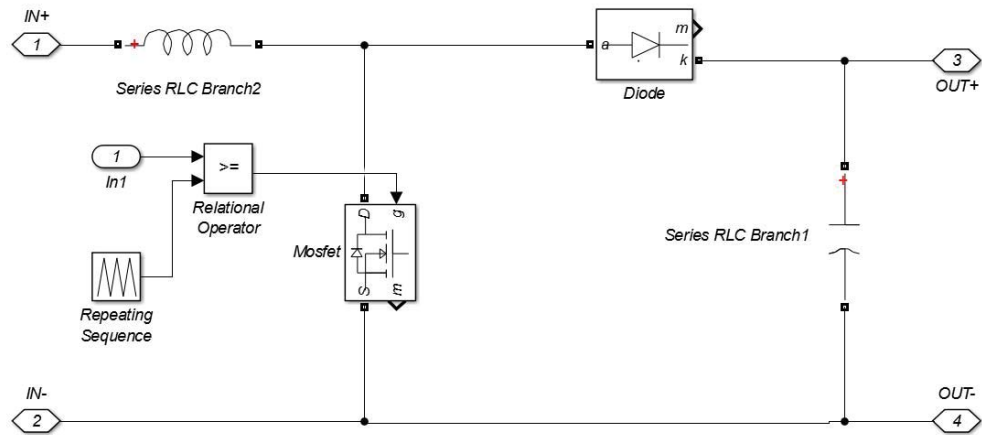


Figure 2.13 – Boost Converter including the control comparator.

The above shown circuit was implemented in the Matlab program. The two inputs labeled IN+ and IN- are connected to the output of the PV array block. The output OUT+ and OUT- are connected to the modular multilevel converter that will be elaborated in the next

section and chapter. In addition the output of perturb and observe maximum power point tracking technique is compared to the Mosfet switch operating signal of the boost converter. This action allow the slight modification of the duty cycle in order to continuously achieve maximum power with the available PV array.

2.6.2 Modular multilevel converter

The typical structure of a Modular Multilevel Converter is shown in Figure 2.14. This converter consists of two arms per phase leg, and each arm has N series identical sub modules (SMs). These submodules consist of two IGBTs along with antiparallel diodes and a local capacitor as shown in Figure 2.15.

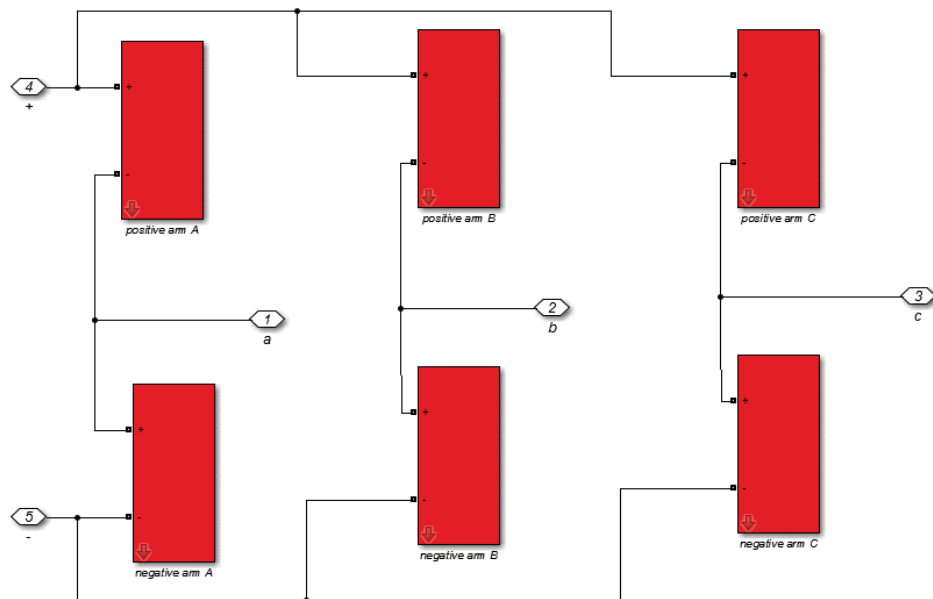


Figure 2.14 – Structure of Modular Multilevel Converter

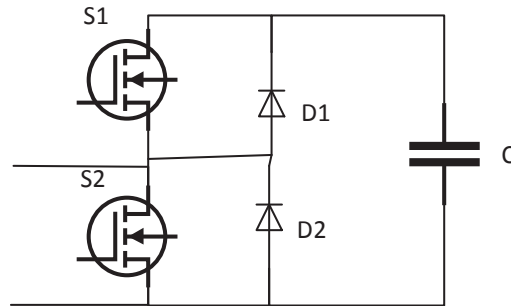


Figure 2.15 – Multilevel converter's sub module

A small inductor is installed in each arm to compensate for the voltage difference, between upper and lower arms, produced when a SM is switched in or out. SMs are controlled in a way that the capacitor is inserted in the circuit or bypassed. The operation of SM is complementary, which means when the first switch (upper one) is on, the second (lower one) is off, and we can say that SM is in on-state. When the second (lower one) is ON and the first switch (upper one) is OFF, then we can say that SM is in off-state. Figure 2.16 shows the conduction paths of a submodule when the current polarity is positive or negative. According to the current direction, the capacitor in the SM can be charged or discharged.

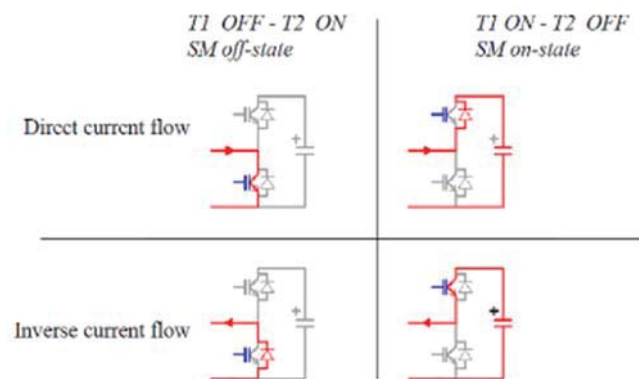


Figure 2.16 – Conduction paths of sub module.

2.7 The system topology

The complete model representing all of the above mentioned PV Arrays, Boost Converter (Including MPPT) and Modular Multilevel Converter is summarized by the general Simulink model shown in Figure 2.17.

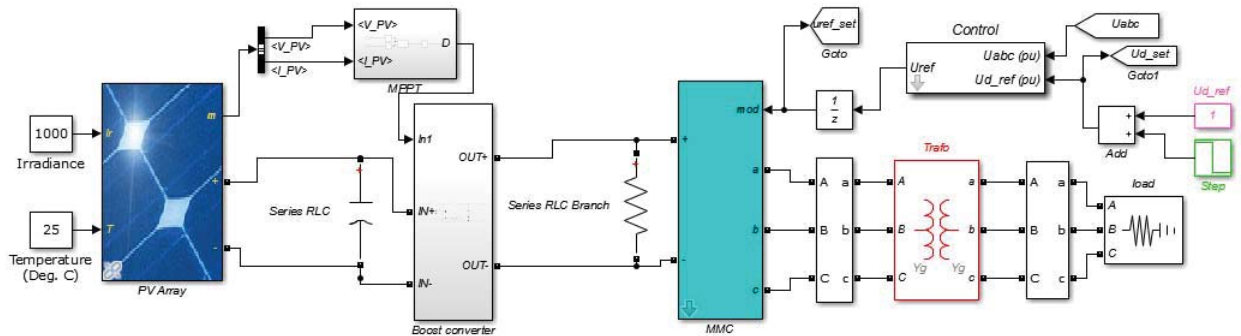


Figure 2.17 – Complete PV system connected to grid.

The next work will be focused on the part connected to the output of the Boost converter, the Modular Multilevel converter including its control will be the main subject of the following chapter.

2.8 Problem Statement

When the MMC operates as an inverter, there are three control objectives that need to be met for appropriate operation. First, the output current or voltage must be controlled at the appropriate magnitude, frequency, and phase. Second, the circulating current flowing through the MMC legs must be controlled at a certain value. Third, the capacitor voltages of the submodules (SMs) must maintain their reference voltage to avoid deterioration of the THD at the output terminals of the MMC [10].

Chapter 3: Modular Multilevel Converter

The structure of a Modular Multilevel Converter is shown in figure 3.1. This three phase converter consists of six arms: two arms for each phase leg. In addition each arm has a number N of series connected identical sub modules (SMs) and an inductor (L) and a resistor (R) that represents the arm's inductance and equivalent resistance respectively. These sub modules consist of two complementary Insulated Gate Bipolar Transistors (i.e., $S_{jm,n}$ and $S'_{jm,n}$) along with antiparallel diodes and a local capacitor (C) as shown in Figure 3.1.

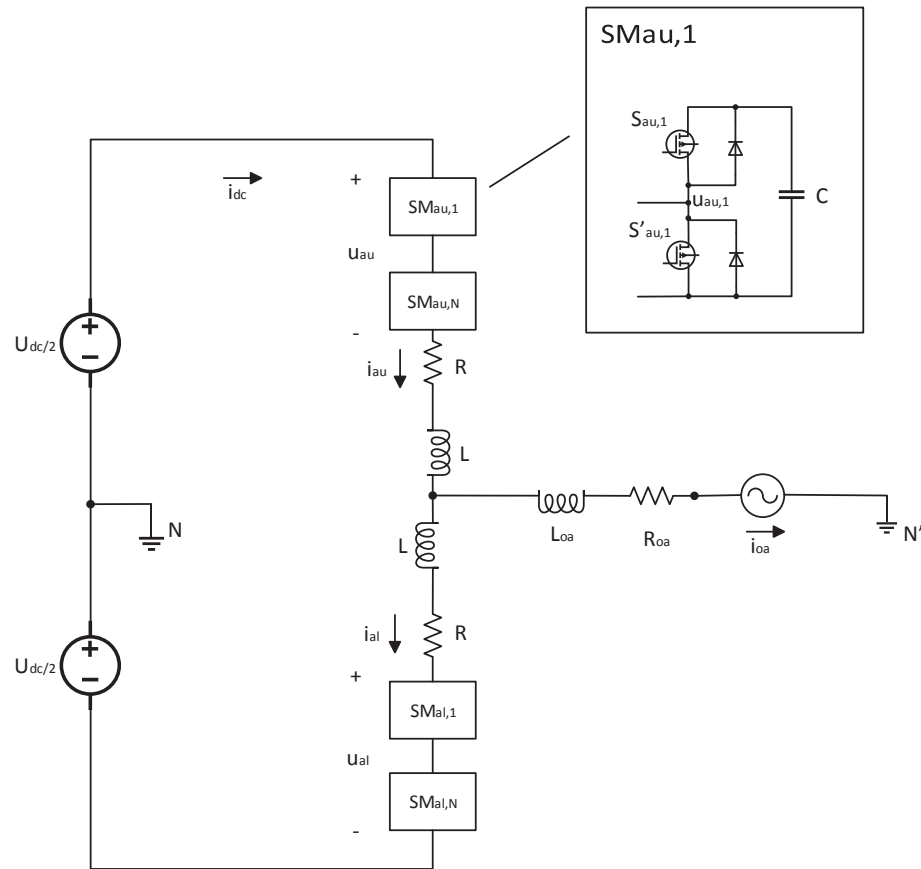


Figure 3.1 – Structure of a three-phase MMC-based inverter and its SM.

In the following equations, to reduce the number of written equation (that are identical but differs in subscripts) by deriving general equation the following subscripts were used:

- j is used to represent the three phases and could then be either a, b or c
- m is used to represent which arm in a particular leg and could be either u (upper arm) or l (lower arm)
- n is used to represent the number of sub-modules and could be 1, 2, 3, ..., N

The symbols used are as follows:

- u_{jm} is the arm voltage
- i_{jm} is the arm current
- u_j is the AC side voltage
- i_{oj} is the output current
- i_{cj} is the circulating current
- L_{oj} is the load inductance
- R_{oj} is the load resistance
- U_{dc} is the DC source voltage
- $u_{jm,n}$ is the capacitor voltage
- C is the sub module capacitance

3.1 Mathematical Model of the MMC

The instantaneous current (i) through the capacitor is related to the instantaneous rate of voltage change $\frac{dv}{dt}$ by Eq. 3.1:

$$i = C \frac{dv}{dt} \quad 3.1$$

Therefore in a sub module the Eq. 3.2 can be issued:

$$\frac{du_{jm,n}}{dt} = \frac{S_{jm,n} i_{jm}}{C} \quad 3.2$$

Where $S_{jm,n}$, that may have either 0 or 1 value, is the switch function of the n^{th} sub module in the arm m of phase j .

From figure 3.1, the relation between the arm voltage and the capacitor voltage in phase j and the switch function could be related by Eq. 3.3:

$$u_{jm} = \sum_{n=1}^N S_{jm,n} u_{jm,n} \quad 3.3$$

Considering a fictitious midpoint in the DC side of figure 3.1 and using Kirchhoff's circuit laws, the following mathematical equations Eq. 3.4 and Eq. 3.5 related to the dynamic behavior of the MMC in phase- j is obtained:

$$u_{ju} + R_{iju} + L \frac{di_{ju}}{dt} + R_{oj}i_{oj} + L_{oj} \frac{di_{oj}}{dt} + u_j = \frac{U_{dc}}{2} \quad 3.4$$

$$u_{jl} + R_{ijl} + L \frac{di_{jl}}{dt} - R_{oj}i_{oj} - L_{oj} \frac{di_{oj}}{dt} - u_j = \frac{U_{dc}}{2} \quad 3.5$$

The upper arm current can be expressed by Eq. 3.6:

$$i_{ju} = \frac{i_{oj}}{2} + i_{cj} \quad 3.6$$

The lower arm current can be expressed by Eq. 3.7:

$$i_{jl} = -\frac{i_{oj}}{2} + i_{cj} \quad 3.7$$

Where i_{cj} and i_{oj} can be calculated by Eq. 3.8 and Eq. 3.9:

$$i_{cj} = \frac{i_{ju} + i_{jl}}{2} \quad 3.8$$

$$i_{oj} = i_{ju} - i_{jl} \quad 3.9$$

Substitute Eq. 3.4 and Eq. 3.9 into Eq. 3.5, and the dynamics of phase j AC side currents can be obtained as:

$$\begin{aligned} \frac{di_{oj}}{dt} &= -\frac{R + 2R_{oj}}{L + 2L_{oj}}i_{oj} - \frac{1}{L + 2L_{oj}}u_{ju} + \frac{1}{L + 2L_{oj}}u_{jl} - \frac{2}{L + 2L_{oj}}u_j \\ &= \frac{u_{jl} - u_{ju} - (R + 2R_{oj})i_{oj} - 2u_j}{L + 2L_{oj}} \end{aligned} \quad 3.10$$

Similarly, the dynamic behavior of the circulating current in phase j can be obtained by substituting Eq. 3.4 and Eq. 3.8 into Eq. 3.5:

$$\frac{di_{cj}}{dt} = -\frac{R}{L}i_{cj} - \frac{1}{2L}u_{ju} - \frac{1}{2L}u_{jl} + \frac{1}{2L}U_{dc} = \frac{U_{dc} - u_{jl} - 2Ri_{cj} - u_{ju}}{2L} \quad 3.11$$

3.2 State Space Matrix presentation

Based on Eq. 3.2, Eq. 3.3, Eq. 3.10, and Eq. 3.11, the state-space equation of the MMC in phase-j can be described as:

$$\dot{\mathbf{x}}(t) = \mathbf{A}(t)\mathbf{x}(t) + \mathbf{D}\mathbf{d}(t) \quad 3.12$$

Where

$\mathbf{x} = [i_{oj}, i_{cj}, u_{ju, 1}, \dots, u_{ju, N}, u_{jl, 1}, \dots, u_{jl, N}]^T$ is the state vector

$\mathbf{d} = [u_j, U_{dc}]^T$ is a perturbation vector

The required value (u_j^*) of u_j is given by:

$$u_j^* = \sqrt{2}U \sin(2\pi ft + \varphi_j) \quad 3.13$$

Where U is the voltage RMS value on the AC side, f is the AC system frequency, and φ_j is the initial phase angle in phase j .

\mathbf{A} is a time-varying structure state matrix given by:

$$\mathbf{A}(t) = \begin{bmatrix} \mathbf{A}_1 & \mathbf{A}_2(t) \\ \mathbf{A}_3(t) & \mathbf{0} \end{bmatrix} \quad 3.14$$

Where \mathbf{A}_1 is a constant $2 \times 2N$ matrix in Eq. 3.15, and \mathbf{A}_2 and \mathbf{A}_3 are time-varying $2 \times 2N$ and $2N \times 2$ matrices in Eq. 3.16 and Eq. 3.20, respectively.

$$\mathbf{A}_1 = \begin{bmatrix} -\frac{R + 2R_{oj}}{L + 2L_{oj}} & 0 \\ 0 & -\frac{R}{L} \end{bmatrix} \quad 3.15$$

$$\mathbf{A}_2(t) = \mathbf{A}'_2 \text{diag}(u(t)) \quad 3.16$$

Where $\mathbf{A}'_2 = [\mathbf{A}'_{21} \quad \mathbf{A}'_{22}]$ is a $2 \times 2N$ matrix, \mathbf{A}'_{21} is a $2 \times N$ matrix given by Eq. 3.17, \mathbf{A}'_{22} is a $2 \times N$ matrix given by Eq. 3.18, and $\mathbf{u}(t)$ is the input control vector, presented in Eq. 3.19.

$$\mathbf{A}'_{21} = \begin{bmatrix} \frac{-1}{L + 2L_{oj}} & \frac{-1}{L + 2L_{oj}} & \cdots & \frac{-1}{L + 2L_{oj}} \\ \frac{-1}{2L} & \frac{-1}{2L} & \cdots & \frac{-1}{2L} \end{bmatrix} \quad 3.17$$

$$\mathbf{A}'_{22} = \begin{bmatrix} \frac{1}{L + 2L_{oj}} & \frac{1}{L + 2L_{oj}} & \cdots & \frac{1}{L + 2L_{oj}} \\ \frac{-1}{2L} & \frac{-1}{2L} & \cdots & \frac{-1}{2L} \end{bmatrix} \quad 3.18$$

$$\mathbf{u}(t) = [S_{ju,1}, S_{ju,2}, \dots, S_{ju,N}, S_{jl,1}, S_{jl,2}, \dots, S_{jl,N}] \quad 3.19$$

$$\mathbf{A}_3(t) = \text{diag}(u(t))\mathbf{A}'_3 \quad 3.20$$

Where \mathbf{A}'_3 is a $2N \times 2$ matrix given by Eq. 3.21:

$$\mathbf{A}'_3 = \begin{bmatrix} 1 & \dots & 1 & -1 & \dots & -1 \\ \frac{1}{2C_{ju,1}} & \dots & \frac{1}{2C_{ju,N}} & \frac{1}{2C_{jl,1}} & \dots & \frac{1}{2C_{jl,N}} \\ 1 & \dots & 1 & 1 & \dots & 1 \\ \frac{1}{C_{ju,1}} & \dots & \frac{1}{C_{ju,N}} & \frac{1}{C_{jl,1}} & \dots & \frac{1}{C_{jl,N}} \end{bmatrix}^T \quad 3.21$$

And \mathbf{D} is the perturbation coefficient $(2N+2) \times 2$ matrix, presented in Eq. 3.22.

$$\mathbf{D} = \begin{bmatrix} \mathbf{D}_1 \\ 0 \end{bmatrix} \quad 3.22$$

Where \mathbf{D}_1 is given by Eq. 3.23:

$$\mathbf{D}_1 = \begin{bmatrix} \frac{-2}{L + 2L_{oj}} & 0 \\ 0 & \frac{1}{2L} \end{bmatrix} \quad 3.23$$

The output voltage of the MMC, such as phase- j , is defined in Eq. 3.24

$$v_{jN} = R_{oj}i_{oj} + L_{oj} \frac{di_{oj}}{dt} + u_j \quad 3.24$$

In $\dot{\mathbf{x}}(t) = \mathbf{A}(t)\mathbf{x}(t) + \mathbf{D}\mathbf{d}(t)$, the control of the system may sometime be to adjust the structure of matrix \mathbf{A} so that $\mathbf{u}_j \rightarrow \mathbf{u}_j^*$ and $\mathbf{U}_{dc} \rightarrow \mathbf{U}_{dc}^*$ [11]. It is the case of an inverter operating alone.

From Eq.3.10, we can get the formula of u_j as follows

$$u_j = -\frac{1}{2}(L + 2L_{oj})\frac{di_{oj}}{dt} - \frac{R}{2}i_{oj} - \frac{1}{2}u_{ju} + \frac{1}{2}u_{jl} \quad 3.25$$

3.3 Reverse Model Predictive Control (RMPC)

The three control targets for conventional MPC used for MMCs are as follows:

1. Balancing of SM capacitor voltages.
2. Tracking of output current, including magnitude, frequency, and phase angle.
3. Suppressing the circulating current

The reverse MPC (R-MPC) strategy, reduces the computational complexity of MPC by decoupling the SM capacitor voltage control and carrying it out in an independent control loop [12]. Figure 3.2 shows the Control scheme of the reverse model predictive control.

Assuming n_u and n_l are the number of on-state SM in the upper and lower arms respectively at next step, the SM capacitor voltages must be sorted as follows

1. Ascending order if the arm current is positive and n_i ($i = u, l$) SMs with the lowest voltages are chosen to be inserted to the arm, and the other SMs are bypassed.
2. Descending order if the arm current is negative and n_i ($i = u, l$) SMs with the highest voltages are chosen to be inserted to the arm, and the other SMs are bypassed.

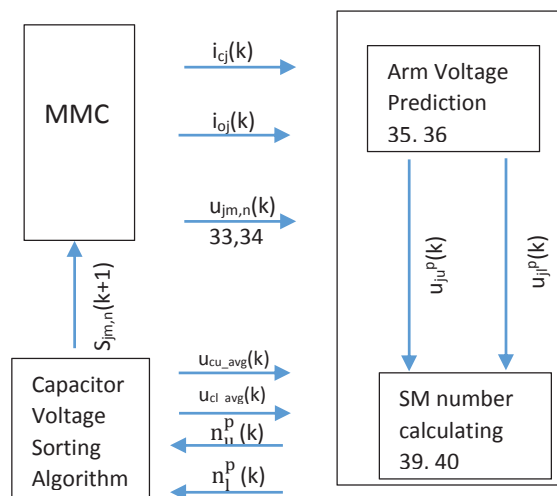


Figure 3.2 – Control scheme of the reverse MPC.

The balancing of SM capacitor voltage is one of key issues in MMC. MPC uses in general sorting method (e.g., bubble sorting) in which all of the SM capacitor voltages have to be sorted in ascending or descending order to determine the inserted SMs with the highest or lowest voltages to finally balance the SM capacitor voltages. But when the number of SMs is large enough the sorting algorithm becomes a hard task. Thus some improved sorting methods are elaborated to minimize the computational complexity. Beneath, the grouping sorting method will be reviewed.

In general, as long as several SMs with the highest or lowest voltages are selected, the voltage balancing is achieved within a certain allowable range of ripples, while the rest SMs need not be sorted and thus reduce the computational problem.

3.4 Grouping-Sorting Optimized Control

The GSOC is proposed to decrease the prediction number of each phase down to $2X+M+3(N=M\times X)$ for the $N+1$ levels MMC [13].

The sub-modules of each arm are divided into M groups and each group contains X sub-modules.

GSO controller takes several tasks, such as sub-module capacitor voltage balancing, the energy balancing between the upper and lower arms and the suppressing of the circulating current.

GSOC is based on two level of operation as shown in Figure 3.3

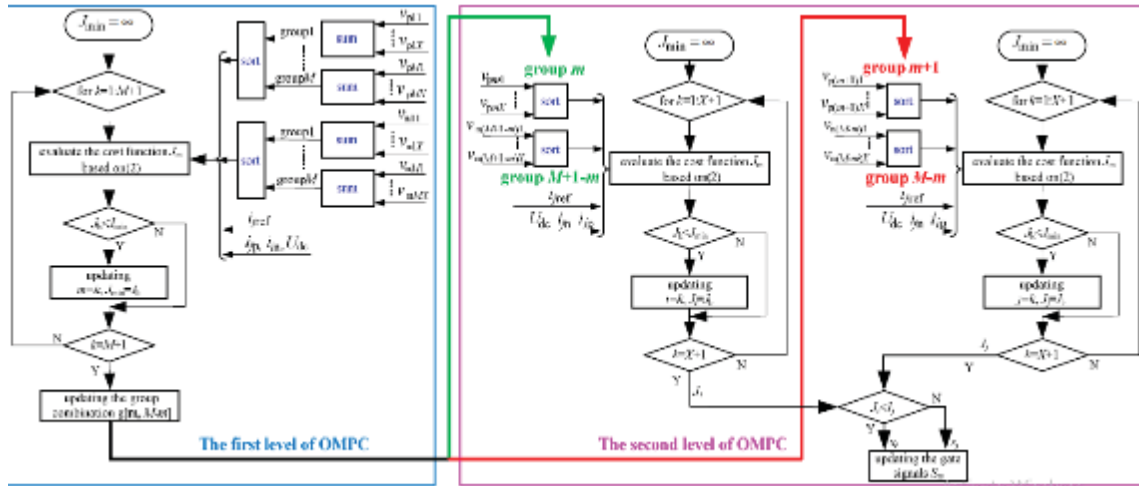


Figure 3.3 – GSOC 1st and 2nd levels

First level of GSOC:

1. The summation of all the sub-module capacitor voltages within each group is obtained.
2. The summation results are sorted in ascending/descending order depending on the charging/discharging current.
3. The group combination $gc[A, B]$ (Where $A=1,2,\dots,M$ and $B=1,2,\dots,M$) corresponding to the minimum value of the cost function (such Eq. 3.26) is determined, by evaluation of the cost function $M+1$ times

By the first level of evaluating cost function, the work mode of each group can be obtained, i.e. the first m groups of upper arm should be conducted and the first $M-m$ groups of lower arm should be conducted.

Second level of GSOC:

1. There are $X+1$ sub-module combinations, denoted by $[A(i), B+1(X-i)]$ (Where $i=0,1,\dots,X$) with No. A group of the upper arm and No. $B+1$ group of the lower arm.
2. Evaluation of Equation (2) $X+1$ times, the optimal sub-module combination corresponding to the minimum cost function value J_i is determined.
3. There are also $X+1$ sub-module combinations, denoted by $[A+1(i), B(X-i)]$ (Where $i=0,1,\dots,X$) with No. $A+1$ group of the upper arm and No. B group of the lower arm.
4. Evaluation of Equation (2) $X+1$ times, the optimal sub-module combination corresponding to the minimum cost function value J_j is determined.
5. The smaller one between J_i and J_j , determines the inserted in sub-modules of the optional groups in the next control period

By carrying out two levels of OMPC, the working mode of each sub-module of next sampling period can be obtained and all the prediction candidates are decreased to $2X+M+3$.

After two levels of OMPC, the switching rates of all the groups and sub-modules are identified for the next sampling period.

The cost function [10] is defined by Eq. 3.26:

$$g = \lambda_0 |i_{oj}^r(k+1) - i_{oj}(k+1)| + \lambda_c |i_{cj}(k+1)| + \lambda_w (|W_{ju}(k+1) - W_r| + |W_{jl}(k+1) - W_r|) \quad 3.26$$

Where λ_o , λ_c , and λ_w are the weighing factors of the cost function and are calculated based on [14], resulting in $\lambda_o = 1$, $\lambda_c = 0.05$, and $\lambda_w = 1 \times 10^{-7}$

And W_r is given by Eq.3.27:

$$W_r = \frac{C}{2N} U_{dc}^2 \quad 3.27$$

And

$$\begin{cases} W_{ju}(k+1) = \frac{C}{2} \sum_{i=1}^N v'_{jui}(k+1)^2 \\ W_{jl}(k+1) = \frac{C}{2} \sum_{i=1}^N v'_{jli}(k+1)^2 \end{cases} \quad 3.28$$

$$\begin{cases} v'_{jui}(k+1) = v_{ju}(M_{jui}) = \begin{cases} v'_{jui}(k) + \frac{i_{ju}}{C} T_s & (\text{inserted in}) \\ v'_{jui}(k) & (\text{bypassed}) \end{cases} \\ v'_{jli}(k+1) = v_{jl}(M_{jli}) = \begin{cases} v'_{jli}(k) + \frac{i_{jl}}{C} T_s & (\text{inserted in}) \\ v'_{jli}(k) & (\text{bypassed}) \end{cases} \end{cases}$$

M_{jui} and M_{jli} are the sorting index of the submodules.

In the following, the RMPC is derived.

From Eq. 3.4 and Eq. 3.5, the arm voltages can be written as follows in Eq. 3.29 and Eq.3.30:

$$u_{ju} = \frac{U_{dc}}{2} - L \frac{di_{cj}}{dt} - \left(\frac{L}{2} + L_{oj} \right) \frac{di_{oj}}{dt} - \left(\frac{R}{2} + R_{oj} \right) i_{oj} - u_j \quad 3.29$$

$$u_{jl} = \frac{U_{dc}}{2} - L \frac{di_{cj}}{dt} + \left(\frac{L}{2} + L_{oj}\right) \frac{di_{oj}}{dt} + \left(\frac{R}{2} + R_{oj}\right) i_{oj} + u_j \quad 3.30$$

By using backward Euler approximation shown in Eq. 3.31,

$$\frac{dx}{dt} = \frac{x(k) - x(k-1)}{T_s} \quad 3.31$$

The AC voltage of the MMC can be expressed by Eq. 3.32:

$$u_j = -\frac{1}{2}(L + 2L_{oj}) \frac{i_{oj}(k) - i_{oj}(k-1)}{T_s} - \frac{R}{2} i_{oj}(k) - \frac{1}{2} u_{ju}(k) + \frac{1}{2} u_{jl}(k) \quad 3.32$$

The discrete-time dynamic models of the arm voltages of MMC can be written as per Eq.

3.33 and Eq. 3.34:

$$u_{ju}(k) = \frac{U_{dc}}{2} - \frac{L}{T_s} [i_{cj}(k) - i_{cj}(k-1)] - \left(\frac{\frac{L}{2} + L_{oj}}{T_s} + \frac{R}{2} + R_{oj}\right) i_{oj}(k) + \left(\frac{\frac{L}{2} + L_{oj}}{T_s}\right) i_{oj}(k-1) - u_j(k) \quad 3.33$$

$$u_{jl}(k) = \frac{U_{dc}}{2} - \frac{L}{T_s} [i_{cj}(k) - i_{cj}(k-1)] + \left(\frac{\frac{L}{2} + L_{oj}}{T_s} + \frac{R}{2} + R_{oj}\right) i_{oj}(k) - \left(\frac{\frac{L}{2} + L_{oj}}{T_s}\right) i_{oj}(k-1) + u_j(k) \quad 3.34$$

Assuming the next-step reference values of control objectives can be tracked without error,

thus, the next-step predicted arm voltages $u_{ju}(k+1)$ and $u_{jl}(k+1)$ can be obtained by

shifting forward the Eq.3.33 and Eq.3.34 to get Eq.3.35 and Eq.3.36:

$$\begin{aligned}
u_{ju}^p(k+1) &= \frac{U_{dc}}{2} - \frac{L}{T_s} [i_{cj}^*(k+1) - i_{cj}(k)] - \left(\frac{\frac{L}{2} + L_{oj}}{T_s} + \frac{R}{2} + R_{oj} \right) i_{oj}^*(k+1) + \left(\frac{\frac{L}{2} + L_{oj}}{T_s} \right) i_{oj}(k) \\
&\quad - u_j^*(k+1)
\end{aligned} \tag{3.35}$$

$$\begin{aligned}
u_{jl}^p(k+1) &= \frac{U_{dc}}{2} - \frac{L}{T_s} [i_{cj}^*(k+1) - i_{cj}(k)] + \left(\frac{\frac{L}{2} + L_{oj}}{T_s} + \frac{R}{2} + R_{oj} \right) i_{oj}^*(k+1) - \left(\frac{\frac{L}{2} + L_{oj}}{T_s} \right) i_{oj}(k) \\
&\quad + u_j^*(k+1)
\end{aligned} \tag{3.36}$$

Where $i_{cj}^*(k+1)$ is the next-step reference value of circulating current, $i_{oj}^*(k+1)$ is the next-step reference value of output current, and $u_j^*(k+1)$ is the next-step reference values of grid voltage.

For the circulating current, the main frequency component is DC, its next-step reference value $i_{cj}^*(k+1)$ can be replaced by the previous reference value $i_{cj}^*(k)$. But for output current and grid voltage, in order to improve the control accuracy, the next-step reference value $i_{oj}^*(k+1)$ and $u_j^*(k+1)$ can be predicted by Eq. 3.37 and Eq. 3.38 based on the formula of the Lagrange extrapolation:

$$i_{oj}^*(k+1) = 3i_{oj}^*(k) - 3i_{oj}^*(k-1) + i_{oj}^*(k-2) \tag{3.37}$$

$$u_j^*(k+1) = 3u_j^*(k) - 3u_j^*(k-1) + u_j^*(k-2) \tag{3.38}$$

At last, the number of next-step on-state SMs can be calculated by Eq. 3.39 and Eq. 3.40:

$$n_u^p = \text{round} \left(\frac{u_u^p(k+1)}{u_{cu_avg}(k)} \right) \tag{3.39}$$

$$n_l^p = \text{round} \left(\frac{u_l^p(k+1)}{u_{cl_avg}(k)} \right) \tag{3.40}$$

Where $u_{cu_avg}(k)$ and $u_{cl_avg}(k)$ are the average arm voltages of the MMC (upper and lower arm). Figure 3.4 shows the complete scheme of the MMC including the control.

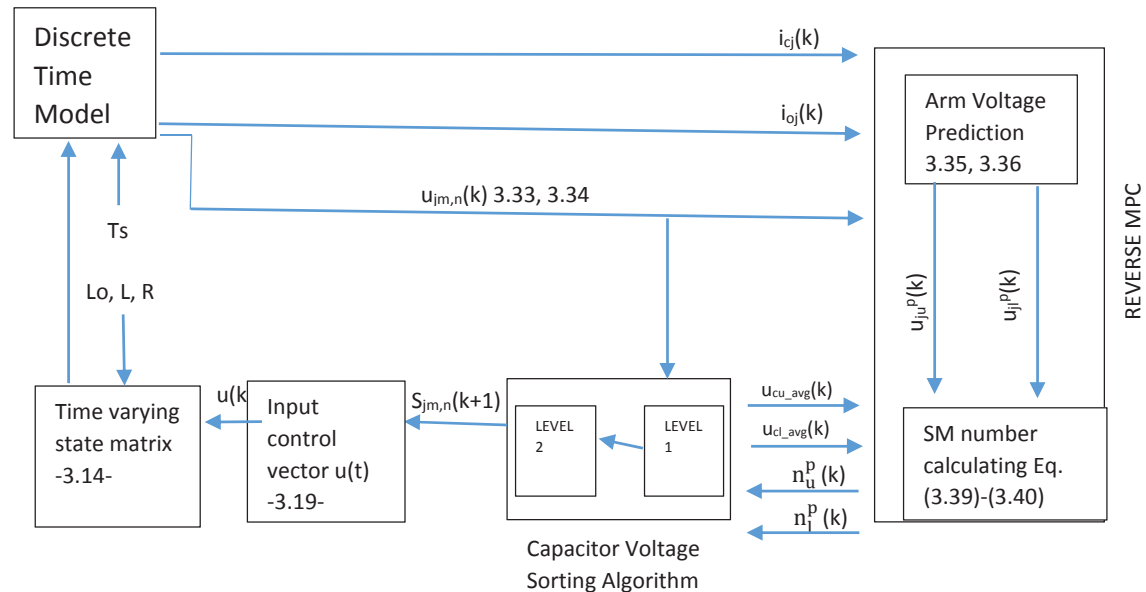


Figure 3.4 – Complete model of the MMC including the RMPC

3.5 Simulation and Results

The model used for the simulation is shown in figure 3.5. This model consist of a hybrid combination of Simulink blocks and MATLAB scripts. Figure 3.5 provide the general summary of the Simulink model. The main parts of this model consists of:

1. MMC Arms
2. DC source
3. Grid/line.
4. Reverse model predictive control block

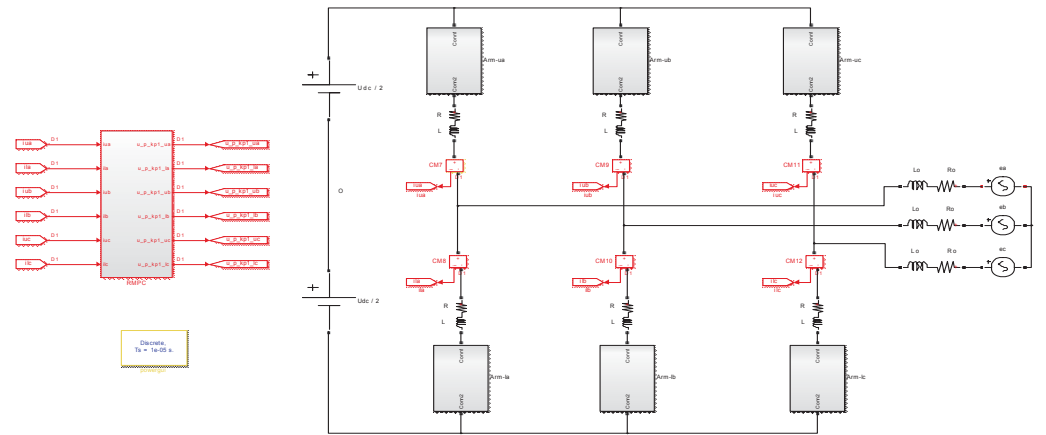


Figure 3.5 – Circuit of the MMC system tied to ideal grid through grid impedances, and the R-MPC control block.

Figure 3.6 on the other side shows the detailed sections of one of the arm namely phase a upper arm. Each arm in the simulation is composed of 20 submodules that are controlled directly through the block (s-function) that determines for each submodule the gate signal.

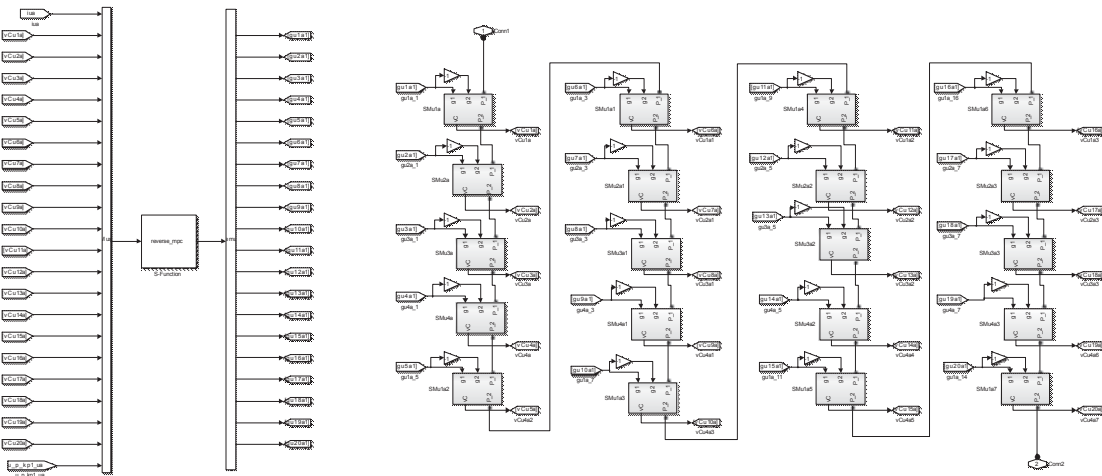


Figure 3.6 – Illustration of the phase-a upper arm subsystem showing the twenty submodules and the block (s-function) that determines the gate signals.

The detailed block of each submodule used in the simulation is shown in figure 3.7. As shown these submodules are half bridge based.

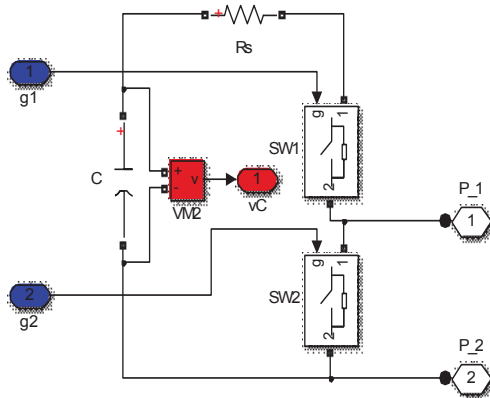


Figure 3.7 – Half-bridge submodule used in the MMC.

The reverse model predictive control shown on the right side of figure 3.5 is elaborated as shown in figure 3.8 and figure 3.9.

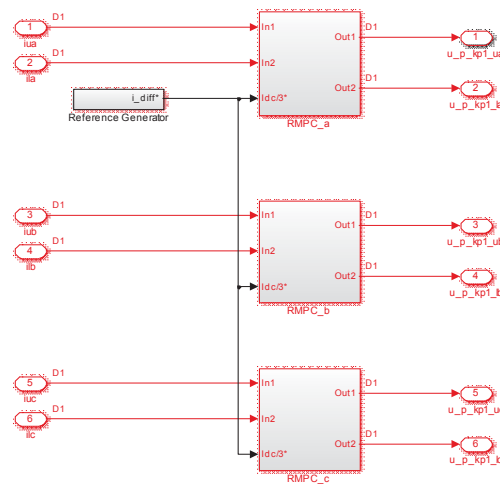


Figure 3.8 – The inside of the R-MPC control block showing the subsystems to derive the RMPc control law for each arm.

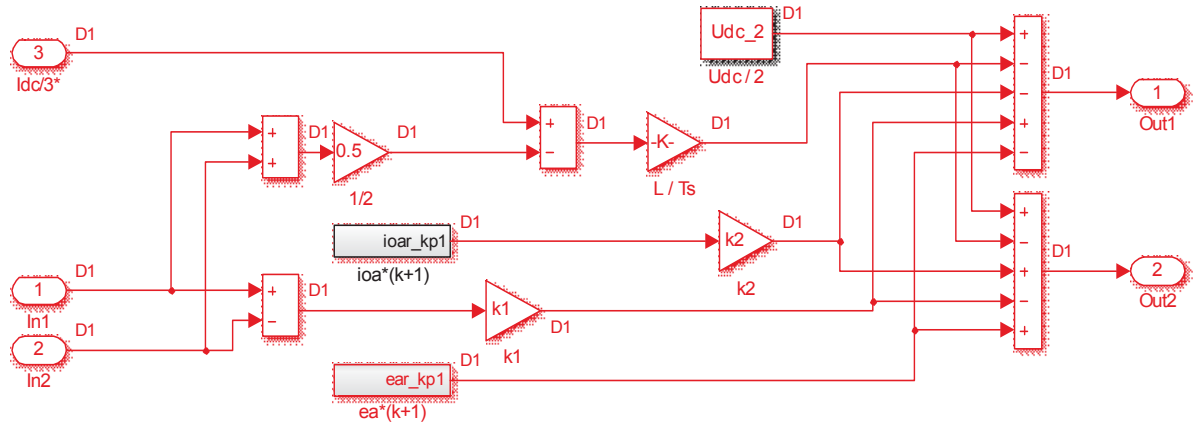


Figure 3.9 – Implementation of the RMPC control law for the two arms of phase-a.

The function inside the Matlab s-function that performs the capacitor voltage sorting and generates the gate signals of arm devices is given by the following Matlab script:

```
function sys = mdlOutputs(~,~,u)
y = zeros(1,20);
v_c_avg = mean(u(2:21));
u_p_kp1 = u(22);
n_p_kp1 = round(u_p_kp1/v_c_avg);

if n_p_kp1 > 20,
    n_p_kp1 = 20;
end
if n_p_kp1 < 1,
    n_p_kp1 = 0;
end

if u(1)> 0,
    [~,I] = sort(u(2:21));
else
    [~,I] = sort(u(2:21),'descend');
end

switch n_p_kp1
    case 0
        y = -ones(1,20);
    case 20
        y = ones(1,20);
    otherwise
```

```

    for i = 1:n_p_kp1
        y(I(i)) = 1;
        for j = n_p_kp1+1:20
            y(I(j)) = -1;
        end
    end
end
sys = yi;

```

The simulation adopted parameters are illustrated in table 3.1.

Table 3.1– System parameters adopted in the simulation

Parameter	Value
Grid rated voltages (V_{LL-rms})	6.1 kV
DC bus voltage (U_{dc})	30 kV
Number of submodules per arm (N)	20
Submodule capacitance (C_{SM})	4000 μ F
Arm inductance (L)	2.5 mH
Arm resistance (R)	0.01 Ω
Output line inductance (L_o)	2 mH
Output line resistance (R_o)	0.01 Ω
Output frequency (f)	50 Hz
Sampling period (T_s)	10 μ s

The simulations are conducted using SimPowerSystems (SPS) blockset in Matlab/Simulink environment. Before $t = 0.1$ s, the MMC system reached steady state, after which the amplitude of the reference output currents experienced two step changes,

stepped up from 40 A to 80 A at $t = 0.1$ s and stepped down from 80 A to 40 A at $t = 0.2$ s as shown in figures 3.10, 3.11 and 3.12.

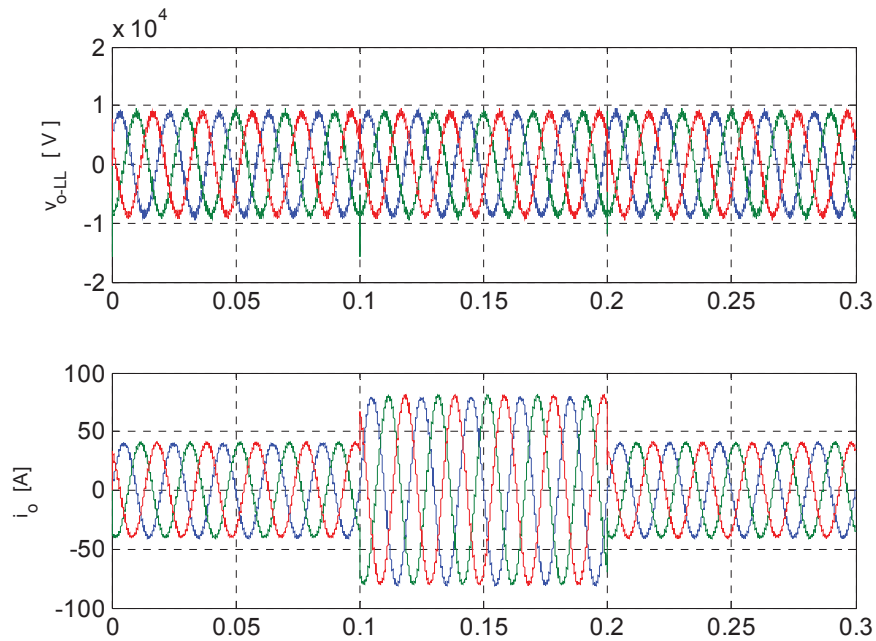


Figure 3.10 – Output-side line-to-line voltages and line currents.

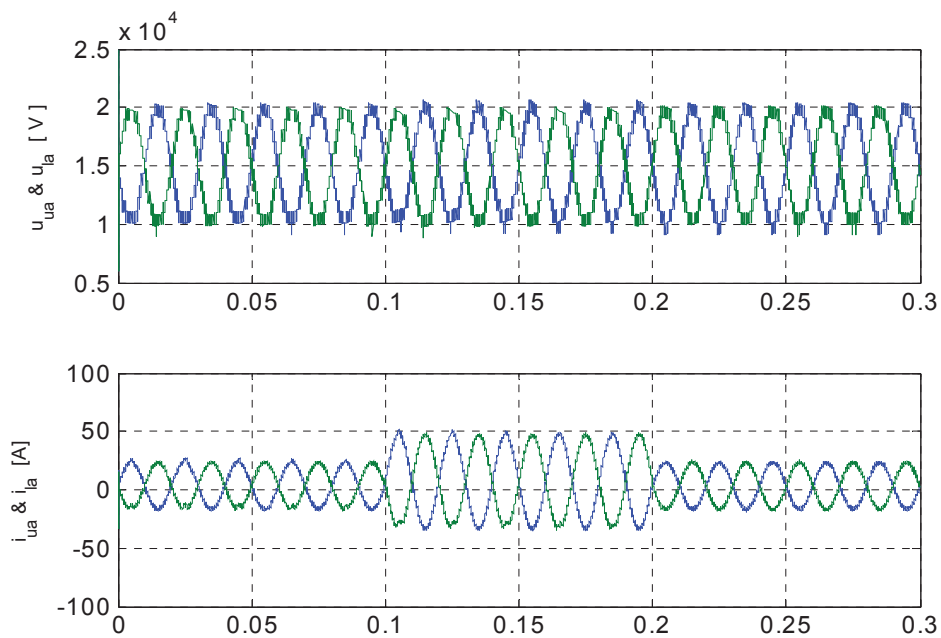


Figure 3.11 – Arm voltages and inner currents of phase-a arms.

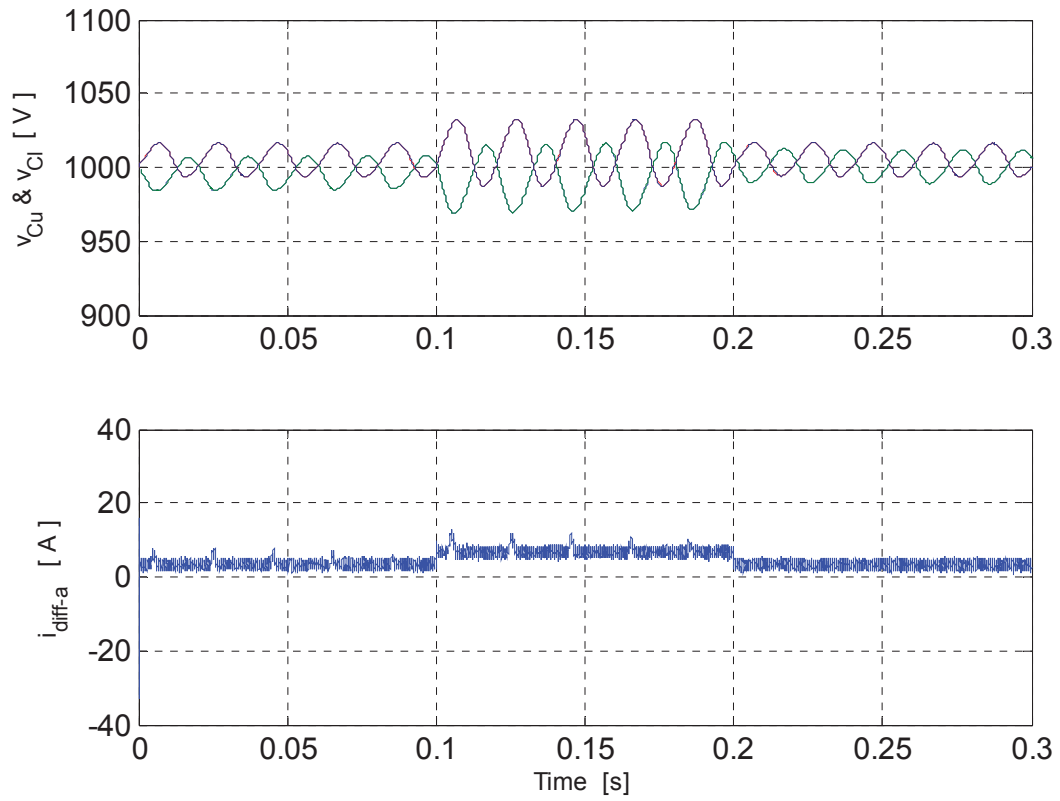


Figure 3.12 – Capacitor voltages and phase-a common-mode current i_{diff} .

Chapter 4: Solar System Study at Notre Dame University Lebanon

4.1 System Design and Objectives

This study allows the design of a PV system that meets the condition of a project while manipulating possible PV system solutions which in particular includes:

- a. Collecting and evaluating meteorological data for the site to determine the available solar resource and environmental conditions.
- b. Evaluating available ground surfaces regarding the suitability of installing a PV system.
- c. Designing and simulating several possible PV systems while considering limitations and restrictions.
- d. Evaluating the economic feasibility of the PV systems designed.

4.2 Methodology

4.2.1 Simulation Software: PVsyst

PVsyst contains databases of meteorological data and PV system components from several reputable manufacturers. This database make from PVsyst a powerful tool for designing and analyzing a PV project. PVsyst version 7.2 [15]. Figure 4.1 summarize the steps taken during the execution of a PV system design and simulation in PVsyst.



Figure 4.1 – Steps taken in PVsyst design.

During the Project Design phase the proposed PV system is firstly defined. Then in the Project Specification phase, the coordinates, the meteorological data and the project settings are specified. Parameters are then classified as mandatory or optional.

The Mandatory parameters such orientation, PV module type, inverter specification and losses are essential and could not be skipped when using the software.

On the other hand, the Optional parameters such module layout and near shading could be kept unspecified and will not prevent obtaining simulation result.

4.2.2 Site Assessment

The available area for installation, orientation and dimensions, near shading objects, and electricity consumption pattern were investigated. Figure 4.2 show the proposed site location which belong to Notre Dame University Louaize and has the following coordinate:

Latitude (°): 33.9528 (North hemisph.)

33Deg.57Min.10Sec. (North hemisph.)

Longitude (°): 35.6117 (East of Greenwich)

35Deg.36Min.42Sec. (East of Greenwich)

Altitude (m): 203 above sea level

Time Zone: 2 corresponding to an average difference

Legal Time – Solar Time = 0h-21m (min. 0h-38min at November 2nd, max. 0h-7m at February 12th)

The geographical location is summarized in Table 4.1.

Table 4.1– Geographical location of Notre Dame University Louaize Lebanon [16]

Latitude	Longitude	Altitude	Time Zone
33.9528	35.6117	203m	UTC+2

These coordinates were used for all weather data and site specific data throughout the study.



Figure 4.2 – Satellite imagery of the location - Notre Dame University Louaize-Zouk Mosbeh Main Campus [16]

5700m² of available rooftop spaces is identified. This area is distributed over the different faculty's roofs of NDU as shown in table 4.2 and in figure 4.3, 4.4, 4.5, 4.6 and 4.7.

Table 4.2– Identified roof areas that are useful for PV installation

Location (Roof Top of)	Approximated Area (m ²)
Engineering Labs	1500
Computer Labs	950
Faculty of Engineering & Faculty of Natural and Applied Sciences	1800
Zone 1	600
Zone 2	750
Total Area (m²)	5600

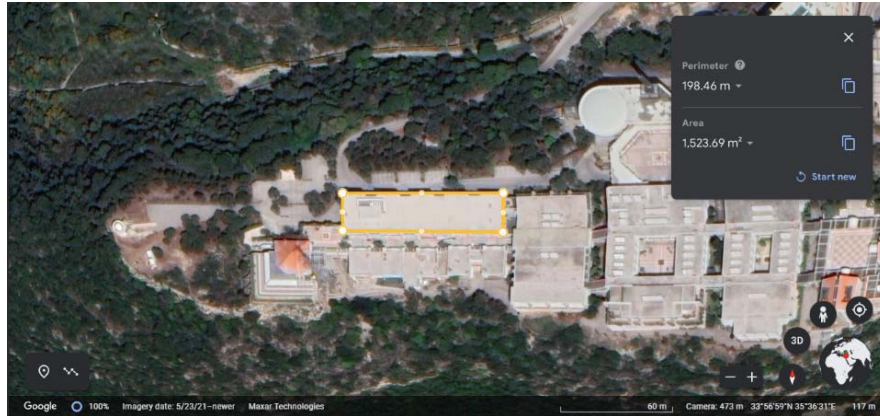


Figure 4.3 – Engineering Labs, Building Dimensions: 80mx19m, Perimeter: 198.5m, Rooftop Area: 1523m² [16]



Figure 4.4 – Faculty of Engineering & Faculty of Natural and Applied Sciences, Building Dimensions: 34.5mx53m, Perimeter: 175m, Rooftop Area: 1827m² [16]



Figure 4.5 – Computer Labs, Building Dimensions: 80mx12.3m, Perimeter: 183m, Rooftop Area: 982m² [16]



Figure 4.6 – Zone 1, Building Dimensions: 36mx18m, Perimeter: 107m, Rooftop Area: 629m² [16]



Figure 4.7 – Area 2, Building Dimensions: 33mx18m, Perimeter: 118m, Rooftop Area: 768m² [16]

4.2.3 Meteorological Data

The next step after defining the latitude, longitude, altitude, time zone and site name, is to import the related monthly meteo data. For this task, PVsyst offers the ability to get data from either Photovoltaic Geographical Information System (PVGIS), The National Solar Radiation Database (NSRDB), Solcast or SolarAnywhere.

The data imported are in hourly values, the values are then averaged and displayed as monthly values.

a. PVGIS Typical Meteorological Year (TMY) data

The PVGIS data available are TMY based on the most recent data reevaluation from the European Commission Joint Research Centre (JRC). The source of data depends of the geographical site you are creating, figure 4.8 shows the areas covered by each source:

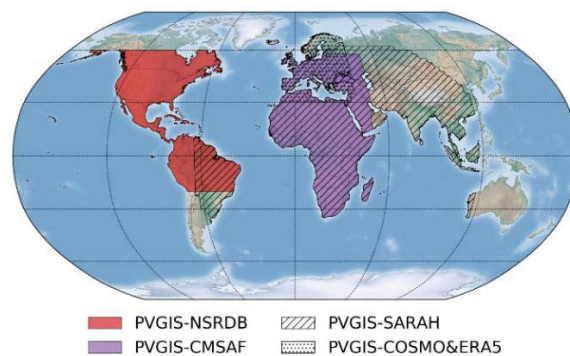


Figure 4.8 – PVGIS source of data depending on the geographical site location

b. NSRDB TMY data

The NSRDB data available are TMY based on the most recent data from the National Renewable Energy Laboratory (NREL). NSRDB data are offered in the areas shown in Figure 4.9.

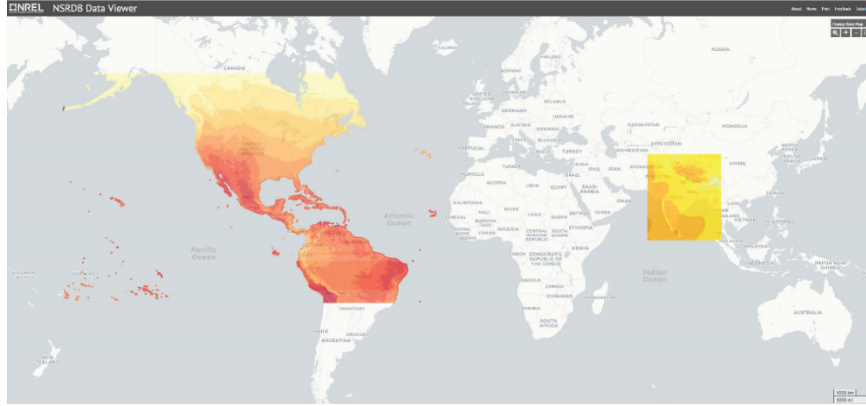


Figure 4.9 – NSRDB data available for the colored areas

c. Solcast TMY data

Solcast TMY P50 data is a collation of historical weather data for a specified location for a one year period. Solcast data are offered in the areas shown in Figure 4.10.

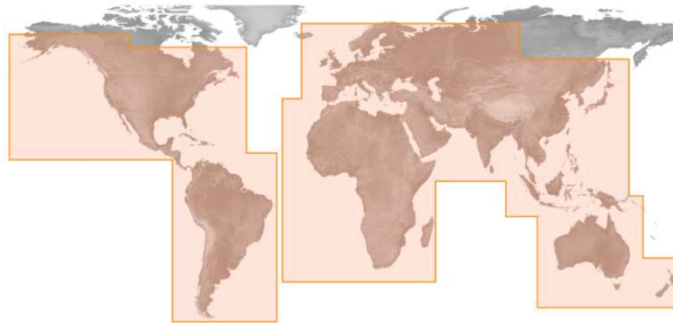


Figure 4.10 –Solcast data available in the highlighted areas

d. SolarAnywhere TGY data

SolarAnywhere TGY data are SolarAnywhere's version of TMY data. The TGY data will include 12 months of actual data from various years in the historical time series. For example, if January of 2010 has the monthly total irradiance closest to the long-term

average monthly total irradiance for all Januarys as calculated in step 1, it will be included in the file. This is illustrated in Figure 4.11.

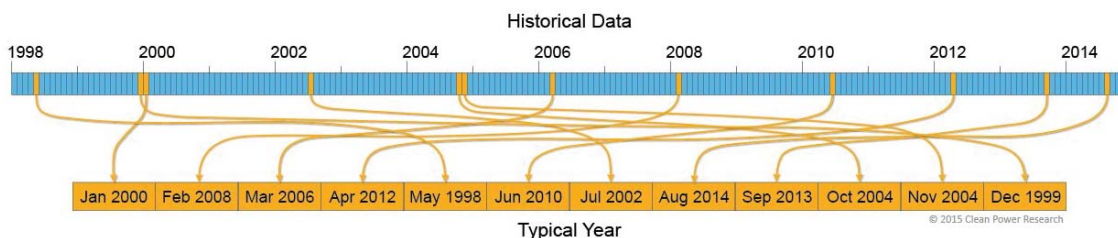


Figure 4.11 – SolarAnywhere TGY data, twelve months of various years

For the NDU project the data were taken based on the PVGIS imported from the TMY.

The obtained results are as shown in table 4.3:

Table 4.3 – Meteorological data based on the PVGIS imported from the TMY [17]

Country	Lebanon			
Region	Asia			
Source	PVGIS TMY: SARA, COSMO or NSRDB			
Latitude	33.9528°			
Longitude	35.6117°			
Altitude	203 m			
Time Zone	2 GMT			
Albedo	0.2			
Values	GlobH	DiffH	Temp	Wind Velocity
Month	kWh/m²	kWh/m²	°C	m/s
January	58.1	36.9	9.9	2.65
February	99.5	38.5	11.1	2.94
March	134.5	60.1	13.5	3.08
April	153.7	63.6	16.5	2.32
May	209.7	80.2	19.9	1.9
June	216.7	84.7	22.4	2.17
July	202.9	90.1	24.4	1.68
August	214	72.8	26.3	1.71
September	159.2	62.2	23.8	1.7
October	141.7	46.6	20.2	1.83
November	86.5	33.6	14.1	1.78
December	75.1	31	12	2.57
Year	1751.7	700.3	17.8	2.19

4.3 Selection of Module and Inverter

When selecting a module to use, the selection may be challenging, since there are several factor that distinguish one panel from other:

- a. Modules available in sizes,
- b. Modules power,
- c. Types and Manufacturer,
- d. Prices
- e. Module Efficiency.
- f. Compliance with international standard
- g. Module warranty.

Although the above listed factors are very important in the module selection, another important factor to consider is the availability of modules in the country or the duration of shipment if to be imported and also which modules installers are familiar with.

The experts focused on three key criteria when making their judgement:

- a. The manufacturer's financial position
- b. Brand reputation
- c. Value for money

Based on the SOLARREVIEWS, Jinko Solar is one of the 10 best solar panel brands in 2022 according to experts [<https://www.solarreviews.com/>]. The JKM-600N solar module was distinguished having substantial efficiency in N-type Series with 21.46% efficiency per cells area. Table 4.4 show the general key characteristic of the selected module.

Table 4.4– Jinkosolar JKM-600N-78HL4-BDV specification [17]

Technology	SI-Mono
Nom. Power (STC)	600Wp
Vmp	45.25V
Voc	55.03V

Number of cells	156
V _{max} (IEC)	1500Vdc
Efficiency/Module area	21.46%

On the other hand, when opting for the best the inverter for a certain application, the following consideration should be made:

- a. Size of the system,
- b. Cost,
- c. Flexibility of the system,
- d. Partial shading,
- e. Number of sub-strings or strings and their orientation.

Based on the above the selected inverter classified as string inverter, the Huawei SUN2000-40KTL-M3-400V inverter was used in the roof mounted PV simulations.

Table 4.5 show the general key characteristic of the selected inverter.

Table 4.5 – Huawei SUN2000-40KTL-M3-400V inverter specification [17]

Input side (DC PV Field)	
Minimum Mpp Voltage	200V
Maximum Mpp Voltage	1000V
Absolute max.PV Voltage	1100V
Output side (AC Grid)	
Triphased	50Hz / 60Hz
Grid Voltage	230Vac / 400Vac, 3W/N+PE
Nominal AC Power	40000W
Maximum Efficiency	98.7%

4.4 Module Orientation and Inter-Row Spacing

When choosing the tilt angle and azimuth angle for a roof mounted PV system, the inter-row spacing must be considered together with the orientation. When choosing the inter-row spacing, an optimization between tilt angle, azimuth angle, area utilization and maximum energy production is done. The modules are oriented in landscape configuration

to reduce the effect of parallel shading on the module cells [17]. Care should be taken to ensure that only modules with the same orientation, angle and shading conditions are connected together in strings

In this design, the optimization by respect to yearly irradiation yield and the condition of no mutual shading from 7am to 4pm was used based on the solar paths at specified site as shown on Fig. 1. Through orientation optimization by PVsyst, an azimuth angle of 0° (since it is feasible due to the orientation of the rooftop of NDU) and a tilt angle of 29° were considered.

Thus, the effective row spacing between the panels are decided by:

- a. Panel Tilt (β)
- b. Panel width (w)
- c. Height difference (H)
- d. Shadow angle and Azimuth angle(α)

The shadow pattern is derived from the tilt as well as the height of the panel. The shadow angle is calculated mostly on the winter solstice when one can experience more shadows for any objects owing to the Sun's position.

The azimuth angle is the angle through which the sun rays penetrate the panels. The tilt angle is decided in such a way that panel is almost perpendicular to the direction of the solar radiation. This ensures the panel to have an optimal generation from solar radiation [29].

The inter-row spacing was then calculated by using Eq. 4.1,

$$d_{row} = w_m \cos \beta_m + w_m \left(\frac{\sin \beta_m \cos(\gamma_s - \gamma_m)}{\tan \alpha} \right) \quad 4.1$$

Where w_m , β_m and γ_m are respectively the width, tilt angle and azimuth angle of the module, and γ_s and α are respectively the azimuth angle and the altitude angle of the Sun as shown in Figure 4.12 .

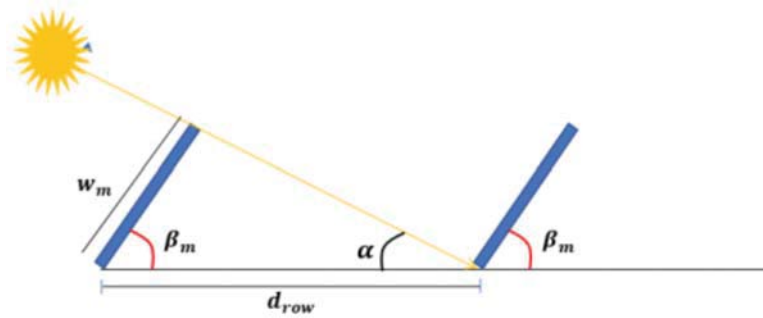


Figure 4.12 – Inter-row spacing for a ground mounted PV system.

In the design, an optimization by respect to yearly irradiation yield and the condition of no mutual shading from 7am to 4pm was used based on the solar paths at specified site as shown on Figure 4.13.

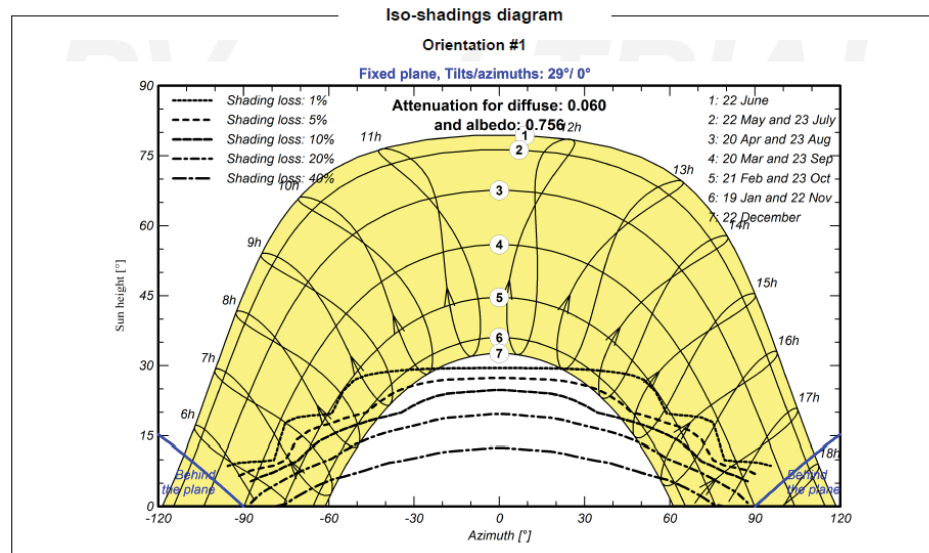


Figure 4.13 – Solar Paths at Zouk Mosbeh [17].

The obtained value of inter-row distance based on table 4.6 and equation will be equal to 193cm. Thus, a 2m pitch is adopted between panels

Table 4.6 – Supports angles and azimuth

Parameter	Value
w_m	113cm (width of the module, since modules are placed in landscape)
β_m	29° (as found ideal for the selected location in Lebanon)
γ_m	0° (due to the orientation of the rooftop of NDU)
γ_s	Averages at 0° (from 7am and 4pm)
α	30° (at 7am and 4pm)

4.4.1 Number of Modules to be installed

Based on section 4.4, the total number PV modules that will be installed will be 1008 and distributed as shown in table 4.7 and figure 4.14.

Table 4.7 – Identified roof areas that are useful for PV installation

Location (Roof of)	Approximated Area (m ²)	Number of installed PV modules	Density of PV (Area of PV modules / Roof Area)
Engineering Labs	1500	9x31=280	52%
Computer Labs	950	5x31=156	45%
Faculty of Engineering & Faculty of Natural and Applied Sciences	1800	26x13=338	52%
Zone 1	600	9x14=126	58%
Zone 2	750	9x12=108	40%
Total	5600	1006	50%

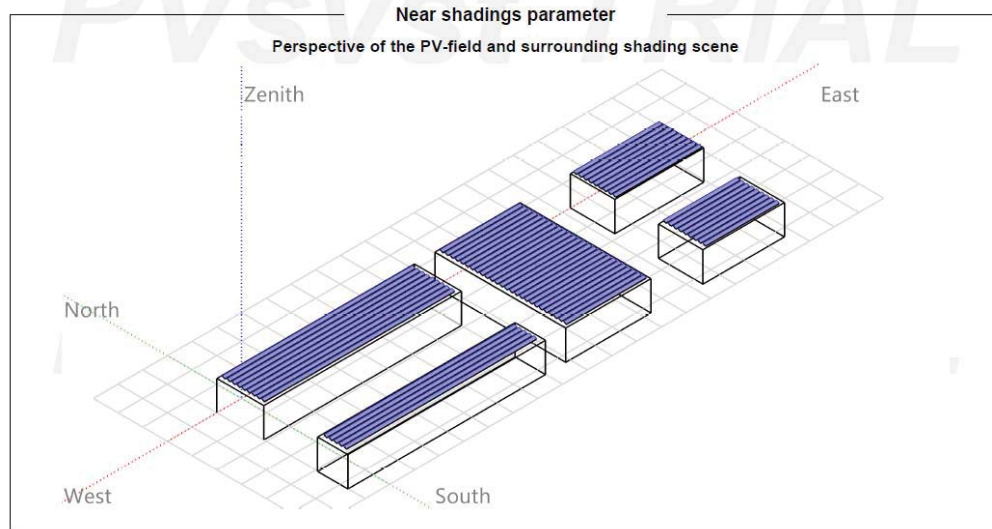


Figure 4.14 – 3D distribution of PV panels on NDUs buildings roofs.

4.5 System Design

Given that the selected PV module is 600Wp and the total installed number of panel that could be hosted on the roof is 1008, then the total installed capacity of the system will be equal to 604.8kW

In general when determining the number of Inverter and number of PV panels per inverter, it is recommended to perfectly size the inverter in order to achieve the maximum overall energy yields from the solar system. In order to check the total number of panels per strings and the number of inverter required based on the previous PV and inverter selection the following steps are performed

Step 1: Finding the minimum string size connected to the inverter

The minimum number of panels that we should put in a string are calculated by dividing the lower limit the MPPT range of the inverter (in this case 200V) by the V_{mp} of the panel (45.25V).

The result is 4.42, which needs to be rounded up to the next whole number. So the minimum string size consists of 5 panels.

Step 2: Finding the maximum string size that doesn't exceed operating voltage

For maximum string size and to ensure that we don't overload the inverter, the maximum DC input (1100V) will be divided by the open circuit voltage V_{oc} of the panel (55.03V).

The result 19.98 is rounded down in order to stay below a maximum threshold. So the maximum number of panels per string is 19 panels.

Step 3: Checking that maximum string size is within MPP range

In the preceding step the maximum string size that keep the inverter operational was found. To ensure that this size is within peak efficiency range, the maximum string size already calculated (19 panels) is multiplied by the voltage at maximum power of the panel V_{mp} (45.25V).

The result 859.75V falls under the higher end of the MPP range (in this application 1000V). Thus everything checks out here.

Based on these calculations, the string size may range from 5 to 19 panels.

Given that the Huawei chosen inverter can host up to 8 strings and since the best configuration consists in using all strings in order to maximize the number of operating (integrated MPPT controller (1MPPT for each 2 strings) 14 panels will be connected in series on each string and a total of 72 strings will be formed. 15 inverters will host panels as shown in table 4.8. In this case, 60 MPP trackers are available (versus 1 MPP trackers

if the central inverter topology was adopted instead). This configuration leads to much less mismatching losses and much higher overall yield.

Table 4.8– Identified roof areas that are useful for PV installation

Location (Roof of)	Number of installed PV modules	Number of Inverters	Number of panel per string	Number of MPPT involved
Engineering Labs	9x31=279	15	14	60
Computer Labs	5x31=155			
Faculty of Engineering & Faculty of Natural and Applied Sciences	26x13=338			
Zone 1	9x14=126			
Zone 2	9x12=108			
Total	1006			

4.6 Shading

Due to the remote location of NDUs building and giving that no surrounding objects can obstruct the sun from the roof mounted PV panels, shading effect could be almost disregarded. The only shading on the roof area occurs during winter months, as the Sun's position in the sky is low enough. Due to the chosen inter-row spacing, no mutual shading occurs from 7am to 4pm during the winter months. The shading is mainly due to mutual shading between the module rows in mornings and afternoons outside the 7am to 4pm time range.

4.7 Economical Evaluation of the PV System

When planning to install a PV system, the first investor need is to check the financial profit acquired by using the system.

To start with the economic analysis of the project at NDU, the two common used term “Payback Time” and “Net Present Value”, in the economical section, must be defined.

a. Payback Time

The payback time refers to the time required for a certain investment to recompense its cost. It is defined in Eq. 4.2 as [18]:

$$\text{payback time} = \frac{\text{total investment}}{\text{annual income}} \quad 4.2$$

b. Net Present Value (NPV)

The Net Present Value (NPV) allows the calculation of the present value of the future cash flows and is common in evaluating a PV system. When NPV is positive the project will be considered profitable.

While the payback time reveals the duration taken to get back the invested money, the NPV on the other side shows the profit one can expect at the end of the investment period. The present value of the lifecycle costs is calculated by Eq. 4.3

$$NPV = \sum_{t=0}^T \frac{\text{Revenue}_t - \text{Costs}_t}{(1+r)^t} \quad 4.3$$

Where

t is the year of operation ,

T is the lifetime of the system,

r is the discount rate,

Revenue_t is the cash inflow,

Costs_t is the cash outflow.

Based on the simulation results, an economic evaluation of the system was performed. Costs are defined in price list from local suppliers. Table 4.9 and 4.10 summarize the economical assumptions and the financing evaluation respectively.

Table 4.9 – Economical Assumptions [17]

Cost of the system			
Installation costs			
Item	Quantity units	Cost USD	Total USD
PV modules			
JKM-800N-78HL4-BDV	1008	204.00	205632.00
Supports for modules	1008	50.00	50400.00
Inverters			
SUN2000-40KTL-M3-380V	15	4000.00	60000.00
Other components			
Accessories, fasteners	4032	1.00	4032.00
Wiring	2000	1.70	3400.00
Surge arrester	135	100.00	13500.00
Studies and analysis			
Engineering	1	25000.00	25000.00
Installation			
Global installation cost per module	1008	100.00	100800.00
Global installation cost per inverter	15	1000.00	15000.00
Grid connection	1	19500.00	19500.00
Taxes			
VAT	1	0.00	42142.80
Total			539406.80
Depreciable asset			320064.00
Operating costs			
Item			Total USD/year
Maintenance			
Cleaning			10000.00
Total (OPEX)			10000.00
Including inflation (1.43%)			11482.48
System summary			
Total installation cost			539406.80 USD
Operating costs (incl. inflation 1.43%/year)			11482.48 USD/year
Produced Energy			1000 MWh/year
Cost of produced energy (LCOE)			0.043 USD/kWh

Financial analysis			
Simulation period			
Project lifetime	20 years	Start year	2023
Income variation over time			
Inflation			1.43 %/year
Production variation (aging)			0.00 %/year
Discount rate			0.00 %/year
Income dependent expenses			
Income tax rate			0.00 %/year
Other income tax			0.00 %/year
Dividends			0.00 %/year
Financing			
Own funds		200000.00 USD	
Loan - Redeemable with fixed annuity - 10 years		339406.80 USD	Interest rate: 5.00%/year
Electricity sale			
Feed-in tariff		0.2000 USD/kWh	
Duration of tariff warranty		1 years	
Annual connection tax		0.00 USD/kWh	
Annual tariff variation		+10.0 %/year	
Feed-in tariff decrease after warranty		20.00 %	
Return on investment			
Payback period		3.7 years	
Net present value (NPV)		2372845.50 USD	
Return on investment (ROI)		439.9 %	

Table 4.10 – Financing Evaluation [17]

Choosing loan duration and interest rate, PVsyst computes automatically the annual financial cost, supposing a loan pay back as constant annuities. The loan duration correspond to the expected lifetime of the system. This procedure is justified since when purchasing a solar system, the customer buys at a time the value of the whole energy consumed during the exploitation. The sum of the annuities and the running costs is the total annual cost. Divided by the effectively produced and used energy, it gives an evaluation of the energy cost (price of the used kWh) [19].

Table 4.11 shows the result of the calculation of payback time and NPV. The system lifetime is assumed to be equal to the module lifetime. The International Energy Agency (IEA) assumes a PV system lifetime of 25 years [20].

Table 4.11 – Payback Time and NPV

Payback Time	3.7 years
Net Present Value	2372845.5 USD

The economical evaluation shows that it will take 3.7 years to make the invested money back and the net present value is positive for all systems. This means that the investment cost will be paid back during the system lifetime.

4.8 Results and Discussion

The PVsyst simulation generates a report of used system configuration and the obtained simulation results. PVsyst calculates the losses and shows them in a loss diagram as illustrated in Figure 4.15.

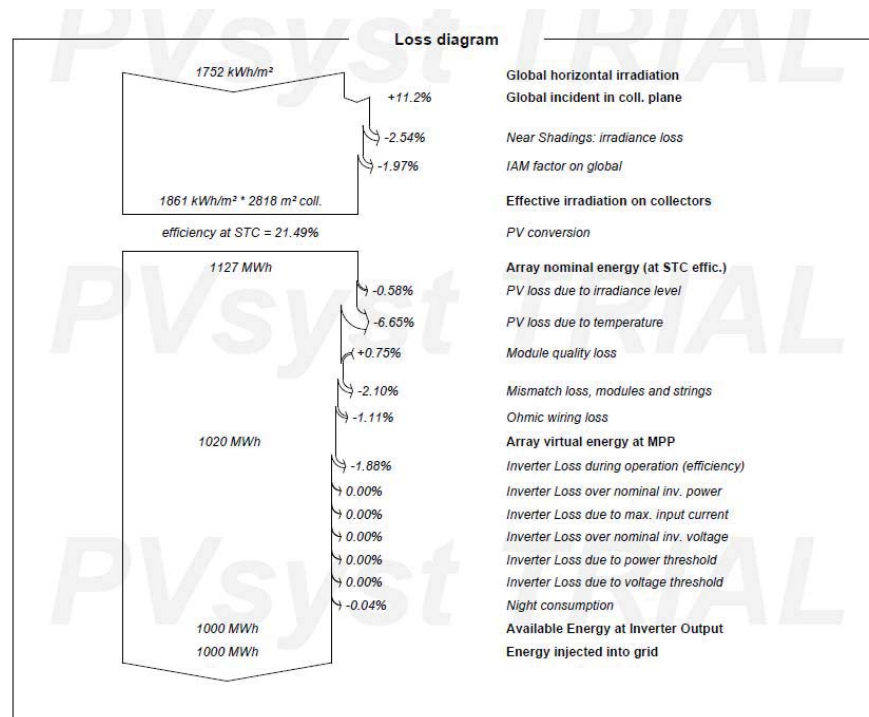


Figure 4.15 – Loss diagram over the whole year [17]

The diagram is normally composed of three parts:

- a- The upper part of the diagram corresponds to the optical losses,
- b- The middle part correspond to the array losses,
- c- The lower part consists of the system losses.

Table 4.12 shows the simulation results for the ground mounted systems. The monthly normalized production and PR for the system is shown in Figure 4.16 and Figure 4.17.

Table 4.12 – Results Overview

System Production	1000MWh/year
Specific Production	1654kWh/kWp/year
Performance Ratio	84.91
Normalized Production	4.53kWh/kWp/day
Array Losses	0.72kWh/kWp/day
System Losses	0.09kWh/kWp/day

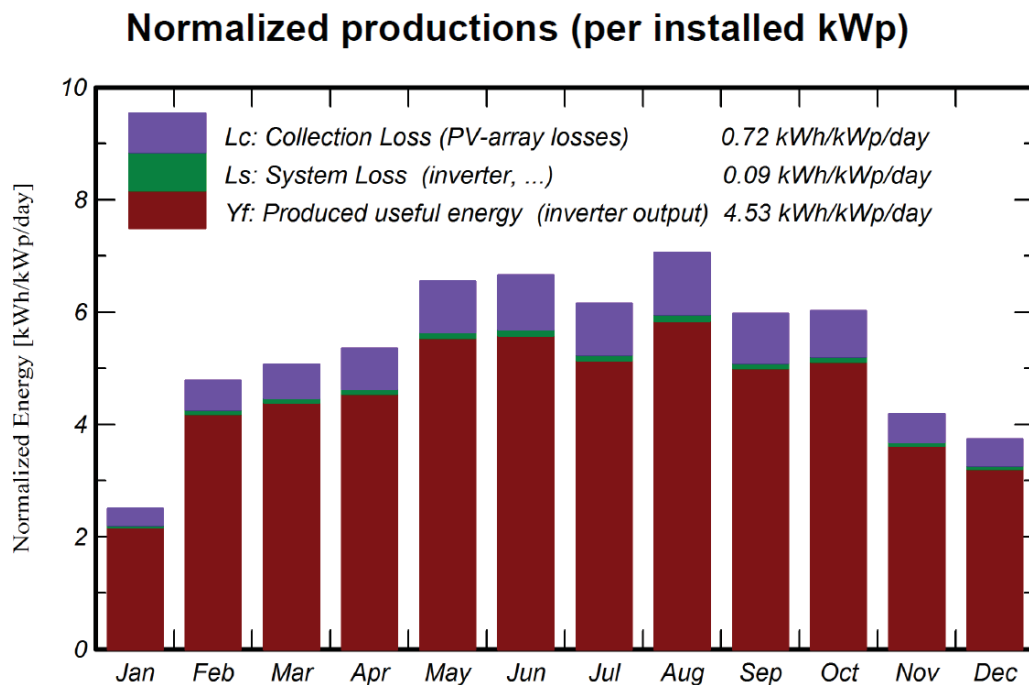


Figure 4.16 – Normalized productions (per installed kWp) [17]

Performance Ratio PR

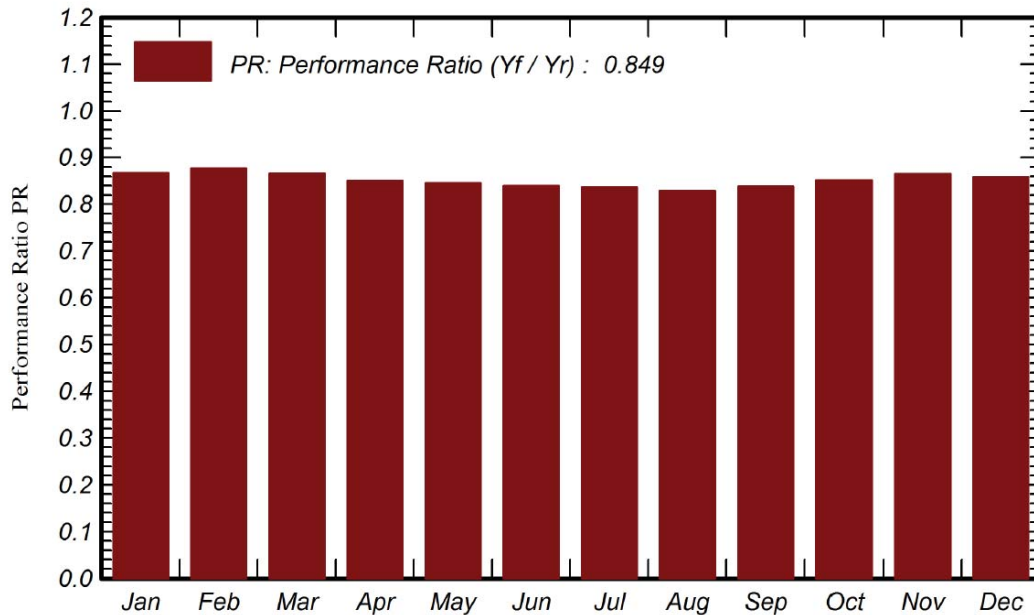


Figure 4.17 – Performance Ratio [17]

The largest optical losses are the near shading irradiance loss and IAM loss as per Figure 4.15. The array and system losses that had the greatest effect on system performance were inverter loss and efficiency loss due to temperatures difference from STC, as shown in Figure 4.15.

Figure 4.17 shows that the performance ratio is higher during winter months than during summer months. This is expected as winter months have lower temperatures and the dust, resulting in lower losses. The normalized production for each month seen in Figure 4.16 shows the array and system losses. Both losses are lower during winter months and increase during summer months. This efficiency loss is highly related to the temperature.

4.9 Conclusion

Using the PVsyst simulation software, the energy yield analysis for 600 kWp PV solar power generation was performed for geographical site at Notre Dame University Lebanon. Although, there are uncertainties regarding the meteorological data and the available solar resource.

It is observed that the efficiency of modules is more sensitive to temperature than the solar irradiation. The normal daily wise is that the efficiency of the plant is high during morning time but low during middle of the day and starts increasing from late afternoon. The efficiency of modules varies from 14.5% to 11.5% with variation in the averaged module temperature from 25°C to 60°C. Hence cooling of solar modules may be desirable to increase the efficiency.

Chapter 5: Case Study - Grid Connected Photovoltaic Project in Lebanon

5.1 Overview and Location Description

Located on the eastern part of the Saint George Bay on Beirut's northern Mediterranean coast, Port of Beirut (POB) is one of the largest and busiest ports on the Eastern Mediterranean. The port is operated and managed by the “Gestion et exploitation du port de Beyrouth”. Container terminal operations are subcontracted to a private consortium called the Beirut Container Terminal Consortium (BCTC). POB has a total area of 1,200,000m² and has 4 basins, 16 quays as shown in Figure 5.1, and a new container terminal at quay 16 capable of handling 745,000 twenty-foot equivalent units per year. Since 1990 after the end of civil war, major updating and expansion program were developed in the Port. Within these programs, the installation of a new PV power plant to reduce the overall energy dependency on fuel and EDL power was the most valued during the current years.

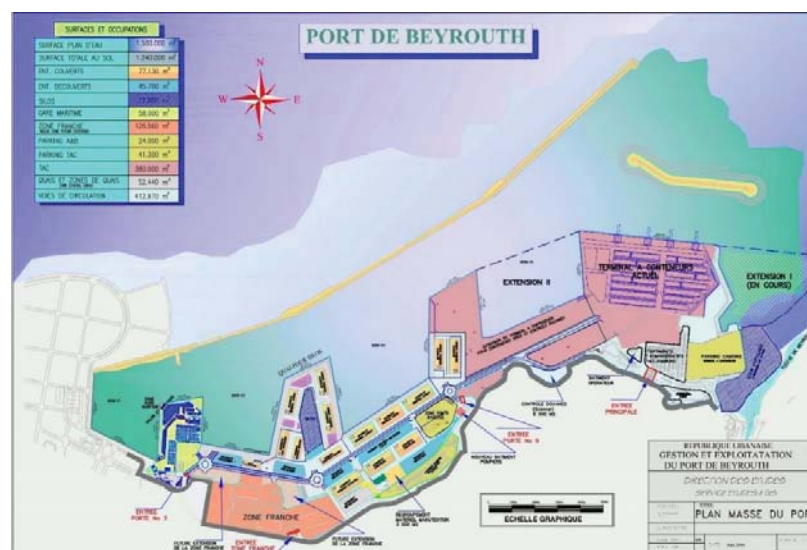


Figure 5.1 – POB General Layout [21]

5.1.1 Port of Beirut Existing Electrical Infrastructure

5.1.1.1 Port of Beirut Emergency Power Plant:

POB emergency power plant consists of three buildings as shown in Figure 5.2:

1. Building 1: Hosting the Generator Room, Control and Low Voltage (LV) Circuit Breakers Room and the Step-up Transformers Room.
2. Building 2: Hosting the Medium Voltage Switchgears and the Power load bank.
3. Building 3: Containing the main fuel tank related to the power plant.

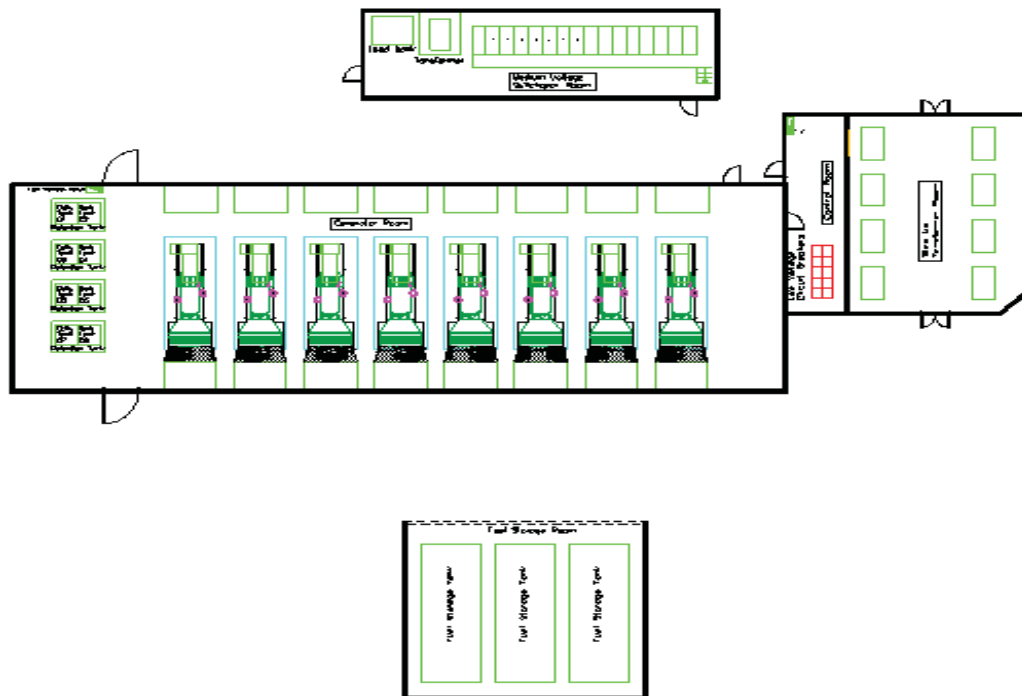


Figure 5.2 – Port of Beirut Power Plant Buildings [22]

The generators room is currently fully equipped with eight sets of 1600kW/2000kVA generators (Marathon alternators driven by Cummins engines). Five out of the eight sets were assembled by SAKR Power Generation and the rest were added by Younes Bros as part of the extension's project of the power plant done in 2015.

Today, POB has a 12.8MW/16MVA emergency power plant fully automated and capable of starting automatically during main power failure events.

On the other side, the control and low voltage circuit breakers' room hosts the main Programmable Logic Controller (load management PLC) capable of controlling the start/stop operation, synchronism, the load management and the operation of the circuit breakers on the LV or the primary sides of the transformers.

Since the Port premises are spread on a very wide area and given that the distances between sources and load are large enough, Medium Voltage transmission is adopted in order to reduce the power losses. In order to achieve the medium voltage level, the generators output voltage (low voltage) is passed through step-up transformers to allow medium voltage distribution toward each of the Port's substations. Copper bus ducts are used to connect each of the eight generators to its related transformer. Then the output of each transformer is connected to an MV switchgear located inside the Medium voltage switchgear room. And the sum up outgoing MV switchgear is connected to the "Poste Principale" station where the automatic transfer (by mean of MV switchgears) between EDL and power plant power is performed. The complete single line diagram related to the POB power plant is shown in Figure 5.3

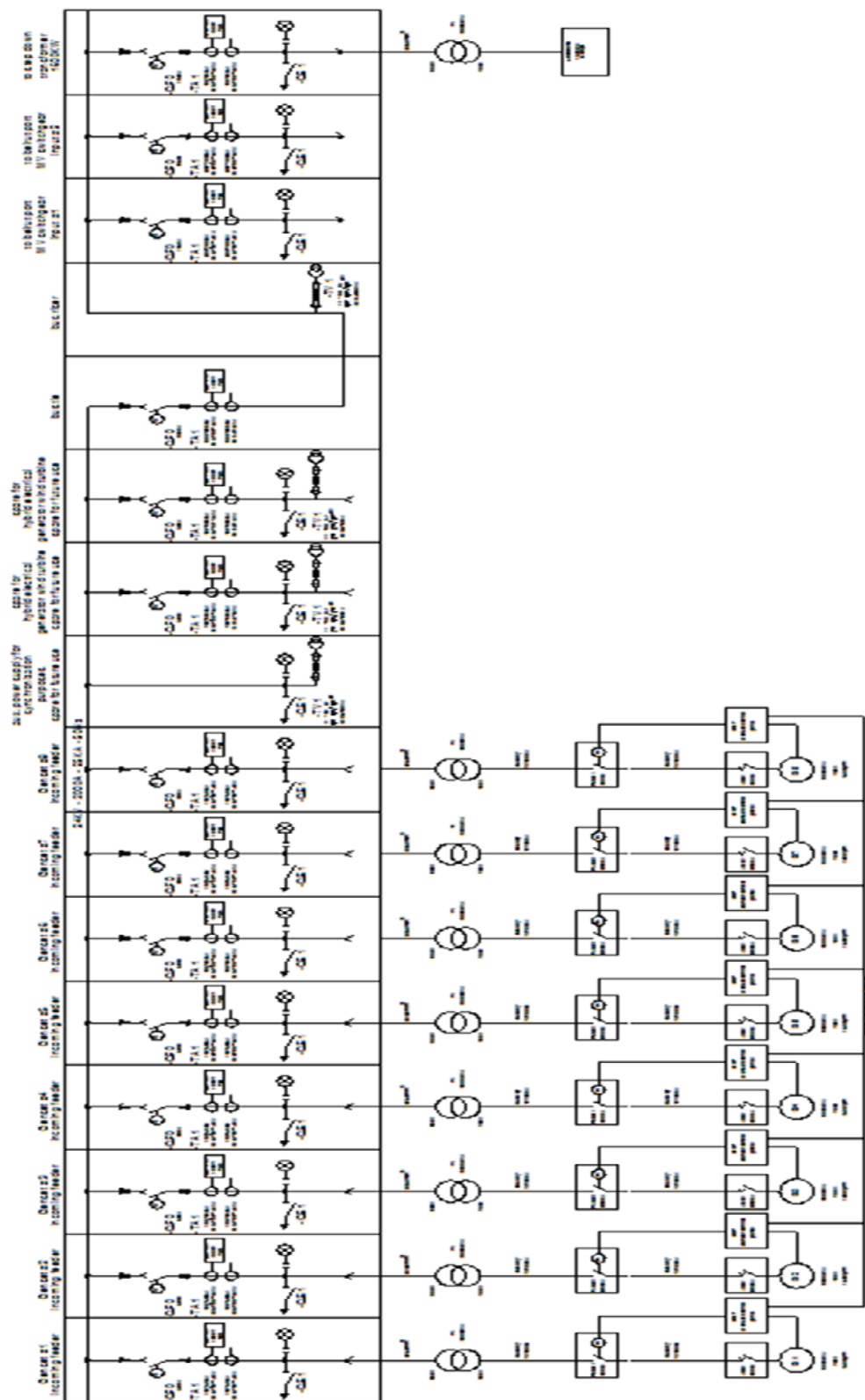


Figure 5.3 –POB Power Plant’s Single Line Diagram [23]

Operation Philosophy of the Port's power plant:

Automatic synchronizing mode

Upon receipt of EDL main power failure signal (detected by the loss of mains phase relay), the PLC will initiate a start procedure to launch all generator sets at the condition of having MV Switchgear of the Outgoing breaker (the one connected to the "Poste Principale") in the open state. Once this condition is met, the load management PLC selects randomly one engine that will close its low voltage circuit breaker on the dead bus bar. This action is used to allow magnetizing the step up transformers. Then after, the PLC will command the rest of generators to launch and synchronize with each other. MV switchgear of the outgoing breaker will then be closed in order to supply the Port's load. Therefore to sum up, at the beginning of the load supply all of the available generator operates simultaneously. After around 10 minutes, the PLC will start the load management and power optimization protocol and will initiate a stop command for supplementary generators, based on the average power read from the Automatic Genset Controllers, and based on the number of Ship to Shore (STS) cranes in operation. Table 5.1 summarize the relation between number of operating generators, STSs and load.

Table 5.1 – Relation between Number of Operating Generators, STSs and Load [22]

KVA	GEN	UP kW	UP %	DOWN kW	DOWN %	MAX kW
2000	1	1000	63			1600
4000	2	2100	66	850	53	3200
6000	3	3350	70	1800	56	4800
8000	4	4450	70	2900	60	6400
10000	5	5600	70	3850	60	8000
12000	6	6700	70	4800	60	9600

14000	7	7800	70	5750	60	11200
16000	8		0	6900	62	12800

UP KW: Call for additional genset when load reach the indicated load

DOWN KW: Call for less genset when load reach the indicated load

Running STS	0	1	2	3	4	5	6	7	8...16
Pcal (kW)	Pmes	Pmes + 800	Pmes + 1600	Pmes + 2000	Pmes + 2400	Pmes + 2400	Pmes + 2400	Pmes + 2400	Pmes + 2400
Pneg (kW)	0	Pmes - 400	Pmes - 800	Pmes - 1200	Pmes - 1600	Pmes - 1600	Pmes - 1600	Pmes - 1600	Pmes - 1600

Pmes: Total actual active power measured

Pcal: Total actual active power required (calculated)

Pneg: Maximum negative active power (calculated)

After receipt of stop signal (for example when main power is restored), a 6.5 minutes cooling period will start by disconnecting the load imposed on the generators.

Power management protocol

The PLC reads the total power provided by each running set, and thus calculates the total power expected to be available by the station, and required for the load. The load is composed of sixteen cranes and other general used load such reefers, lighting, power sockets, administration building, maintenance building, customs and security buildings, BCTC building necessities...). The PLC compares system load requirements with on bus generator capacity. Additional generators shall automatically be added or removed from the bus according to system load demand. When the STS cranes are off, generators are started and stopped based on the existing demanded load:

- A generator's contribution is added immediately to the system if the total actual load reaches 70% of the total power on bus generator powers.

- A generator's contribution is removed from the system if the total actual load is less than 60% of the total minus one of the on bus generator power for an adjustable period of time.

When the STS cranes are running, another scenario is applied. In other words, the PLC reads two different signals (Uploading, downloading) from each crane in order to properly apply the load management protocol. First, The PLC reads from each crane a signal "Crane On" activated just when the crane is started up. This signal will allow the PLC to calculate the predicted power to be needed and taken into consideration that will be necessary to keep the operation of the plant optimized if any load variation occurs. The PLC calculates the actual existing load, adds to it the power needed each time the crane motor will start (On or lifting up) or apply the brake (Down or lifting down) and define the total expected needed load. Thus, based on the total expected needed load, the PLC will calculate the number of sets to be started, and initiate the starting procedure just before the crane is actually operating. On the other hand, the second signal to be read is the "Down" signal. This Signal is used to allow the PLC to manage the Loadbanks contribution depending on the number of operating cranes and on the number of running generators. When the STS crane is unloading, it generates active power in the reverse direction. To compensate this negative power and protect the alternators from high reverse power faults, the PLC reads from each crane the signal "hub brake" and calculates the negative active power that the system will face. Based on this calculation, the PLC command the necessary number of resistors from the auxiliary load bank to be added or removed from the total system load to absorb the reverse power.

5.1.1.2 Poste Principale:

Switching between EDL and Port's generators power is made inside the "Poste Principale" building. Therefore this building host the most critical MV distribution equipment related to the operation of the Port. In fact, two incoming switchgears interlocked between each other allow, using dedicated control (PLC), the automatic transfer switching between the power sources. Then after the resulting power from EDL or generators is then distributed through MV switchgears and MV cables to two main groups:

1. Ship to Shore Cranes' load fed through the "Cellule Portique" MV substations.
2. The Rest of port load fed through MV to LV substation referred by "LT1, LT2, LT2', LT3, LT4, LT5, LT6".

In order to ensure a high level of redundancy and in order to allow easy and flexible maintenance work, each of the above mentioned group is fed using two different path of MV cables and switchgears (loop configuration).

The power single line diagram related to the "Poste Principale" and the rest of substations inside the Port are shown in Figure 5.4.

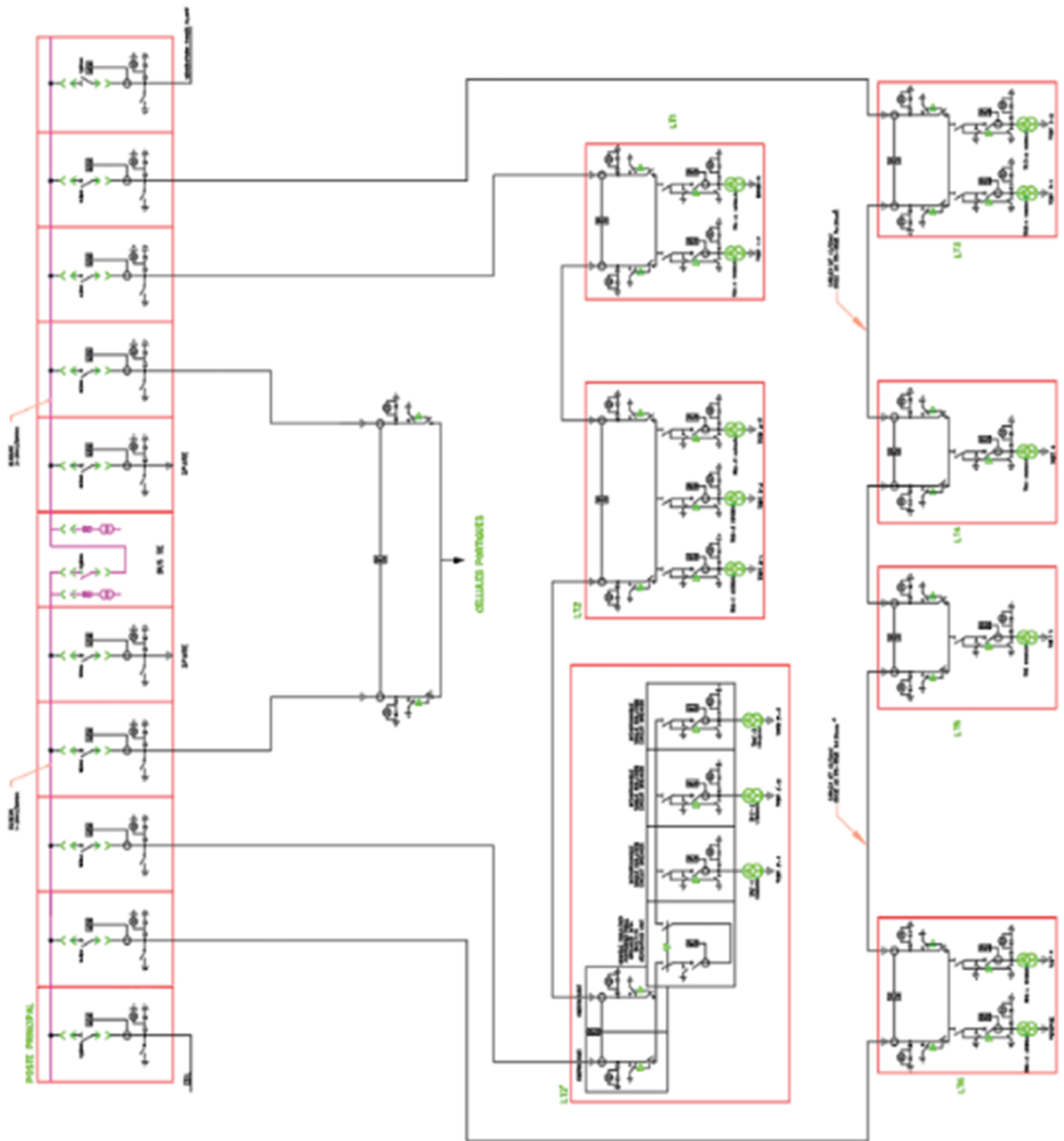


Figure 5.4 – POB Complete Single Line Diagram [24]

LT5 and LT6 are currently disconnected due to the high level of damages that they have after the 4th of August Port's blast.

5.2 Executive Summary

Port of Beirut (POB), represented by its administration GEPB, has the intention to rely on a renewable energy source for their daily activity. The adoption of this type of energy will definitely push the POB to a green environment ensuring financial revenue following a short return on investment period of time.

The form of renewable energy to abide by, is the solar energy by installing photovoltaic (PV) panels and converting the sun energy to electrical power sufficient to cover the POB requested demand load.

Given the above, the hybrid PV solution is proposed in which the PV panels, in addition to being synchronized with EDL, are also synchronized with the POB private generators power plant thus, in case of EDL failure the load on the generators will be minimized yielding a lower fuel consumption.

Many challenges may face the kickoff of this project, these challenges are listed here below and are considered as the main issue of this study:

- A. POB demand load
- B. Renewable energy capacity requested from POB
- C. PV panels location & type of installation:
 - 1. Floating PV panels
 - 2. Roof Installation
 - 3. Carports Installation

- D. Connecting the renewable energy to the POB grid:
 - 1. Converting the received energy to medium voltage
 - 2. Excavation and routing to main substation
- E. Approximate cost estimate
- F. Return on investment (ROI)

Reference to the above points described in the following sections, the project benefits are significant and most importantly the ROI will yield considerable yearly amount of money that can be invested in other different sectors/projects, not to forget the reputation on power savings over the EDL grid that can benefit from it different other consumers.

5.3 Description of the Project

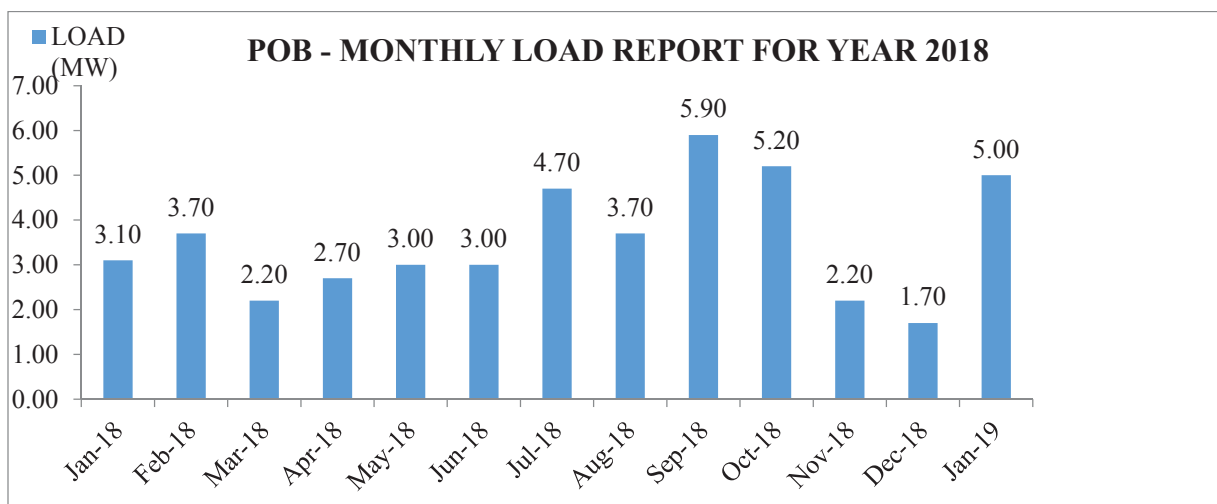
As briefly described in the above section, the challenges of this project constitute the several parts this study is made of.

5.3.1 POB demand load

Over a period of 12 months, random data and readings were acquired in order to avoid an overdesign for the PV system. This allowed determining POB demand load.

Table 5.2 shows that an average demand load of 3.7MW is needed for the POB to normally operate.

Table 5.2 – POB Monthly Load Report over one year



December 2018 load, shall be excluded from the calculation since during that day, maintenance on the Ship to Shore (STS) Cranes was being conducted and hence they were disconnected from the grid.

5.3.2 PV Panels location & type of installation

Given the port heavy operation and harsh environment, the PV dimensioning, location and type of installation of the PV constituted a major challenge and will be described here below.

The location & type of installation of the PV will be briefed into three options:

- Option 1: Floating PV panels
- Option 2: Roof Installation
- Option 3: Carports Installation

5.3.2.1 Option 1: Floating PV Panels

a- Description

Floating PV panels system allows standard PV panels to be installed on large bodies of water such as: drinking water reservoirs, quarry lakes, irrigation canals, remediation and tailing ponds, and hydro-electric dam reservoirs. Solar panels need to be affixed to a floating structure that keeps them above the surface. It's also common to install floating solar structures on large, man-made bodies of water, such as reservoirs

Application for sea installation is still minimal and no previous experience in Lebanon.

Example of floating PV installation as per Figure 5.5:

Location: Kelseyville country, California, USA

Size: 252 kilowatts



Figure 5.5 –Example of floating PV installation (Kelseyville country, California, USA, 252 kW)

a- Pros

- The system is scalable.
- Material used is high density thermoplastic which is eco-friendly.

- Recyclable material.
- High efficient thanks to the cooling effect of water on PV panels.

b- Cons

- Requires a deep study of the location in order to assess the environmental conditions that characterize the site. However, the floating system requires the below conditions:

- Maximum water speed 1 m/s (not applicable in Lebanon)
- Maximum waves height 0.8 meters (not applicable in Lebanon)
- Wind speed ~ 50 m/s

- Requires anchoring from sides and center. Depth in this case will be studied in details.
- Has a high effect on animals and vegetable life beneath it as it obscure the sun light to reach the water.
- Materials are to be ordered and customized.
- Requires a big area inside the sea.

c- Cost of installation

It typically requires a higher price than installing solar farms on rooftops, solid ground or on carports. This is due to the fact that every project requires special and customized design based on specific data such as: water depth, water level variations, wind speed, current

speed, wave height, the total air resistance caused by the moored application. That's why its price depends on each specific project and the environmental conditions that the system needs to handle.

5.3.2.2 Option 2: Roof installation

a- Description

Installing photovoltaic (PV) solar panels on building roofs is already common and considered as the traditional most economical alternative.

Warehouses have a great potential for rooftop electricity generation, since the existing roofs have an enormous area and most importantly their structure can support the added weight of PV panels without requiring major reinforcement. No special design or special mounting devices are needed.

This does not mean that a structural survey is not needed. A structural engineer shall check the site and the warehouses where PV installation is intended to be done to verify and validate the installation.

Example of PV roof installation as per Figure 5.6:

Location: SMLC PEPSICO Lebanon

Size: 1MWp



Figure 5.6 –Example of PV roof installation: SMLC PEPSICO Lebanon

b- Pros

- Common application.
- No need for special design.
- Fast and easy deployment.
- Cost effective.
- Easy maintenance.
- Use of dead areas.

c- Cons

- Not scalable, limited to the roof area.
- Access to roof via special means.
- Roof strengthening might be needed in some areas.
- Roof asbestos shall be dismantled and replaced by trapezoidal metal sheets

d- Cost of installation

The installation of PV panels on warehouses roofs is considered as the most economical cost effective solution, especially in POB case where the warehouses are available and there is relatively big area allowing installation of requested capacity without loss of any ground level area.

5.3.2.3 Option 3: Carports Installation

Several meetings with POB administration were conducted and it was requested to achieve a capacity equal to the maximum renewable energy that can be installed, given the limited places we have near POB main power substation “Poste Principale”. The first study was submitted before the August 2020 explosion of Port of Beirut and consisted in making the installation on the roof of warehouses number 13, 14 and 15 [25]. After the catastrophic explosion, the warehouses were totally destroyed and the study was updated and it was based on a newly available location and different type of PV installation which is solar carports at the administration parking area.

Solar carports are overhead shades designed as parking area shelters with solar panels mounted on them. These structures have multiple similarities with the ground mounted panels, which are mostly installed on the ground, instead of rooftops. The major difference between ground-mounted panels and solar carports is that carports are much taller as shown in Figure 5.7, to help accommodate parked cars. Also, solar carports are more space-efficient than ground-mounted solar panels. Solar carports are meant to offer shelter to vehicles parked below them, as well as efficiently generate electricity. They are ideal for large parking areas.



Figure 5.7 –Example of Solar Carports Installation: 16.3 MW solar array on a car park in Corbas, France
The parking area around administration building will allow the installation of around 1900 photovoltaic modules as per Figure 5.8, 530W peak each, providing a total capacity of around 1MW peak.

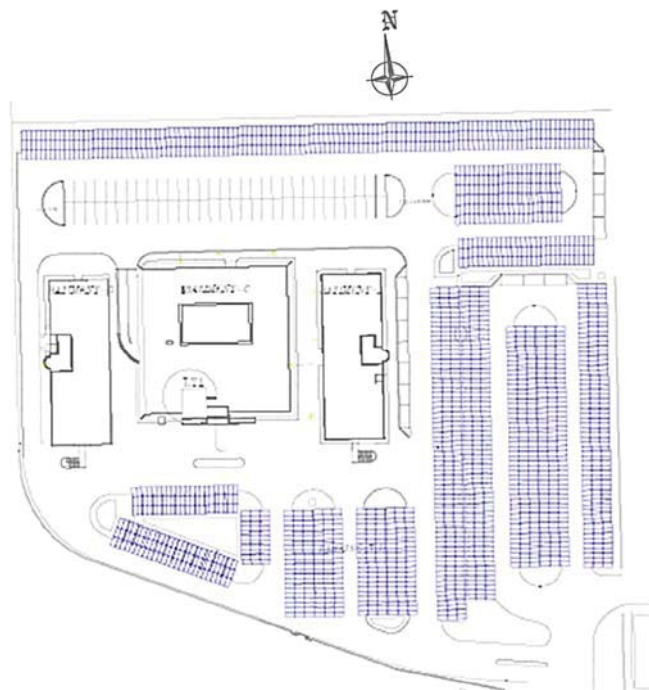


Figure 5.8 – Port Parking PV layout

A part of the parking will not be used to install photovoltaic modules because of the high shades from the buildings.

5.4 Selected Material for the Port's Project

5.4.1 PV Panels

The chosen panel for the Port project is the “LR5-72HBD-530M” manufactured by LONGISOLAR red characterized by the following [26]:

1. A weight of 32.3kg
2. Dimension of 2256x1133x35mm
3. Operational temperature between -40°C and 85°C
4. Maximum power of 530W (Standard Testing Conditions (STC))
5. Open circuit voltage of 49.2V (STC)
6. Short circuit current of 13.71A (STC)
7. Voltage at maximum power 41.35V (STC)
8. Current at maximum power 12.82A (STC)
9. Module efficiency of 20.7%
10. Current-Voltage and Power-Voltage curves at different temperature and at different irradiance are shown in the Figures 5.9, 5.10 and 5.11.

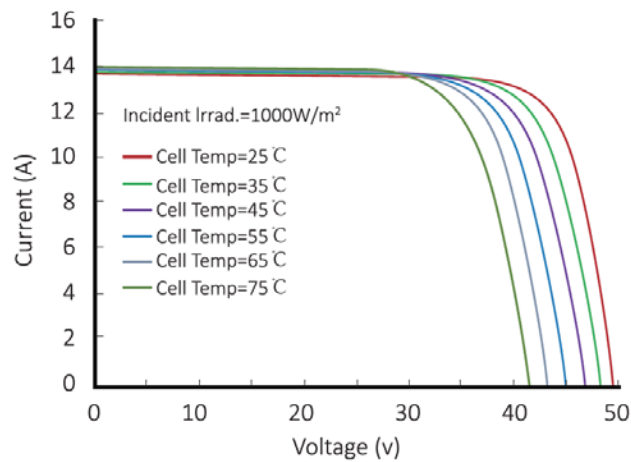


Figure 5.9 – Current Voltage relation of LR5-72HBD-530M at different cell temperature [26]

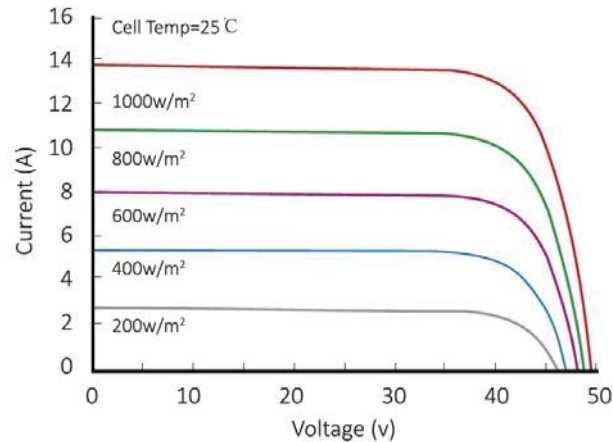


Figure 5.10 – Current Voltage relation of LR5-72HBD-530M at different incident irradiances [26]

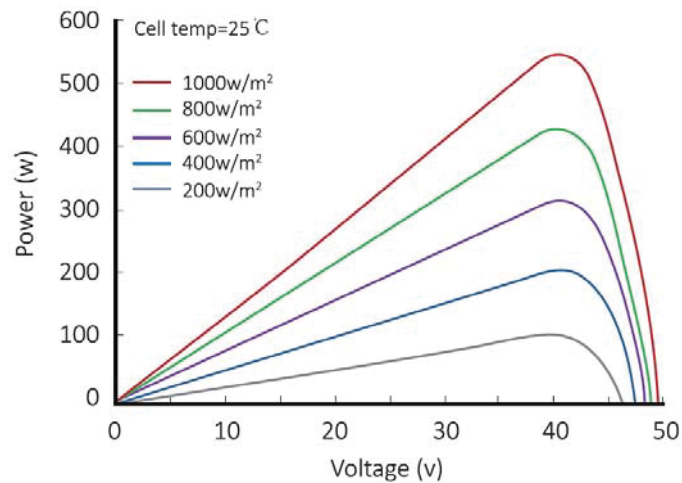


Figure 5.11 –Power Voltage curve of LR5-72HBD-530M at different incident irradiances [26]

5.4.2 Inverter

For the Port application, and among different PV-topologies, the string inverters is more preferably chosen for the following reasons:

1. String inverters have the best watt specific price overall.
2. Less DC cabling.
3. The AC voltage is high enough (around 800V) which allows reduction in the AC cabling cost or the cost of connection to the LV totalizer and transformers.

4. The high DC voltage 1,500Vdc which allows also for cheaper DC side cabling.
5. String inverters have a higher efficiency than central inverters (around 99.1%).
6. Centralized inverters are very heavy and would require additional infrastructure and civil works.
7. Decentralized plants can be handled, serviced and maintained locally without manufacturer specialists unlike for the central inverters.
8. String inverters are readily available in stock in case of any breaks down while the centralized inverters are not.
9. Very high availability in string inverters: if one fails, the remaining ones will keep on generating electricity.
10. Central inverters have 1 MPP tracker while in decentralized systems, each inverter has several MPP trackers.

Figure 5.12 shows the circuit diagram of a Huawei SUN2000-105KTL-H1 string inverter [27]. This inverter is typical to the inverters that will be used in the POB project and is characterized by the following:

1. A number of input of 12 or in other words the ability of connecting and monitoring 12 photovoltaic strings.
2. An efficiency of 99%
3. 6 MMPTs
4. Protection degree of IP65.
5. Integrated surge arresters Type II for both DC and AC sides.
6. Maximum input voltage of 1500Vdc.
7. Maximum short circuit current per MPPT of 33A

8. Maximum AC apparent power of 116kVA
9. Maximum output current of 84.6A
10. MPPT operating voltage range 600V to 1500V

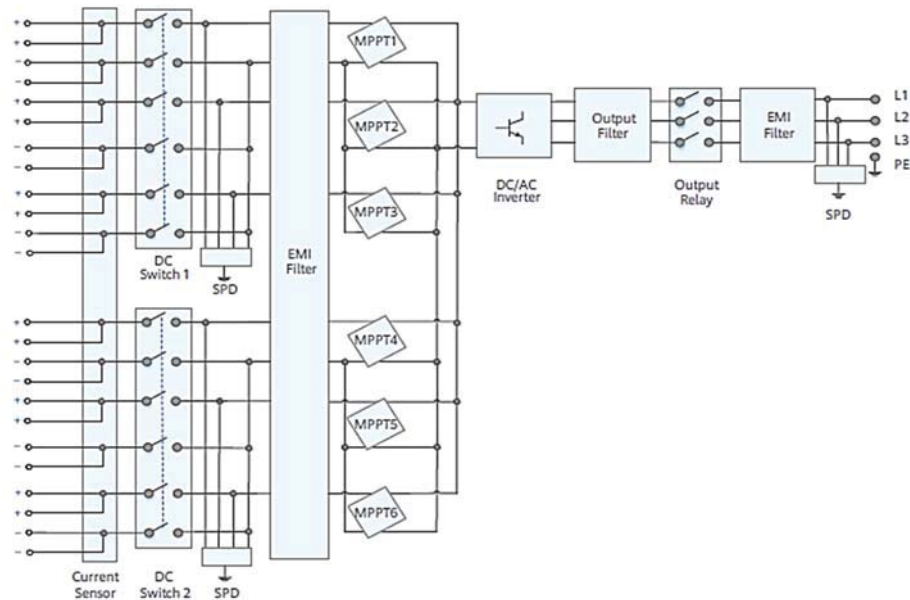


Figure 5.12 –Circuit diagram of a Huawei SUN2000-105KTL-H1 string inverter [27]

5.5 System Configuration

5.5.1 Determining number of Inverter and number of PV panels per inverter

The fact that installing an inverter whose maximum capacity is higher than the nominal capacity of solar panel array may be an option if the system may be expanded at some point in the future, but in general it is recommended to perfectly size the inverter in order to achieve the maximum overall energy yields from the solar system.

In order to check the total number of panels per strings and the number of inverter required based on the previous PV and inverter selection the following steps are performed

Step 1: Finding the minimum string size connected to the inverter

The minimum number of panels that we should put in a string are calculated by dividing the lower limit the MPPT range of the inverter (in this case 600V) by the V_{mp} of the panel (41.35V).

The result is 14.51, which needs to be rounded up to the next whole number. So the minimum string size consists of 15 panels.

Step 2: Finding the maximum string size that doesn't exceed operating voltage

For maximum string size and to ensure that we don't overload the inverter, the maximum DC input (1500V) will be divided by the open circuit voltage V_{oc} of the panel (49.2V).

The result 30.48 is rounded down in order to stay below a maximum threshold. So the maximum number of panels per string is 30 panels.

Step 3: Checking that maximum string size is within MPP range

In the preceding step the maximum string size that keep the inverter operational was found. To ensure that this size is within peak efficiency range, the maximum string size already calculated (30 panels) is multiplied by the voltage at maximum power of the panel V_{mp} (41.35V).

The result 1240.5V falls under the higher end of the MPP range (in this application 1500V). Thus everything checks out here.

Based on these calculations, the string size may range from 15 to 30 panels.

Given that the Huawei chosen inverter can host up to 12 strings and since the best configuration consists in using all strings in order to maximize the number of operating (integrated MPPT controller) 18 panels will be connected in series on each string and a total of 216 panels will be installed on each inverter. Thus 9 string inverters will be used ($1900(\text{panels}) / 216(\text{panels/inverter}) = 9$ inverters) for this project. In this case, 54 MPP trackers are available versus 4 MPP trackers if the central inverter option was adopted. This configuration leads to much less mismatching losses and much higher yield.

Using block design and String Inverters

Most utility-scale plants are designed in blocks since it is the most cost-effective design. Likewise, the project is divided into 4 blocks. By doing so, the work becomes systematic and less cluttered. The medium voltage components of each block are also the same in terms of capacity and specifications, which also reduces the Capital Expenditures (CAPEX) and thus the Levelized Cost of Energy (LCOE).

An analysis was done and based on the locations and distances one new substation was chosen to be introduced.

It is to be noted that both inverters and the switchgear (LV totalizer, transformer LV to MV and MV switchgear, auxiliary transformer) will be placed inside this substation. This substation will incubate separately

1. Inverters
2. LV totalizer
3. Transformer LV to MV
4. MV switchgear

5.5.3 Estimated monthly PV output in KWh for 1MWp PV installation

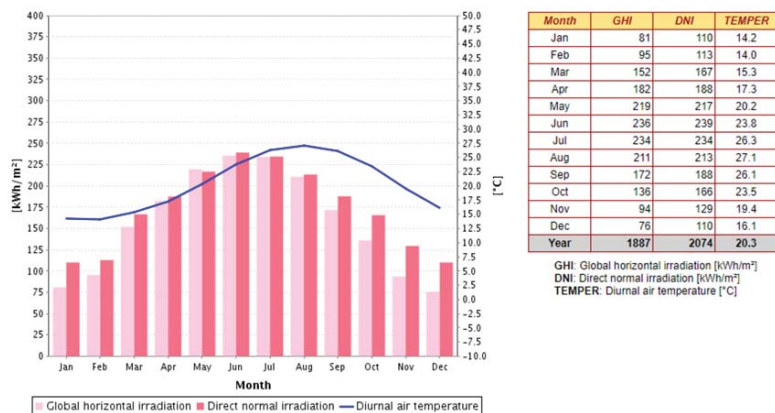
The effective power resulting from such installation is totally related to the solar irradiance and solar data in Lebanon over the years.

The Solar Map shown in Figure 5.13 and the yearly Global Horizontal Irradiation (GHI) shown in Table 5.3 show that a Global GHI in Beirut area ranges between 1500KWh/KWp to 1800KWh/KWp per year [28].



Figure 5.13 –Lebanon Solar GHI Map [28]

Table 5.3 – Yearly GHI chart and table [28]

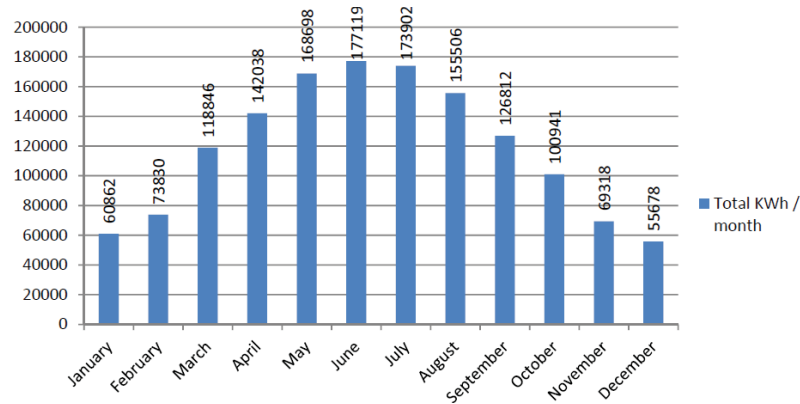


	Jan	Feb	Mar	Apr	May	Jun	Jul	Aug	Sep	Oct	Nov	Dec	Annual
Average Sunlight Hours/ Day	04:13	05:03	06:09	08:06	10:00	11:36	11:36	10:46	09:36	07:54	06:40	04:44	08:02
Average Daylight Hours & Minutes/ Day	10:09	10:54	11:54	12:59	13:53	14:21	14:08	13:22	12:20	11:15	10:22	09:55	12:00
Sunny & (Cloudy) Daylight Hours (%)	42 (58)	47 (53)	52 (48)	63 (37)	73 (27)	82 (18)	83 (17)	81 (19)	79 (21)	71 (29)	65 (35)	48 (52)	67 (33)
Sun altitude at solar noon on the 21st day (°)	36.3	45.6	56.4	68.1	76.4	79.6	76.6	68.3	56.8	45.3	36.2	32.8	56.5

Based on Table 5.3, Table 5.4 shows us the estimated daily KWh on a monthly basis following weather data retrieved over 30 years timeline.

Table 5.4 – Estimated monthly PV output in KWh for 1MWp PV installation at POB [28]

	Total KWh / month	Total KWh / day
January	60862	1963
February	73830	2637
March	118846	3834
April	142038	4735
May	168698	5442
June	177119	5904
July	173902	5610
August	155506	5016
September	126812	4227
October	100941	3256
November	69318	2311
December	55678	1796



From the Table 5.4, it is clear how much the daily KWh varies between the months and that its greater efficiency is between April to August.

5.6 PV KWh output compared to POB KWh consumption

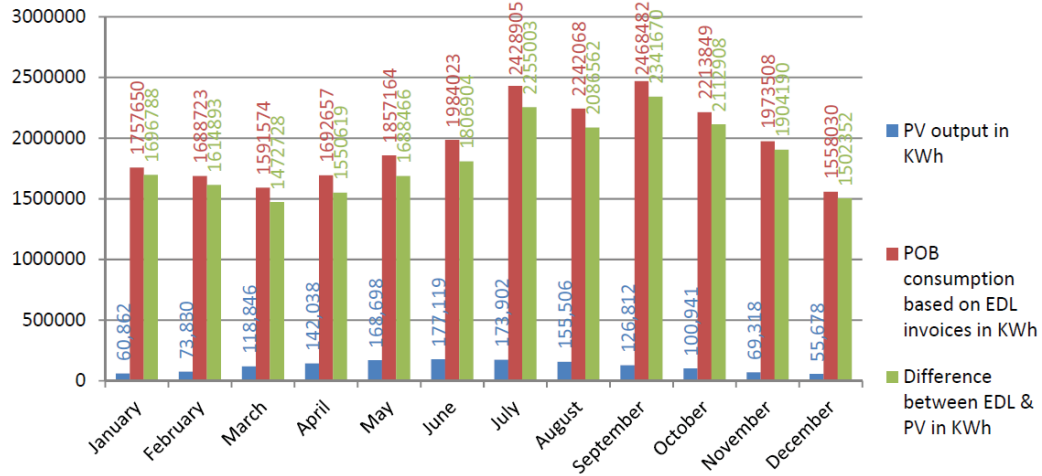
Given the received EDL invoices showing POB power consumption, and compared to the recent above Table 5.4 showing the monthly PV output KWh, we end up by the below

Table 5.5:

Table 5.5 – PV KWh output compared to POB KWh consumption

	PV output in KWh	POB consumption based on EDL invoices in KWh	Difference between EDL & PV in KWh
	KWh / month		
January	60,862	1,757,650	1,696,788
February	73,830	1,688,723	1,614,893
March	118,846	1,591,574	1,472,728
April	142,038	1,692,657	1,550,619
May	168,698	1,857,164	1,688,466
June	177,119	1,984,023	1,806,904
July	173,902	2,428,905	2,255,003
August	155,506	2,242,068	2,086,562
September	126,812	2,468,482	2,341,670

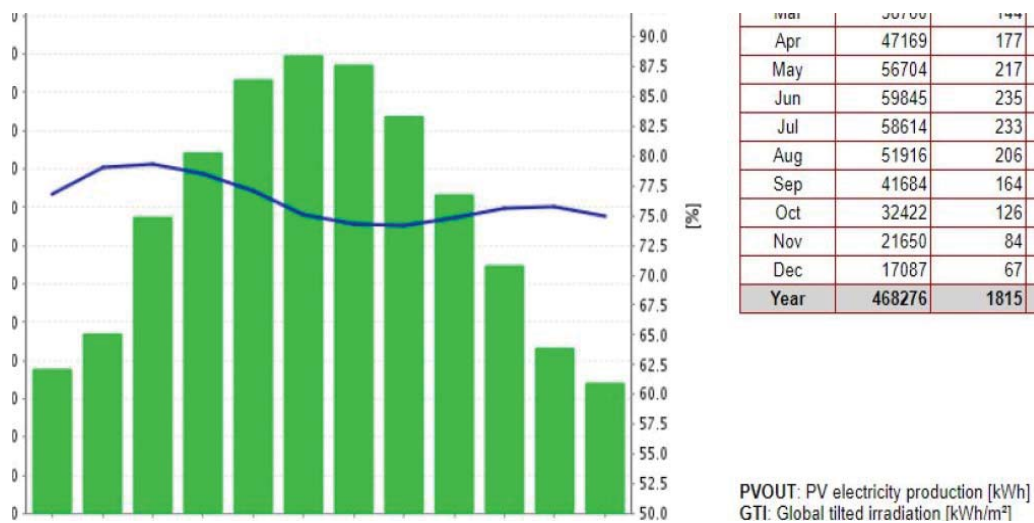
October	100,941	2,213,849	2,112,908
November	69,318	1,973,508	1,904,190
December	55,678	1,558,030	1,502,352
Total	1,423,550	23,456,633	22,033,083



5.7 Energy captured from solar carports according to orientation

- PV output from carports facing South (339KW peak) is shown in Table 5.6

Table 5.6 – South Orientation PVout calculation for 1MWp installation

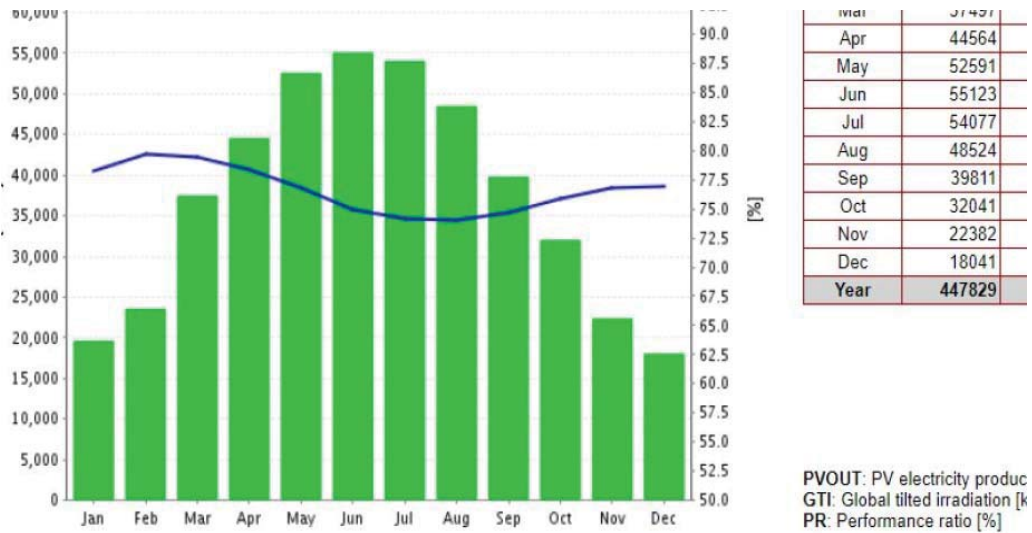


The estimated yearly total output resulting from South Orientation with approximate total

339KW peak installed is A=468,276KWh.

- PV output from carports facing West (311KW peak) is shown in Table 5.7.

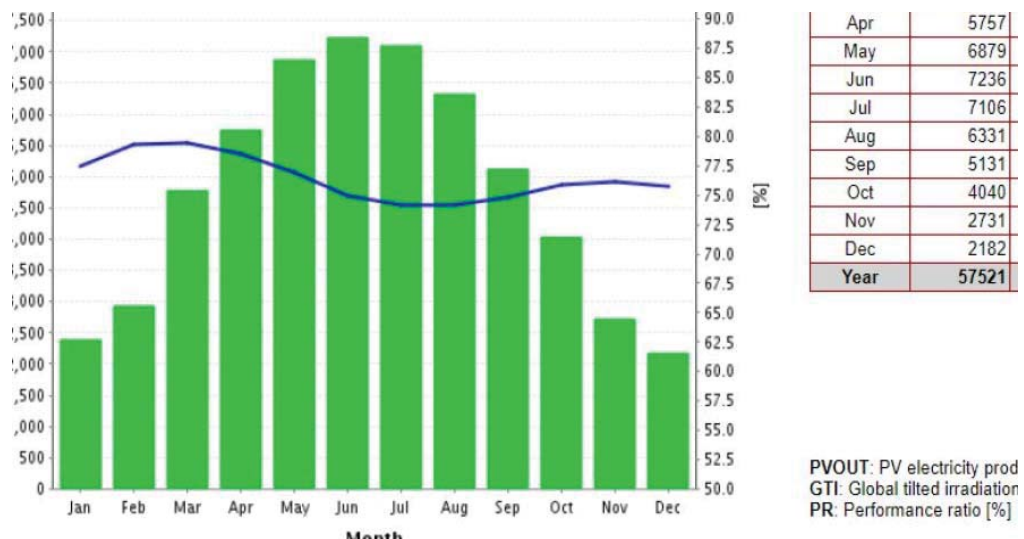
Table 5.7 – East Orientation PV out calculation for 1MWp installation



The estimated yearly total output resulting from West Orientation with approximate total 311KW peak installed is C=447,829KWh.

- PV output from carports facing South West (41KW peak) is shown in Table 5.8.

Table 5.8 – South West Orientation PV out calculation for 1MWp installation



The estimated yearly total output resulting from South West Orientation with approximate total 311KW peak installed is $D=57,521\text{KWh}$.

Therefore from above four tables we note that for 1MW peak installation, the PV installation can grant us a maximum of $E=A+B+C+D=1,423,550\text{KWh}$

5.8 Connecting the renewable energy to the POB grid

Solar energy will be converted to medium voltage (20kV) and connected to the main substation “Poste Principale” as per previous proposals. A technical room shall be built near the parking space to house the LV panel, step up transformer and MV switchgears.

Figure 5.14 shows the schematic for the photovoltaic installation:

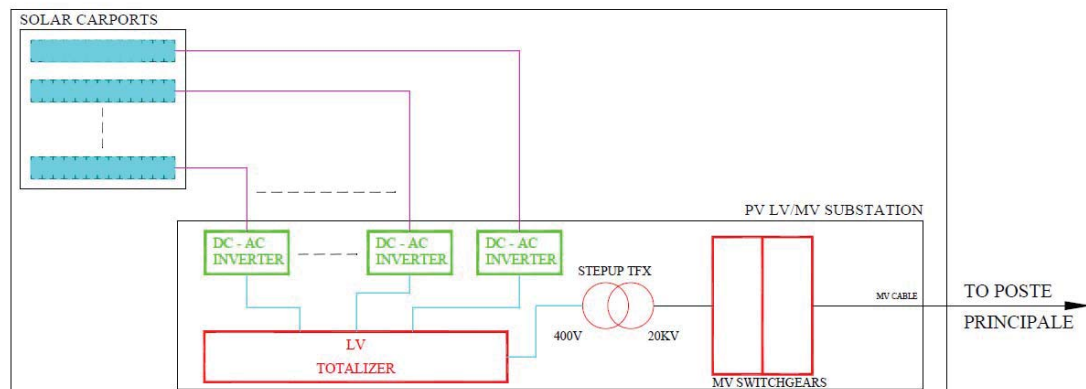


Figure 5.14 –PV installation Schematic

5.9 Approximate Cost Estimate and Return on Investment

An important consideration that PV system owners need to be aware of is the value that the system brings to them. In order to cover this requirement, an engineering economic analysis is developed so that the economic figures are clearly seen. This is done by calculating expected value of the electricity to be generated by the installation and over the lifetime period and then providing that value in dollars per installed watt. For the time

being, solar installations are most impacted by the price of electricity, the rate at which this price is changing, or by various design concerns such as system reliability. Table 5.9 shows the approximate cost of the project.

Table 5.9 – Cost Estimate of the project

PV PANELS	\$300,000.00
STRING INVERTERS	\$60,000.00
PV PANELS INSTALLATION + DC CABLES	\$40,000.00
LV COMPONENTS	\$250,000.00
MAIN STRUCTURE + MOUNTING DEVICES	\$300,000.00
SUB TOTAL	\$950,000.00
Wp price	\$0.95
MV SUBSTATION	\$135,000.00
MV CABLING + EXCAVATION	\$80,000.00
TOTAL	\$1,165,000.00
Wp price	\$1.165

In economic feasibility part, the net present value (NPV) and Return on Investment (ROI) or payback period (PBP) method are analyzed. The NPV as an economic indicator is defined as the value of all future cash flows, calculated at the discount rate. Positive NPV represents an indicator of a potentially feasible project and is provided by Eq. 5.1:

$$NPV = \sum_{n=0}^N \frac{B_n}{(1+i)^n} - \sum_{n=0}^N \frac{C_n}{(1+i)^n} = PVB - PVC \quad 5.1$$

Where

B_n is the expected benefit at the end of the year n ,

C_n is the expected cost at the end of year n ,

i is the discount rate,

n is the project duration in years,

N is the project period,

PVB is the present value benefit

PVC is the present value cost.

The return on investment is substantially indicated by the payback period of the project as stated in Eq. 5.2. The project investment is unacceptable with respect to economics when the ROI presents a high value (long payback periods). ROI does not incorporate the time value of money; moreover, assumptions on discount or interest rates are not required.

Otherwise, the shorter ROI indicates the better investment.

$$ROI \text{ (years)} = \frac{\text{Initial investment (USD)}}{\text{Annual saving } \left(\frac{\text{USD}}{\text{years}}\right)} \quad 5.2$$

From the calculation in above sections:

- The estimated yearly total output from PV panels will be **E**-----
- Approximate EDL rate on MV per KWh is **F**-----
(EDL rate is increased by 30% as per the annunciation of MoEW new plan)
- Yearly maintenance fees-----
- POB shall yearly benefit from is **G**-----
- The total cost of installation of the recommended option is **H**-----
-
- Return on investment is **ROI**-----

$$\mathbf{E} \rightarrow \mathbf{A+B+C+D} = 1,423,550 \text{KWh}$$

$$\mathbf{F} \rightarrow 240 \text{ lbp}$$

$$\mathbf{Y} \rightarrow 18,500 \text{ USD}$$

$$\mathbf{G} \rightarrow \mathbf{E * F} = 341,652,000 \text{ lbp}$$

Or 226,260 USD at USD exchange rate

$$1510 \text{ lbp}$$

$$\mathbf{H} \rightarrow 1,165,000 \text{ USD}$$

$$\mathbf{ROI} \rightarrow \mathbf{H/G} = \mathbf{5.3 \text{ years}}$$

5.10 Connecting the renewable energy to the POB Grid

Given the high renewable energy capacity of 1MWp, the focus was on connecting it directly to POB grid in order to benefit the maximum from all the power generated.

For this purpose, the only solution is to convert the solar energy to medium voltage (20kv) and connect it to the main substation “Poste Principale”.

5.10.1 Excavation and routing to main substation

The last but not least is the MV distribution. In this challenge, the major issue is to find the best routing of the cables in order to execute the excavation avoiding any existing crossing.

Once the MV cables reach the “Poste Principale”, a modification inside this substation is required in order to allow for additional MV switchgear. Figure 5.15 shows the excavation, duct banks and MV cables routing from the PV installation toward the “Poste Principale” station.



Figure 5.15 –Excavation and routing to Poste Principale

5.10.2 Converting the received energy to medium voltage

To convert the solar energy to medium voltage, two options can be adopted as described below:

5.10.2.1 Option 1: String inverters with Independent MV substation

One of the options to convert the solar energy to medium voltage distribution is via string inverters connected to an independent MV substation dedicated for the PV installation.

Allocation for step up transformers, MV switchgears and LV switchgears will be granted inside the independent MV substation taking into consideration port environment as already done in other installed substations.

5.10.2.2 Option 2: Packaged Solution

Another option to convert the solar energy to medium voltage distribution is via connection to a pre-assembled packaged unit that includes the LV parts, Step-Up Transformer and MV switchgear distribution unit.

Both above options are valid and can be executed in our project. However, the recommended solution would be to abide by option 1 for the below listed advantages over option 2:

- The MV substation will be completely independent from the PV System integrator.
- Maintenance of this MV substation will be under same existing maintenance contract of substations inside quay16A.

- Construction of this MV substation will follow same applicable sections and details to avoid water flooding.

Chapter 6: Conclusion

Using the PVsyst simulation software, energy analysis of PV solar system is done. The software was used to tackle the complete aspects needed to design a PV project and to check its feasibility. The simulation allowed the analysis of the power revenue based on credible meteorological data and based on selection among wide range of available solar system manufacturer. In addition the economical part of the project was elaborated and predefined user tools were used to allow easy and reliable economic calculation. The obtained simulation results allowed the comparison of system performance in function of the environmental conditions and in function of shadings and other sources of losses.

This work also introduced a new topology to connect the largescale PV system to the grid. The PV power is injected to the grid through MMC. The use of MMC improve power quality and reduce the grid component such as transformer and filter. The MMC is controlled by using R-MPC technique which is a recently powerful and robust control strategy. The simulation results show a satisfactory performance of the proposed topology. Stability of the proposed topology was achieved. The MMC converter proposed has various advantages when compared to conventional inverters due to the reduction in harmonics, elimination of transformer thereby reducing the losses.

A case study consisting in the installation of a large scale PV system in Lebanon was also mentioned. This PV system is located at Port of Beirut. The complete project implementation was elaborated and the return on investment was calculated.

Appendices

Appendix A: PVsyst Report for NDU Main Campus

PVsyst - Simulation report

Grid-Connected System

Project: NDU Solar

Variant: New simulation variant

Sheds on a building

System power: 605 kWp

Zouq Mosbeh - Lebanon



Project: NDU Solar

Variant: New simulation variant

PVsyst V7.2.16

VCO, Simulation date:
22/07/22 13:05
with v7.2.16

Project summary

Geographical Site

Zouq Mosbeh
Lebanon

Situation

Latitude 33.95 °N
Longitude 35.61 °E
Altitude 203 m
Time zone UTC+2

Project settings

Albedo 0.20

Meteo data

Zouq Mosbeh
PVGIS api TMY

System summary

Grid-Connected System

PV Field Orientation

Fixed plane
Tilt/Azimuth 29 / 0 °

Sheds on a building

Near Shadings

Linear shadings

User's needs

Unlimited load (grid)

System information

PV Array

Nb. of modules 1008 units
Pnom total 605 kWp

Inverters

Nb. of units 15 units
Pnom total 600 kWac
Pnom ratio 1.008

Results summary

Produced Energy 1000 MWh/year Specific production 1654 kWh/kWp/year Perf. Ratio PR 84.91 %

Table of contents

Project and results summary	2
General parameters, PV Array Characteristics, System losses	3
Near shading definition - Iso-shadings diagram	4
Main results	5
Loss diagram	6
Special graphs	7
Cost of the system	8
Financial analysis	9
CO ₂ Emission Balance	11



PVsyst V7.2.16

VC0, Simulation date:
22/07/22 13:05
with v7.2.16

General parameters

Grid-Connected System		Sheds on a building	
PV Field Orientation		Sheds configuration	
Orientation		Nb. of sheds	58 units
Fixed plane		Sizes	
Tilt/Azimuth	29 / 0 °	Sheds spacing	2.00 m
		Collector width	1.13 m
		Ground Cov. Ratio (GCR)	56.7 %
		Shading limit angle	
		Limit profile angle	28.5 °
Horizon		Near Shadings	
Free Horizon		Linear shadings	
		Models used	
		Transposition	Perez
		Diffuse	Imported
		Circumsolar	separate
		User's needs	
		Unlimited load (grid)	

PV Array Characteristics

PV module		Inverter	
Manufacturer	Jinkosolar	Manufacturer	Huawei Technologies
Model	JKM-600N-78HL4-BDV	Model	SUN2000-40KTL-M3-380V
(Original PVsyst database)		(Original PVsyst database)	
Unit Nom. Power	600 Wp	Unit Nom. Power	40.0 kWac
Number of PV modules	1008 units	Number of inverters	15 units
Nominal (STC)	605 kWp	Total power	600 kWac
Modules	72 Strings x 14 In series	Operating voltage	200-1000 V
At operating cond. (50°C)		Max. power (=>40°C)	44.0 kWac
Pmpp	560 kWp	Pnom ratio (DC:AC)	1.01
U mpp	589 V		
I mpp	951 A		
Total PV power		Total inverter power	
Nominal (STC)	605 kWp	Total power	600 kWac
Total	1008 modules	Number of inverters	15 units
Module area	2818 m ²	Pnom ratio	1.01

Array losses

Thermal Loss factor		DC wiring losses		Module Quality Loss				
Module temperature according to irradiance		Global array res.	10 mΩ	Loss Fraction	-0.8 %			
Uc (const)	20.0 W/m ² K	Loss Fraction	1.5 % at STC					
Uv (wind)	0.0 W/m ² K/m/s							
Module mismatch losses		Strings Mismatch loss						
Loss Fraction	2.0 % at MPP	Loss Fraction	0.1 %					
IAM loss factor	Incidence effect (IAM): Fresnel, AR coating, n(glass)=1.526, n(AR)=1.290							
0°	30°	50°	60°	70°	75°	80°	85°	90°
1.000	0.999	0.987	0.962	0.892	0.816	0.681	0.440	0.000



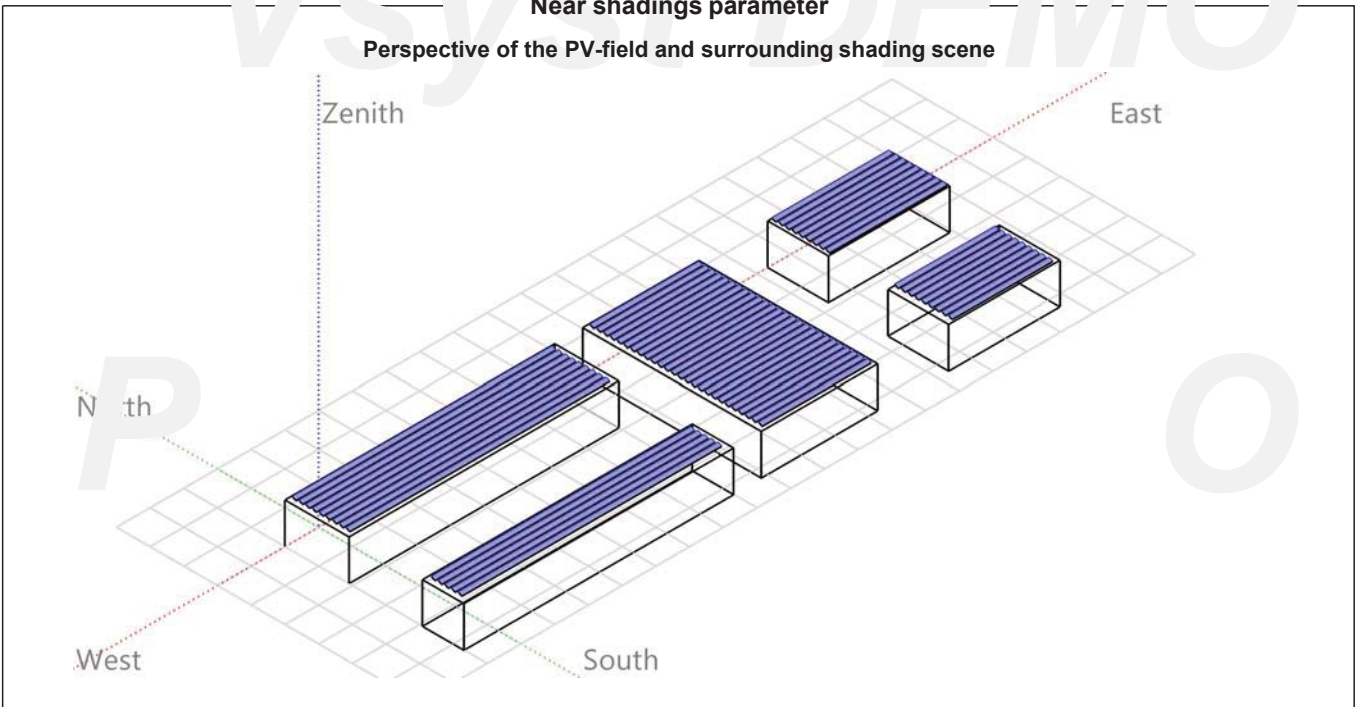
PVsyst V7.2.16

VC0, Simulation date:
22/07/22 13:05
with v7.2.16

Vsyst DEMO

Near shadings parameter

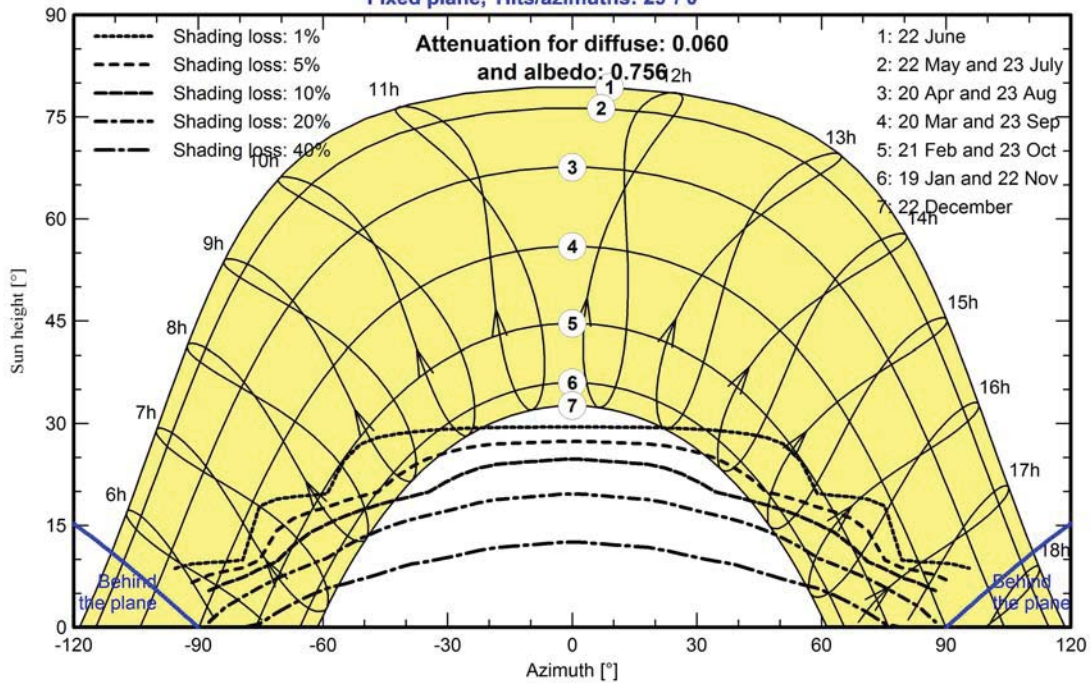
Perspective of the PV-field and surrounding shading scene



Iso-shadings diagram

Orientation #1

Fixed plane, Tilts/azimuths: 29°/ 0°



Vsyst DEMO



PVsyst V7.2.16

VC0, Simulation date:
22/07/22 13:05
with v7.2.16

Main results

System Production

Produced Energy 1000 MWh/year Specific production 1654 kWh/kWp/year
Performance Ratio PR 84.91 %

Economic evaluation

Investment

Global 539406.80 USD
Specific 0.89 USD/Wp

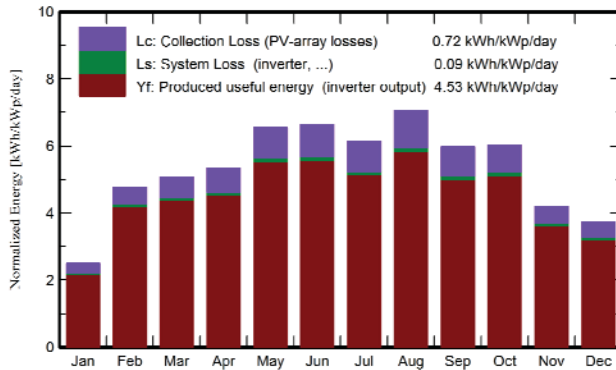
Yearly cost

Annuities Run. 43954.73 USD/yr
costs Payback period 3.7 years

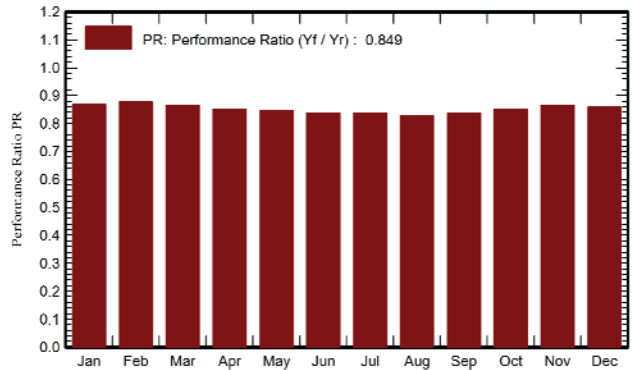
LCOE

Energy cost 0.04 USD/kWh

Normalized productions (per installed kWp)



Performance Ratio PR



Balances and main results

	GlobHor	DiffHor	T_Amb	GlobInc	GlobEff	EArray	E_Grid	PR
	kWh/m ²	kWh/m ²	°C	kWh/m ²	kWh/m ²	MWh	MWh	ratio
January	58.1	36.91	9.86	77.5	72.1	41.5	40.6	0.867
February	99.5	38.49	11.14	133.8	129.0	72.3	70.9	0.877
March	134.5	60.12	13.48	157.0	150.9	83.9	82.3	0.867
April	153.7	63.58	16.54	160.4	153.5	84.1	82.5	0.850
May	209.7	80.18	19.85	203.0	194.1	105.9	103.8	0.846
June	216.7	84.69	22.38	199.5	189.8	103.2	101.3	0.839
July	202.9	90.06	24.42	190.6	180.8	98.3	96.5	0.837
August	214.0	72.82	26.29	218.8	209.8	111.8	109.7	0.829
September	159.2	62.23	23.77	179.1	171.9	92.6	90.8	0.838
October	141.7	46.64	20.23	186.5	180.3	97.9	96.0	0.851
November	86.5	33.57	14.05	125.7	120.1	67.0	65.7	0.865
December	75.1	31.05	12.04	115.9	108.6	61.3	60.2	0.858
Year	1751.7	700.34	17.88	1947.8	1861.0	1019.8	1000.2	0.849

Legends

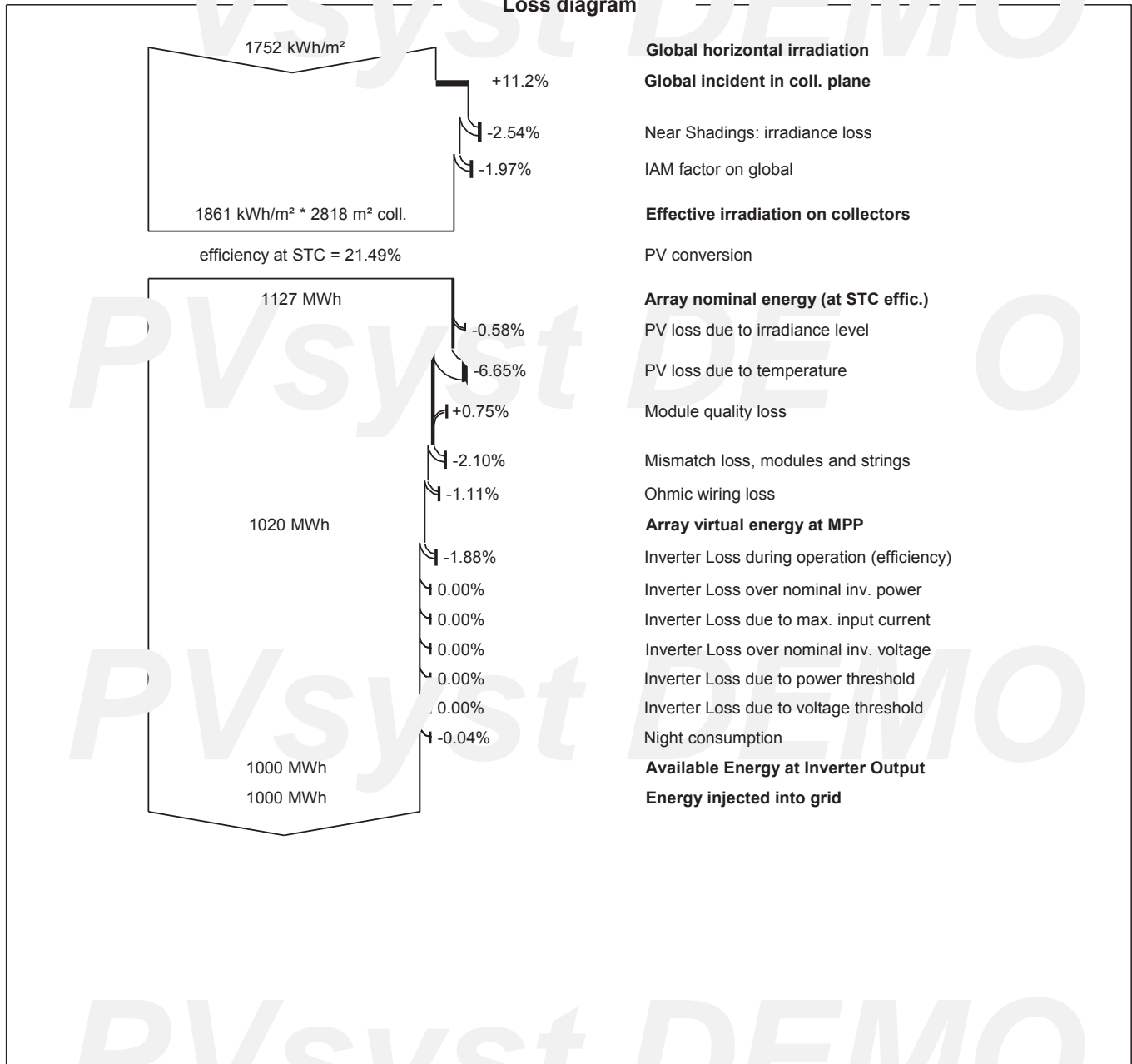
GlobHor	Global horizontal irradiation	EArray	Effective energy at the output of the array
DiffHor	Horizontal diffuse irradiation	E_Grid	Energy injected into grid
T_Amb	Ambient Temperature	PR	Performance Ratio
GlobInc	Global incident in coll. plane		
GlobEff	Effective Global, corr. for IAM and shadings		



PVsyst V7.2.16

VCO, Simulation date:
22/07/22 13:05
with v7.2.16

Loss diagram



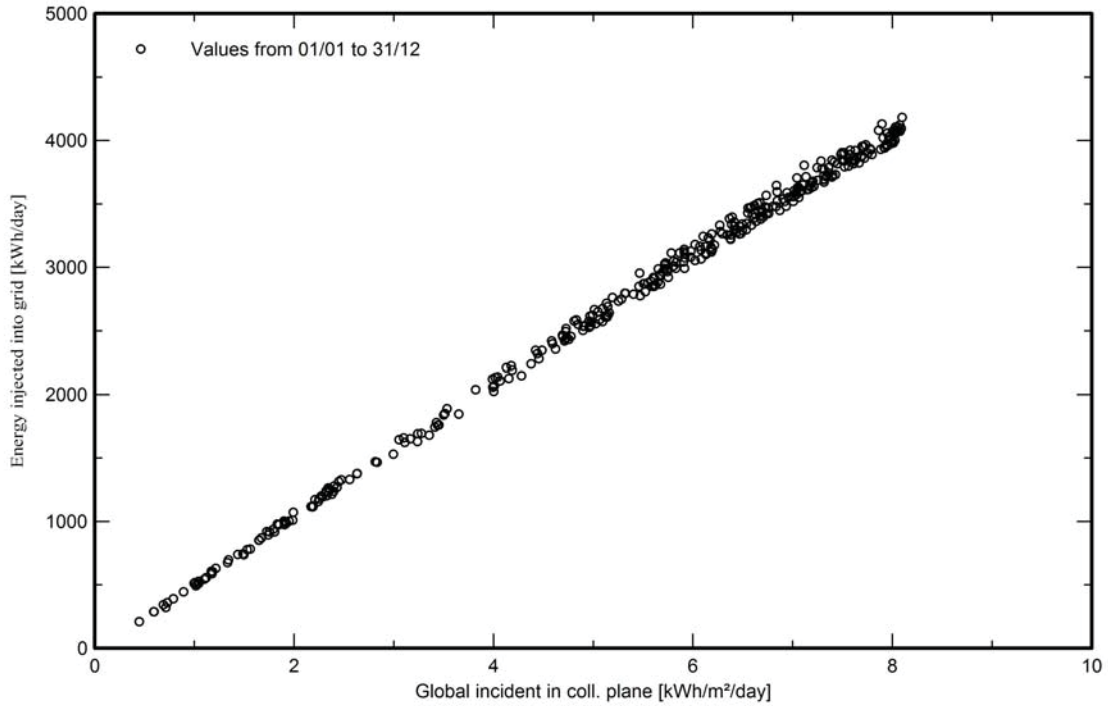


PVsyst V7.2.16

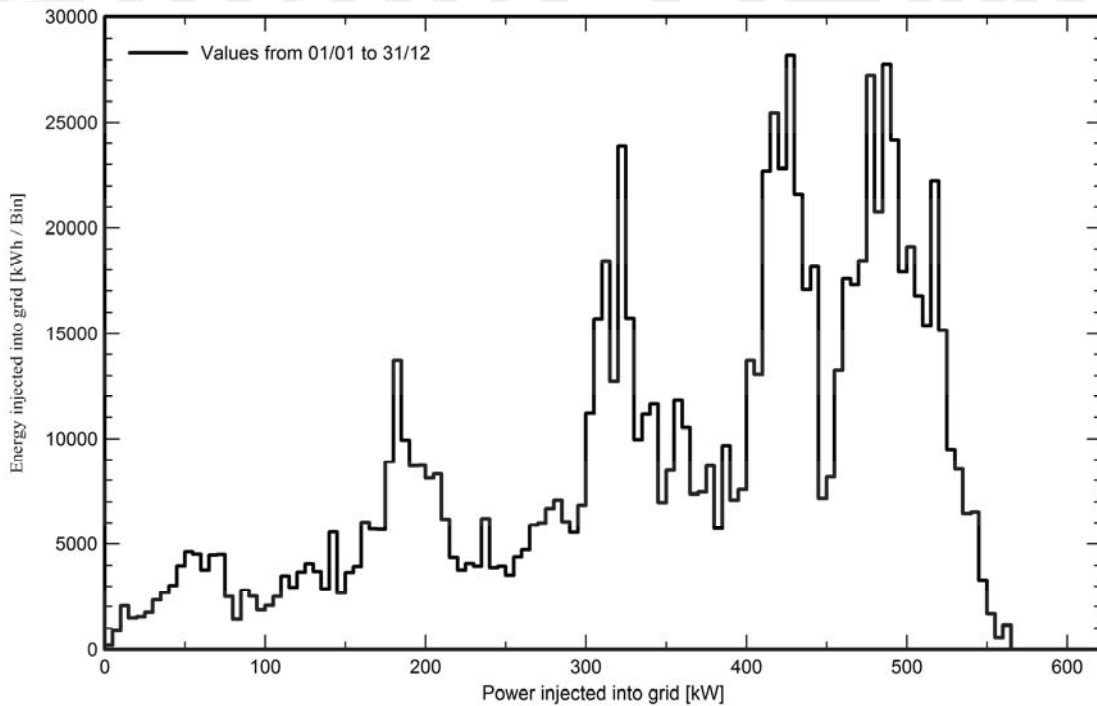
VC0, Simulation date:
22/07/22 13:05
with v7.2.16

Special graphs

Daily Input/Output diagram



System Output Power Distribution





PVsyst V7.2.16

VC0, Simulation date:
 22/07/22 13:05
 with v7.2.16

Cost of the system

Installation costs

Item	Quantity units	Cost USD	Total USD
PV modules			
JKM-600N-78HL4-BDV	1008	204.00	205632.00
Supports for modules	1008	50.00	50400.00
Inverters			
SUN2000-40KTL-M3-380V	15	4000.00	60000.00
Other components			
Accessories, fasteners	4032	1.00	4032.00
Wiring	2000	1.70	3400.00
Site arranger	135	100.00	13500.00
Studies and analysis			
Engineering		25000.00	25000.00
Installation			
Global installation cost per module	1008	100.00	100800.00
Global installation cost per inverter	15	1000.00	15000.00
Grid connection	1	19500.00	19500.00
Taxes			
VAT	1	0.00	42142.80
Total			539406.80
Depreciable asset			320064.00

Operating costs

Item	Total USD/year
Maintenance	
Cleaning	10000.00
Total (OPEX)	10000.00
Including inflation (1.43%)	11482.48

System summary

Total installation cost	539406.80 USD
Operating costs (incl. inflation 1.43%/year)	11482.48 USD/year
Produced Energy	1000 MWh/year
Cost of produced energy (LCOE)	0.043 USD/kWh



PVsyst V7.2.16

VC0, Simulation date:
22/07/22 13:05
with v7.2.16

Financial analysis

Simulation period

Project lifetime 20 years Start year 2023

Income variation over time

Inflation 1.43 %/year
Production variation (aging) 0.00 %/year
Discount rate 0.00 %/year

Income dependent expenses

Income tax rate 0.00 %/year
Other income tax 0.00 %/year
Dividends 0.00 %/year

Financing

Own funds 200000.00 USD
Loan - Redeemable with fixed annuity - 10 years 339406.80 USD Interest rate: 5.00%/year

Electricity sale

Feed-in tariff 0.2000 USD/kWh
Duration of tariff warranty 1 years
Annual connection tax 0.00 USD/kWh
Annual tariff variation +10.0 %/year
Feed-in tariff decrease after warranty 20.00 %

Return on investment

Payback period 3.7 years

Return on investment (ROI) 439.9 %

Detailed economic results (USD)

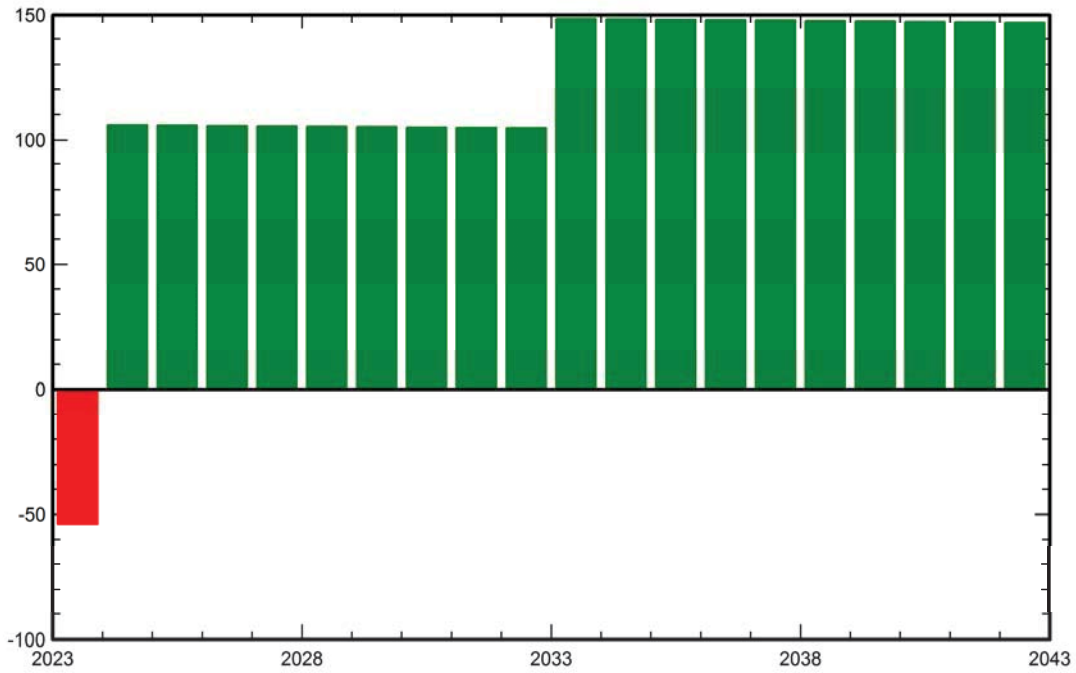
	Electricity sale	Loan principal	Loan interest	Run. costs	Deprec. allow.	Taxable income	Taxes	After-tax profit	Cumul. profit	% amort.
2023	200126	26984	16970	10000	0	173156	0	146171	-53829	32.1%
2024	160101	28334	15621	10143	0	134337	0	106003	52174	57.0%
2025	160101	29750	14204	10288	0	135608	0	105858	158033	82.1%
2026	160101	31238	12717	10435	0	136949	0	105711	263744	107.5%
2027	160101	32800	11155	10584	0	138361	0	105562	369305	133.2%
2028	160101	34440	9515	10736	0	139850	0	105410	474716	159.1%
2029	160101	36162	7793	10889	0	141419	0	105257	579972	185.3%
2030	160101	37970	5985	11045	0	143071	0	105101	685074	211.9%
2031	160101	39868	4086	11203	0	144811	0	104943	790017	238.7%
2032	160101	41862	2093	11363	0	146645	0	104783	894800	265.9%
2033	160101	0	0	11526	0	148575	0	148575	1043375	293.4%
2034	160101	0	0	11690	0	148410	0	148410	1191786	320.9%
2035	160101	0	0	11858	0	148243	0	148243	1340029	348.4%
2036	160101	0	0	12027	0	148074	0	148074	1488102	375.9%
2037	160101	0	0	12199	0	147902	0	147902	1636004	403.3%
2038	160101	0	0	12374	0	147727	0	147727	1783731	430.7%
2039	160101	0	0	12551	0	147550	0	147550	1931282	458.0%
2040	160101	0	0	12730	0	147371	0	147371	2078653	485.4%
2041	160101	0	0	12912	0	147189	0	147189	2225841	512.6%
2042	160101	0	0	13097	0	147004	0	147004	2372845	539.9%
Total	3242042	339407	100141	229650	0	2912252	0	2572845	2372845	539.9%



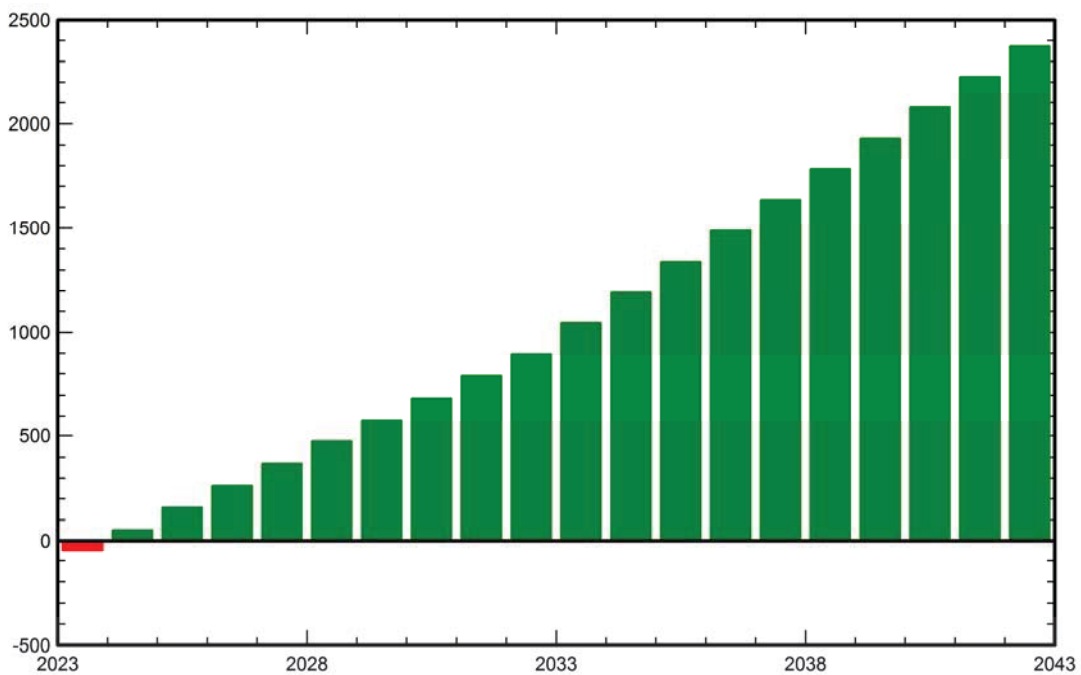
PVsyst V7.2.16

VC0, Simulation date:
22/07/22 13:05
with v7.2.16

Financial analysis
Yearly net profit (kUSD)



Cumulative cashflow (kUSD)





PVsyst V7.2.16

VCO, Simulation date:
 22/07/22 13:05
 with v7.2.16

CO₂ Emission Balance

Total: 17499.1 tCO₂

Generated emissions

Total: 1090.94 tCO₂

Source: Detailed calculation from table below:

Replaced Emissions

Total: 21425.3 tCO₂

System production: 1000.25 MWh/yr

Grid Lifecycle Emissions: 714 gCO₂/kWh

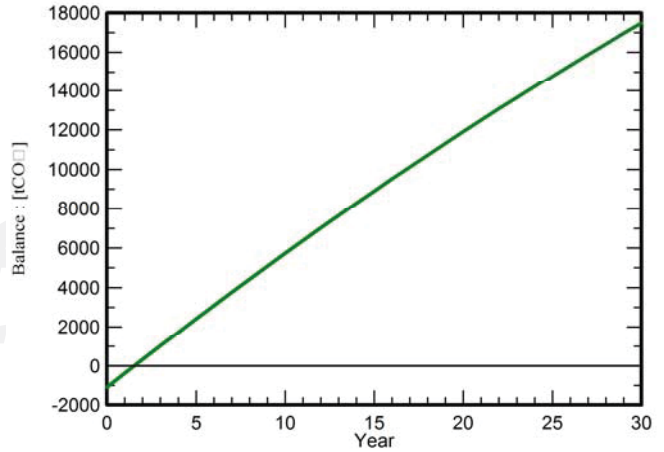
Source: IEA List

Country: Lebanon

Lifetime: 30 years

Annual degradation: 1.0 %

Saved CO₂ Emission vs. Time



System Lifecycle Emissions Details

Item	LCE	Quantity	Subtotal
			[kgCO ₂]
Modules	1713 kgCO ₂ /kWp	605 kWp	1035853
Supports	4.76 kgCO ₂ /kg	10080 kg	48005
Inverters	472 kgCO ₂ /units	15.0 units	7

Appendix B: PV panel Jinko JKM590-610N-78HL4-BDV-F1-EN

Tiger Neo N-type 78HL4-BDV 590-610 Watt

BIFACIAL MODULE WITH
DUAL GLASS

N-Type

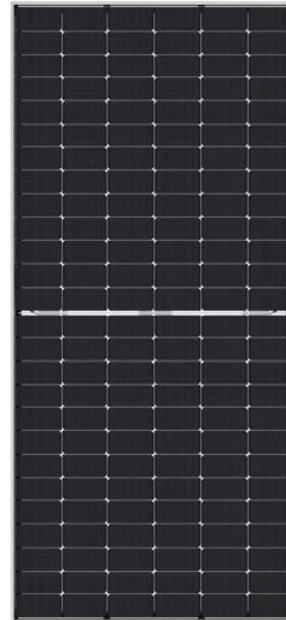
Positive power tolerance of 0~+3%

IEC61215(2016), IEC61730(2016)

ISO9001:2015: Quality Management System

ISO14001:2015: Environment Management System

ISO45001:2018
Occupational health and safety management systems



Key Features



SMBB Technology

Better light trapping and current collection to improve module power output and reliability.



PID Resistance

Excellent Anti-PID performance guarantee via optimized mass-production process and materials control.



Higher Power Output

Module power increases 5-25% generally, bringing significantly lower LCOE and higher IRR.



Hot 2.0 Technology

The N-type module with Hot 2.0 technology has better reliability and lower LID/LETID.

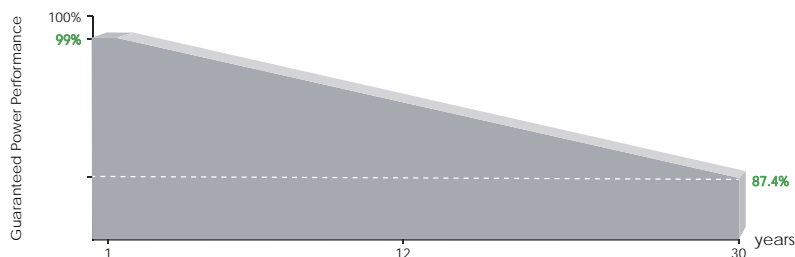


Enhanced Mechanical Load

Certified to withstand: wind load (2400 Pascal) and snow load (5400 Pascal).



LINEAR PERFORMANCE WARRANTY

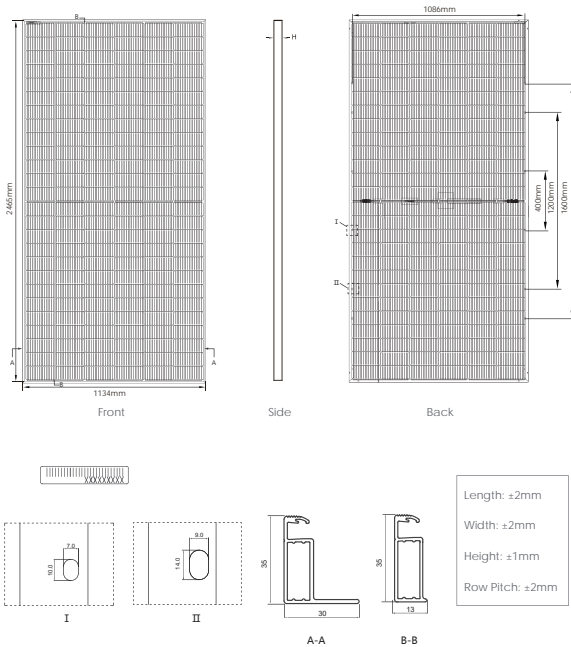


12 Year Product Warranty

30 Year Linear Power Warranty

0.40% Annual Degradation Over 30 years

Engineering Drawings

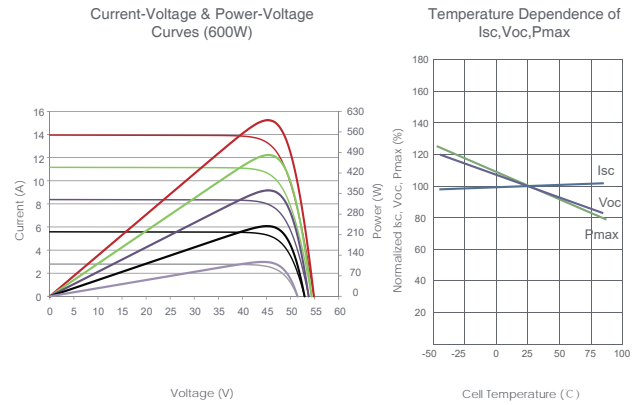


Packaging Configuration

(Two pallets = One stack)

31pcs/pallets, 62pcs/stack, 496pcs/ 40'HQ Container

Electrical Performance & Temperature Dependence



Mechanical Characteristics

Cell Type	N type Mono-crystalline
No. of cells	156 (2×78)
Dimensions	2465×1134×35mm (97.05×44.65×1.38 inch)
Weight	34.6kg (76.38 lbs)
Front Glass	2.0mm, Anti-Reflection Coating
Back Glass	2.0mm, Heat Strengthened Glass
Frame	Anodized Aluminium Alloy
Junction Box	IP68 Rated
Output Cables	TUV 1×4.0mm ² (+): 400mm, (-): 200mm or Customized Length

SPECIFICATIONS

Module Type	JKM590N-78HL4-BDV		JKM595N-78HL4-BDV		JKM600N-78HL4-BDV		JKM605N-78HL4-BDV		JKM610N-78HL4-BDV	
	STC	NOCT	STC	NOCT	STC	NOCT	STC	NOCT	STC	NOCT
Maximum Power (Pmax)	590Wp	444Wp	595Wp	447Wp	600Wp	451Wp	605Wp	455Wp	610Wp	459Wp
Maximum Power Voltage (Vmp)	44.91V	41.89V	45.08V	42.00V	45.25V	42.12V	45.42V	42.23V	45.60V	42.35V
Maximum Power Current (Imp)	13.14A	10.59A	13.20A	10.65A	13.26A	10.71A	13.32A	10.77A	13.38A	10.83A
Open-circuit Voltage (Voc)	54.76V	52.02V	54.90V	52.15V	55.03V	52.27V	55.17V	52.41V	55.31V	52.54V
Short-circuit Current (Isc)	13.71A	11.07A	13.79A	11.13A	13.87A	11.20A	13.95A	11.26A	14.03A	11.33A
Module Efficiency STC (%)	21.11%		21.29%		21.46%		21.64%		21.82%	
Operating Temperature(°C)	-40°C~+85°C									
Maximum system voltage	1500VDC (IEC)									
Maximum series fuse rating	30A									
Power tolerance	0~+3%									
Temperature coefficients of Pmax	-0.30%/°C									
Temperature coefficients of Voc	-0.25%/°C									
Temperature coefficients of Isc	0.046%/°C									
Nominal operating cell temperature (NOCT)	45±2°C									
Refer. Bifacial Factor	80±5%									

BIFACIAL OUTPUT-REAR SIDE POWER GAIN

		5%		15%		25%	
		Maximum Power (Pmax)	Module Efficiency STC (%)	Maximum Power (Pmax)	Module Efficiency STC (%)	Maximum Power (Pmax)	Module Efficiency STC (%)
5%	Maximum Power (Pmax)	620Wp	625Wp	630Wp	635Wp	641Wp	
	Module Efficiency STC (%)	22.16%	22.35%	22.54%	22.73%	22.91%	
15%	Maximum Power (Pmax)	679Wp	684Wp	690Wp	696Wp	702Wp	
	Module Efficiency STC (%)	24.27%	24.48%	24.68%	24.89%	25.10%	
25%	Maximum Power (Pmax)	738Wp	744Wp	750Wp	756Wp	763Wp	
	Module Efficiency STC (%)	26.38%	26.61%	26.83%	27.05%	27.28%	

*STC: Irradiance 1000W/m² Cell Temperature 25°C AM=1.5
 NOCT: Irradiance 800W/m² Ambient Temperature 20°C AM=1.5 Wind Speed 1m/s

References

- [1] The MathWorks, INC., MATLAB, version R2016a (Natick, MA: The MathWorks, Inc., 2016), <https://www.mathworks.com>.
- [2] International Renewable Energy Agency, “Statistics Time Series - Trends in Renewable Energy”, IRENARETimeSeries, Available: <https://www.irena.org/Statistics/View-Data-by-Topic/Capacity-and-Generation/Statistics-Time-Series>.
- [3] Lebanese Republic Ministry of Energy and Water, “Updated Policy Paper for the Electricity Sector”, March 2019, Available: https://www.energyandwater.gov.lb/mediafiles/articles/doc-100515-2019_05_21_04_27_25.pdf
- [4] M.Manikandan, N.Deepa Arun, P.Sivaranjini, M.Suresh, R.Ashok Kumar, “Developing an Equivalent Circuit Model Based M-File for Solar Photovoltaic Applications”, International Journal of Advanced Research in Electrical Electronics and Instrumentation Engineering, Vol. 4, Issue 9, September 2015
- [5] V. Singh, A.N. Tiwari, “Study and Comparison of various types of Converters used for Solar PV: A Review”, 2018 International Conference on Power Energy, Environment and Intelligent Control (PEEIC), G. L. Bajaj Inst. of Technology and Management Greater Noida, U. P., India, Apr 13-14, 2018
- [6] K. Boudaraia, H. Mahmoudi, A. Abbou, M. Hilal, "Buck converter MPPT control of a photovoltaic system", Multimedia Computing and Systems (ICMCS) 2016 5th International Conference on, pp. 783-787, 2016, ISSN 2472-7652
- [7] H Oldenkamp, IJ. Jong, "AC modules: past present and future", Proceedings of Workshop Installing the Solar Solution, vol. 98, 1998.
- [8] A. Fernandez-Infantes, J. Contreras and J. L. Bernal-Agustin, “Design of grid connected PV systems considering electrical, economical and environmental aspects: A practical case”, Renewable Energy, 2005, pp. 2049.
- [9] T. Esum, P. Chapman, “Comparison of Photovoltaic Array Maximum Power Point Tracking Techniques”, IEEE TRANSACTIONS ON ENERGY CONVERSION, VOL. 22, NO. 2, JUNE 2007
- [10] B. Gutierrez, SS. Kwak, “Modular Multilevel Converters (MMCs) Controlled by Model Predictive Control With Reduced Calculation Burden”, IEEE TRANSACTIONS ON POWER ELECTRONICS, VOL. 33, NO. 11, pp. 9176-9187, Nov 2018

- [11] M. Liu, Z. Li, X. Yang, "A Universal Mathematical Model of Modular Multilevel Converter with Half-Bridge", *Energies* 2020, 13, 4464
- [12] W. Guan, S. Huang, D. Luo, F. Rong, "A Reverse Model Predictive Control Strategy for a Modular Multilevel Converter", *Energies* 2019, 12, 297
- [13] P. Liu, Y. Wang, W. Cong, W. Lei, "Grouping-Sorting-Optimized Model Predictive Control for Modular Multilevel Converter With Reduced Computational Load", *IEEE TRANSACTIONS ON POWER ELECTRONICS*, VOL. 31, NO. 3, pp.1896-1907, Mar 2016
- [14] J. Rodriguez and P. Cortes, *Predictive Control of Power Converters and Electrical Drives*. Hoboken, NJ, USA: Wiley, 2012.
- [15] PVsyst version 7.2, Copyright (c) 2009-2010, Victor Derevyanko, <https://www.pvsyst.com>
- [16] Google Earth Version 9.171.0.0-Web Assembly with threads, <https://earth.google.com/>
- [17] Pvsyst contextual help (built-in software). URL <http://files.pvsyst.com/help/index.html>
- [18] Arno H. M. Smets, Klaus Jäger, Olindo Isabella, René A. C. M. M. van Swaaij, and Miro Zeman. *Solar energy : the physics and engineering of photovoltaic conversion, technologies and systems*. UIT Cambridge, Cambridge, 2016. ISBN 978-1-906860- 32-5.
- [19] PVsyst. (2018, November). Economic evaluation. Retrieved from http://files.pvsyst.com/help/economic_evaluation.htm
- [20] Michael Taylor and Eun young So. *Projected Costs of Generating Electricity 2015 edition*, . URL <https://www.iea.org/publications/freepublications/publication/projected-costs-of-generating-electricity-2015-edition.html>.
- [21] Port of Beirut Official website, <http://www.portdebeyrouth.com>
- [22] Port of Beirut As-Built drawing and operation documents, Project Reference: POB Extension of Existing Power Plant, Younes Bros, April 2015
- [23] Port of Beirut As-Built drawing, Project Reference: POB Power Plant, SAKR, 2007

- [24] Port of Beirut Tender drawing, Project Reference: POB Infrastructure, SERT Consultants, 2012
- [25] P. Salameh, N. Mendalek, “Planning of Photovoltaic Power Plant in the Middle East”, 6th IEEE International Energy Conference (ENERGYCON), 2020
- [26] LONGISOLAR LR5-72HBD-530 https://en.longi-solar.com/home/products/Hi_MO5.html
- [27] Huawei SUN2000-105KTL-H1, <https://support.huawei.com/enterprise/en/network-energy/sun2000-pid-7551590>
- [28] World Bank official website, Global Solar Atlas, Location Lebanon, <https://olc.worldbank.org/content/global-solar-atlas>
- [29] Jake Lomansoc, Ricard Jun Roloma, Kim Seer Paller, Design and Simulation of 100 kWp Solar Photovoltaic (PV) Grid Connected Power Plant Using PVsyst.

References

- [1] The MathWorks, INC., MATLAB, version R2016a (Natick, MA: The MathWorks, Inc., 2016), <https://www.mathworks.com>.
- [2] International Renewable Energy Agency, “Statistics Time Series - Trends in Renewable Energy”, IRENARETimeSeries, Available: <https://www.irena.org/Statistics/View-Data-by-Topic/Capacity-and-Generation/Statistics-Time-Series>.
- [3] Lebanese Republic Ministry of Energy and Water, “Updated Policy Paper for the Electricity Sector”, March 2019, Available: https://www.energyandwater.gov.lb/mediafiles/articles/doc-100515-2019_05_21_04_27_25.pdf
- [4] M.Manikandan, N.Deepa Arun, P.Sivaranjini, M.Suresh, R.Ashok Kumar, “Developing an Equivalent Circuit Model Based M-File for Solar Photovoltaic Applications”, International Journal of Advanced Research in Electrical Electronics and Instrumentation Engineering, Vol. 4, Issue 9, September 2015
- [5] V. Singh, A.N. Tiwari, “Study and Comparison of various types of Converters used for Solar PV: A Review”, 2018 International Conference on Power Energy, Environment and Intelligent Control (PEEIC), G. L. Bajaj Inst. of Technology and Management Greater Noida, U. P., India, Apr 13-14, 2018
- [6] K. Boudaraia, H. Mahmoudi, A. Abbou, M. Hilal, "Buck converter MPPT control of a photovoltaic system", Multimedia Computing and Systems (ICMCS) 2016 5th International Conference on, pp. 783-787, 2016, ISSN 2472-7652
- [7] H Oldenkamp, IJ. Jong, "AC modules: past present and future", Proceedings of Workshop Installing the Solar Solution, vol. 98, 1998.
- [8] A. Fernandez-Infantes, J. Contreras and J. L. Bernal-Agustin, “Design of grid connected PV systems considering electrical, economical and environmental aspects: A practical case”, Renewable Energy, 2005, pp. 2049.
- [9] T. Esum, P. Chapman, “Comparison of Photovoltaic Array Maximum Power Point Tracking Techniques”, IEEE TRANSACTIONS ON ENERGY CONVERSION, VOL. 22, NO. 2, JUNE 2007
- [10] B. Gutierrez, SS. Kwak, “Modular Multilevel Converters (MMCs) Controlled by Model Predictive Control With Reduced Calculation Burden”, IEEE TRANSACTIONS ON POWER ELECTRONICS, VOL. 33, NO. 11, pp. 9176-9187, Nov 2018

- [11] M. Liu, Z. Li, X. Yang, “A Universal Mathematical Model of Modular Multilevel Converter with Half-Bridge”, *Energies* 2020, 13, 4464
- [12] W. Guan, S. Huang, D. Luo, F. Rong, “A Reverse Model Predictive Control Strategy for a Modular Multilevel Converter”, *Energies* 2019, 12, 297
- [13] P. Liu, Y. Wang, W. Cong, W. Lei, “Grouping-Sorting-Optimized Model Predictive Control for Modular Multilevel Converter With Reduced Computational Load”, *IEEE TRANSACTIONS ON POWER ELECTRONICS, VOL. 31, NO. 3, pp.1896-1907, Mar 2016*
- [14] J. Rodriguez and P. Cortes, *Predictive Control of Power Converters and Electrical Drives*. Hoboken, NJ, USA: Wiley, 2012.
- [15] PVsyst version 7.2, Copyright (c) 2009-2010, Victor Derevyanko, <https://www.pvsyst.com>
- [16] Google Earth Version 9.171.0.0-Web Assembly with threads, <https://earth.google.com/>
- [17] Pvsyst contextual help (built-in software). URL <http://files.pvsyst.com/help/index.html>
- [18] Arno H. M. Smets, Klaus Jäger, Olindo Isabella, René A. C. M. M. van Swaij, and Miro Zeman. *Solar energy : the physics and engineering of photovoltaic conversion, technologies and systems*. UIT Cambridge, Cambridge, 2016. ISBN 978-1-906860- 32-5.
- [19] PVsyst. (2018, November). Economic evaluation. Retrieved from http://files.pvsyst.com/help/economic_evaluation.htm
- [20] Michael Taylor and Eun young So. *Projected Costs of Generating Electricity 2015 edition*, . URL <https://www.iea.org/publications/freepublications/publication/projected-costs-of-generating-electricity-2015-edition.html>.
- [21] Port of Beirut Official website, <http://www.portdebeyrouth.com>
- [22] Port of Beirut As-Built drawing and operation documents, Project Reference: POB Extension of Existing Power Plant, Younes Bros, April 2015
- [23] Port of Beirut As-Built drawing, Project Reference: POB Power Plant, SAKR, 2007

- [24] Port of Beirut Tender drawing, Project Reference: POB Infrastructure, SERT Consultants, 2012
- [25] P. Salameh, N. Mendalek, “Planning of Photovoltaic Power Plant in the Middle East”, 6th IEEE International Energy Conference (ENERGYCON), 2020
- [26] LONGISOLAR LR5-72HBD-530 https://en.longi-solar.com/home/products/Hi_MO5.html
- [27] Huawei SUN2000-105KTL-H1, <https://support.huawei.com/enterprise/en/network-energy/sun2000-pid-7551590>
- [28] World Bank official website, Global Solar Atlas, Location Lebanon, <https://olc.worldbank.org/content/global-solar-atlas>
- [29] Jake Lomansoc, Ricard Jun Roloma, Kim Seer Paller, Design and Simulation of 100 kWp Solar Photovoltaic (PV) Grid Connected Power Plant Using PVsyst.